SUPPORTING INFORMATION

$[Pd_3Sn_8Bi_6]^{4-}$: A 14-vertex Sn/Bi Cluster embedding a Pd_3 Triangle

Felicitas Lips,[1] Rodolphe Clérac,[2,3] Stefanie Dehnen[1,*]

[1] Fachbereich Chemie and Wissenschaftliches Zentrum für Materialwissenschaften, Philipps-Universität Marburg, Hans-Meerwein-Straße, D-35032 Marburg, Germany, email: dehnen@chemie.uni-marburg.de;
[2] CNRS, UPR 8641, Centre de Recherche Paul Pascal (CRPP), Equipe "Matériaux Moléculaires Magnétiques", 115 avenue du Dr. Albert Schweitzer, Pessac, F-33600, France; Université de Bordeaux, UPR 8641, Pessac, F-33600, France
[3] Université de Bordeaux, UPR 8641, Pessac, F-33600, France

Content:

1 Experimental Details

1.1 General

All manipulations and reactions were performed in an argon or nitrogen atmosphere using standard Schlenk or glovebox techniques. Ethylenediamine (*en*) (Aldrich, 99%) and toluene (technical grade) were freshly distilled prior to use. [2.2.2]crypt [1] (Merck) and Bis[1,2-bis(diphenylphosphino)ethane]palladium(0) (Aldrich) were dried in vacuum for 13 h. The precursor $[K([2.2.2]crypt)]_2[Sn_2Bi_2]\cdot en$ was prepared according to the literature.[2]

1.2 Synthesis of $[K([2.2.2]crypt)]_4[Pd_3Sn_8Bi_6]$

193 mg (0.125 mmol) $[K([2.2.2]crypt)]_2[Sn_2Bi_2]\cdot en$ was weighed out into a Schlenk tube and then dissolved in *en* (3 mL). The color of this solution is dark-reddish brown. Another Schlenk tube was filled with 147 mg (0.163 mmol) of Bis[1,2-bis(diphenylphosphino)ethane]palladium(0) and then suspended in toluene (1 mL). An orange suspension is obtained. The orange suspension was added to the dark-reddish brown solution while stirring powerfully. The reaction mixture was allowed to stirr for 3 hours. The dark brown reaction solution was filtered through a standard glass frit and carefully layered by toluene (4 mL). After 3 days black rhombus-like plates of $[K([2.2.2]crypt)]_4[Pd_3Sn_8Bi_6]$ (**1**) formed at the wall of the Schlenk tube in approximately 15% yield based on the starting material. Semi-quantitative energy-dispersive X-ray spectroscopy (EDX) analyses of several crystals confirmed the composition of **1** (see below).

2 Details of the X-ray Diffraction Measurement, Structure Solution and Refinement

2.1 General

Single crystal X-ray diffraction data for **1** (Table S1) were collected on a Stoe IPDS2T diffractometer at 100 K with MoK_α radiation (λ = 0.71073 Å). The structure was solved by direct methods and refined with full matrix least squares against F^2 using SHELXS-97 und SHELXL-97 [3].

Table S1. X-ray measurement and structure solution of **1**.

Compound	**1**
Empirical formula	$C_{73.19}H_{148.26}Bi_6K_4N_{9.19}O_{24}Pd_3Sn_8$
Formula weight /g·mol^{-1}	4220.21
Crystal color, shape	black rhombus-like plate
Crystal size /mm^3	0.36×0.09×0.03
Crystal system	triclinic
Space group	P-1
a /Å *b* /Å *c* /Å	13.825(3) 16.323(3) 27.335(6)
α /° β /° γ /°	76.22(3) 82.55(3) 65.90(3)
V /Å^3	5465(2)
Z	2
ρ_{calc} /g·cm^{-3}	2.56
$\mu(Mo_{K\alpha})$ /mm^{-1}	12.1
2Θ range /°	9.22-54.33
Reflections measured	38203
Independent reflections	18832
R(int)	0.0932
Ind. reflections ($I > 2\sigma(I)$)	13080
Parameters	1314
Restraints	2245
R_1 ($I > 2\sigma(I)$)	0.0772
wR_2 (all data)	0.2058
GooF (all data)	0.966
Max. peak/hole /e$^-$·Å^{-3}	2.95/-3.47
Absorption correction type [4]	numerical
Min. /Max. transmission	0.095, 0.411

2.2 Details of the structure refinement for Compound 1

Due to rotational disorder the electron density for three C atoms of the [2.2.2]crypt-fragment of the third $[K([2.2.2]crypt)]^+$ ion could not be localized. The influence of the disorder for the [2.2.2]crypt-fragments of the fourth $[K([2.2.2]crypt)]^+$ was much stronger so that the electron density could only be localized in parts. Therefore the electron density around the fourth potassium atom was fitted for the known structural fragment of [2.2.2]crypt and refined as fixed group. The potassium atom of this countercation is located close to the inversion center resulting in two orientations. Placing the potassium atom at the exact position of the inversion center resulted in remarkably higher isotropic displacement parameters and was therefore not maintained. In order to maintain the overall geometry of the disordered $[K([2.2.2]crypt)]^+$ cations similar to the ordered species in the first refinement stages the appropriate SAME restraints were applied. However, in order to achieve a fully-anisotropic disorder model, it was necessary to enable some conformational freedom and to subtitute SAME restraints with an extensive set of soft DFIX restraints (all C-N bonds at 1.42(5) Å, C-C at 1.54(5) Å, C-O at 1.43(5) Å, K-N at 2.95(5) Å, K-O at 2.78(5) Å; for 1,3-distances, in order to keep angles at values reasonable within 3σ: N...C at 2.5(1) Å, C...O at 2.5(1) Å, C...C at 2.4(1) Å).

Numerous attempts to introduce different disorder models and to refine occupancies as free variables led to the following conclusions. In both disordered cations most plausible option is to introduce two disorder components. In case of one $[K([2.2.2]crypt)]^+$ cation (with K3 atom) for both disorder components occupancies should be fixed at 0.5 (also for both disorder components the same K atom position had to be assumed by the use of the corresponding EXYZ/EADP constraints). In case of the second cation (with K4 atom) it is better to refine the occupancies, adding to a full occupancy (the final refined occupancies are 0.54(2) and 0.46(2), respectively). In all cases a combination of EADP and ISOR constraints / SIMU restraints was necessary to achieve convergence.

All first stages of refinement often required the use of damping least-squares shifts, which was steadily removed at the end. Additionally, anti-bumping DFIX restraints (-2.00(1) Å) had to be applied to some H...H distances. Also, in order to keep some minor disorder component atoms from shifting away their distances to the neighbouring major disorder component atoms had to be restrained (C88...C50, C82...C53, C81...C52, O27...O16, O29...O17).

Voids in the crystal structure seem to be occupied by disordered ethylenediamine molecules (it was also possible to remove them by use of a SQUEEZE [5] routine, however, in this model we do not introduce SQUEEZE). Two sites were found with disordered centrosymmetric *en* molecules (with N1N and N2N atoms, respectively). Occupancies for these molecules were refined as free variables to obtain the following final values: 0.73(4) and 0.46(7), respectively (the higher-occupancy *en* molecule was refined anisotropically). The resulting structure model does not contain any voids, which could accomodate disordered potassium cations - this clearly confirms the assumed anion charge of -4.

H atoms of the ordered [2.2.2]crypt-fragments/disordered *en* molecules were calculated using the HFIX 23 command. H atoms for the disordered K[2.2.2]crypt-countercation/amine H atoms from *en*

molecules have not been considered (for the cation H atoms in order to avoid the necessity to include restraints on H...H distances, which would affect other restraints).

The highest peak/hole of the final difference Fourier map (2.95 $e^{-}\cdot Å^{-3}$/–3.47 $e^{-}\cdot Å^{-3}$) are located at 0.56 Å from Sn1 and at 0.68 Å from Bi2, respectively. All first 40 maxima on the final difference Fourier map (down to 1.16 $e^{-}\cdot Å^{-3}$) are located in the neighbourhood of heavy atoms. Figure S1 and S2 show fragments of the crystal structure of compound **1**.

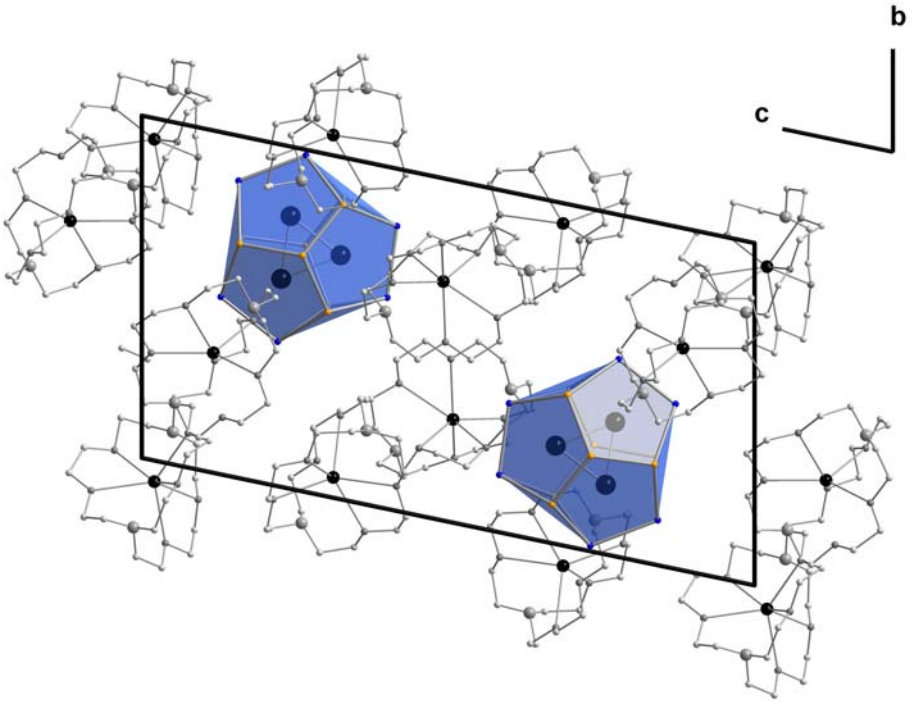

Figure S1. Packing of anions and cations in the crystal structure of compound **1**. View along the crystallographic *a* axis. Color code: Pd: black, Sn orange , Bi blue, K black, N dark gray, O medium gray, C light gray. H atoms have been omitted for claritiy.

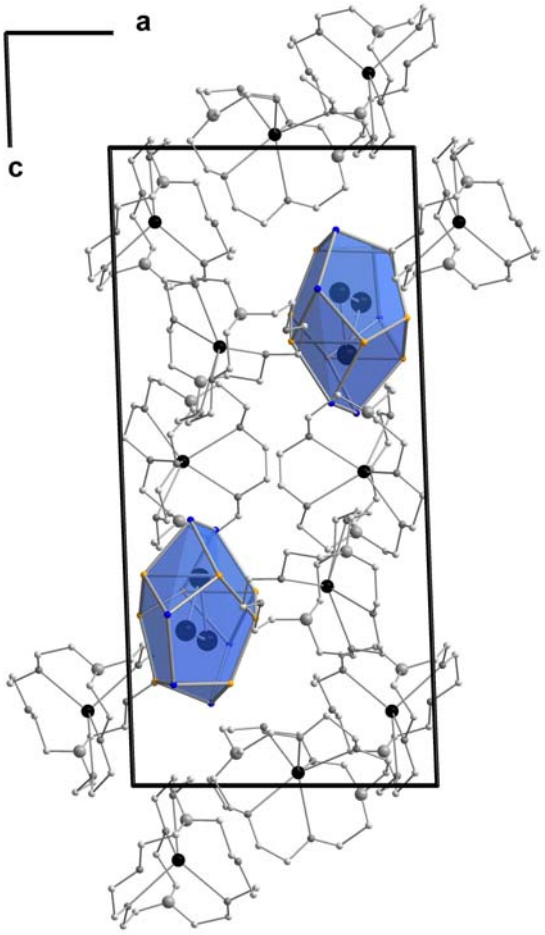

Figure S2. Packing of anions and cations in the crystal structure of compound **1**. View along the crystallographic *b* axis. Color code: Pd: black, Sn orange , Bi blue, K black, N dark gray, O medium gray, C light gray. H atoms are omitted for claritiy.

3 Energy Dispersive X-ray (EDX) Spectroscopy Analysis

3.1 General

EDX analysis on **1** (Table S2) was performed using the EDX device Voyager 4.0 of Noran Instruments coupled with the electron microscope CamScan CS 4DV. Data aquisition was performed with an acceleration voltage of 20 kV and 100 s accumulation time. For the analyses multiple single crystals were used and the data recorded both: various times on one single crystal and various times on other single crystals.

Table S2. EDX analysis of **1** (Sn, Bi, Pd, K).

Element	k-ratio	ZAF	Atom %	Atomic ratio observed (calc)	Element wt %	wt % Err. (1-sigma)
Sn-L	0.2326	1.428	36.19	7.61	33.20	+/- 0.65
Bi-M	0.4714	1.046	30.51	6.42	49.30	+/- 0.72
Pd-L	0.0802	1.466	14.29	3.01	11.75	+/- 0.79
K-L	0.0424	1.354	19.01	4	5.75	+/- 0.40
Total			100.00	21.04	100.00	

4 Magnetic measurement

The magnetic susceptibility measurements were obtained with the use of a Quantum Design SQUID magnetometer MPMS-XL housed at the Centre de Recherche Paul Pascal. This magnetometer works between 1.8 and 300 K for dc applied fields ranging from –7 to 7 T. Measurements were performed on microcrystalline samples of 6.1 mg, prepared in a glove box under argon and sealed in a polyethylene plastic bag.

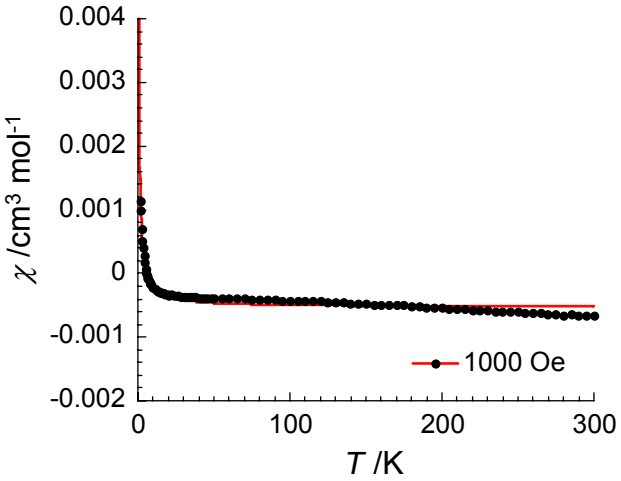

Figure S3. χ vs T plot for **1** at H_{dc} = 1000 Oe (χ being the molar magnetic susceptibility defined as M/H per complex). The solid red line is the best fit obtained with a Curie Law in order to estimate the presence of 0.9% of an S = ½ paramagnetic impurity (based on the molecular weight of **1**) and the diamagnetism of **1** at –5.3 10^{-4} cm^3/mol.

5 Electrospray Ionization Mass Spectrometry (ESI-MS) Investigations

5.1 General

ESI-MS has been performed on a Finnigan LTQ-FT spectrometer by Thermo Fischer Scientific in the negative ion mode: Spray voltage 3.90 kV, capillary temperature 300°C, capillary voltage -11 V, tube lens voltage -108.38 V, with sheath gas.

5.2 ESI-MS investigation of the reaction mixture

The reaction mixture, after 3 hours reaction time, was analyzed in the ethylenediamine/toluene solvent mixture. The overview of the ESI mass spectrum of the reaction mixture is given in Figure S4.
Figures S5-S7 show zooms of identifiable peaks:
at m/z = 655.76; four-atom fragment $[Sn_2Bi_2]^-$
at m/z = 746.84; four-atom fragment $[Sn_1Bi_3]^-$
at m/z = 1338.35; nine-atom fragment $[Sn_6Bi_3]^-$
at m/z = 1402.61; ten-atom fragment $[PdSn_6Bi_3]^-$

For the other peaks the identification failed. In these cases, it was obvious that the organic material is part of the detected species – at least as fragments – which complicated the assignment.

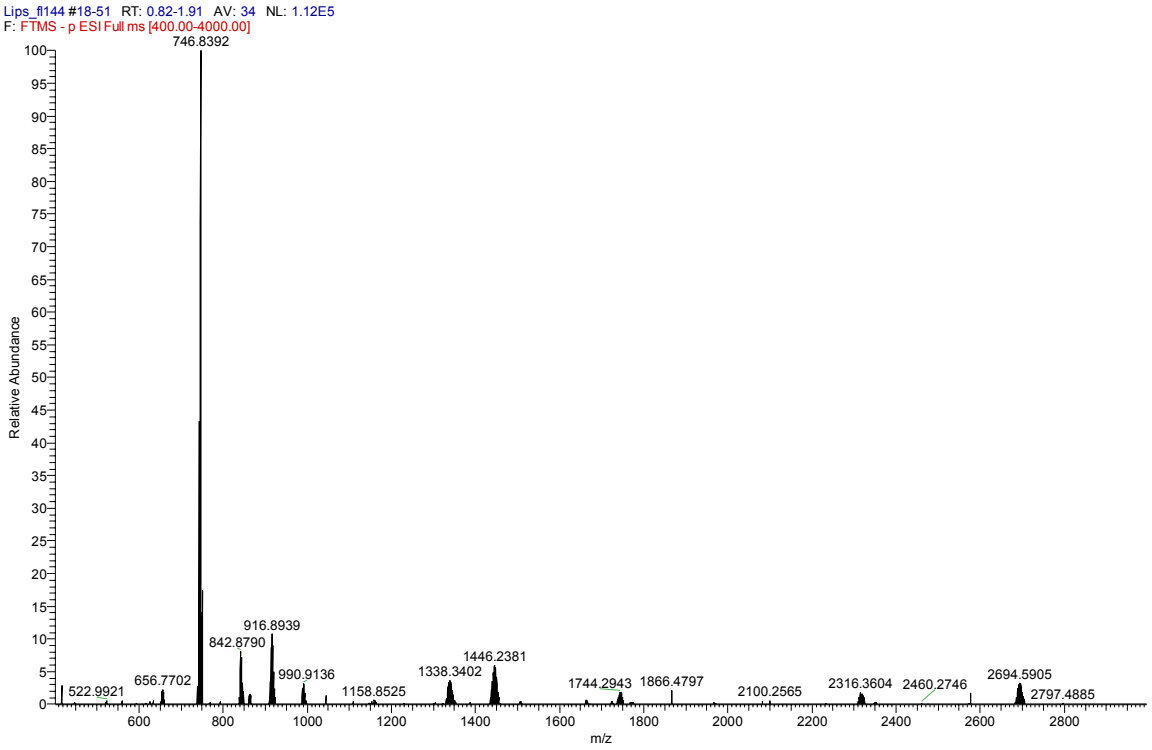

Figure S4. Overview of the ESI mass spectrum of the reaction mixture.

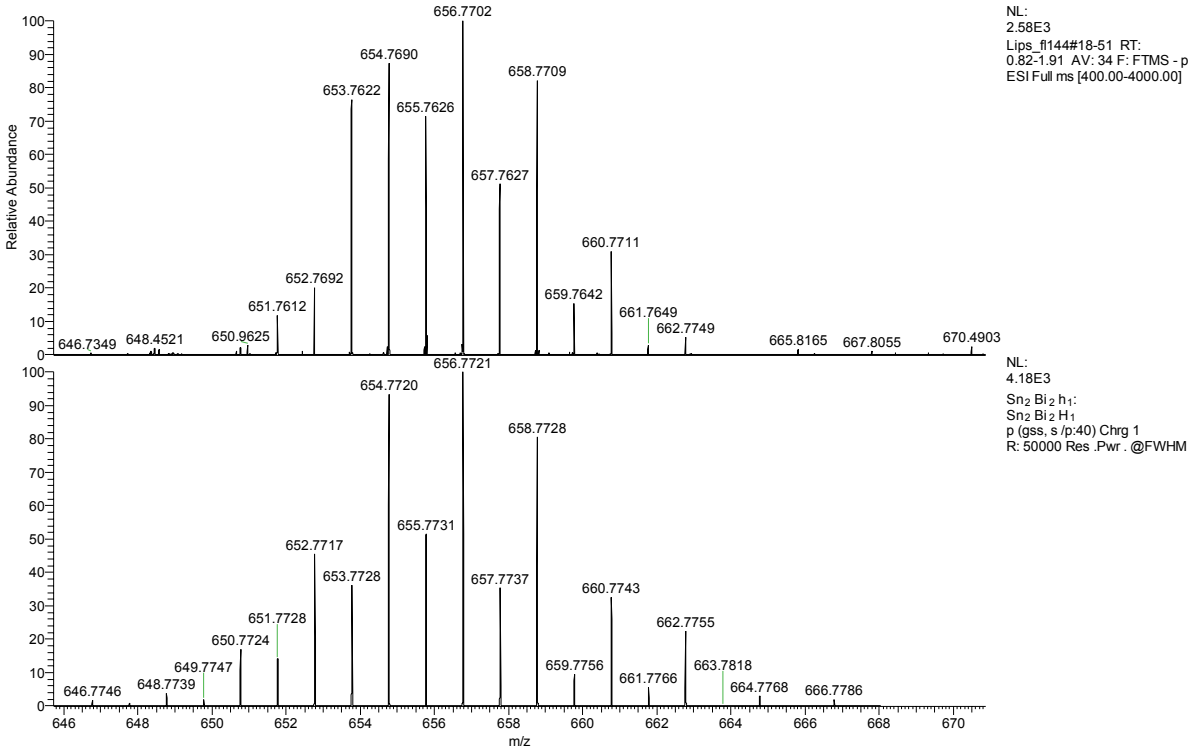

Figure S5. Measured (top) and simulated (bottom) spectrum of the fragment $[Sn_2Bi_2H]^-$.

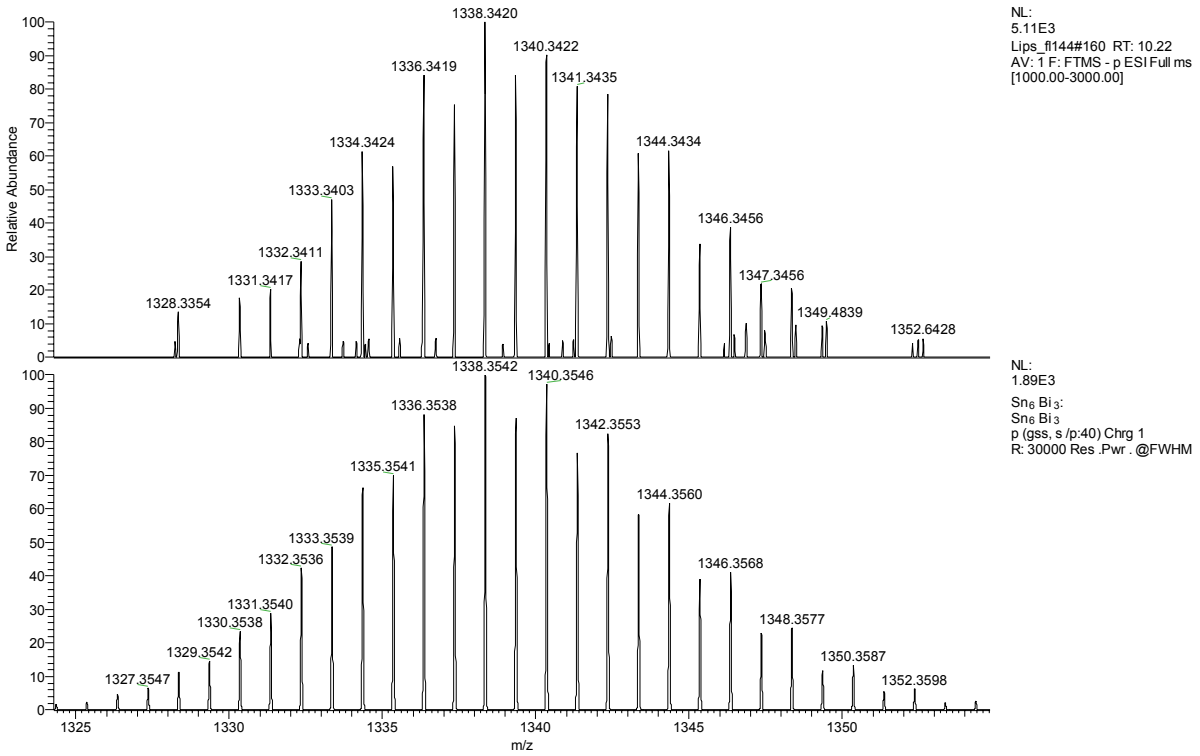

Figure S6. Measured (top) and simulated (bottom) spectrum of the fragment $[Sn_6Bi_3]^-$.

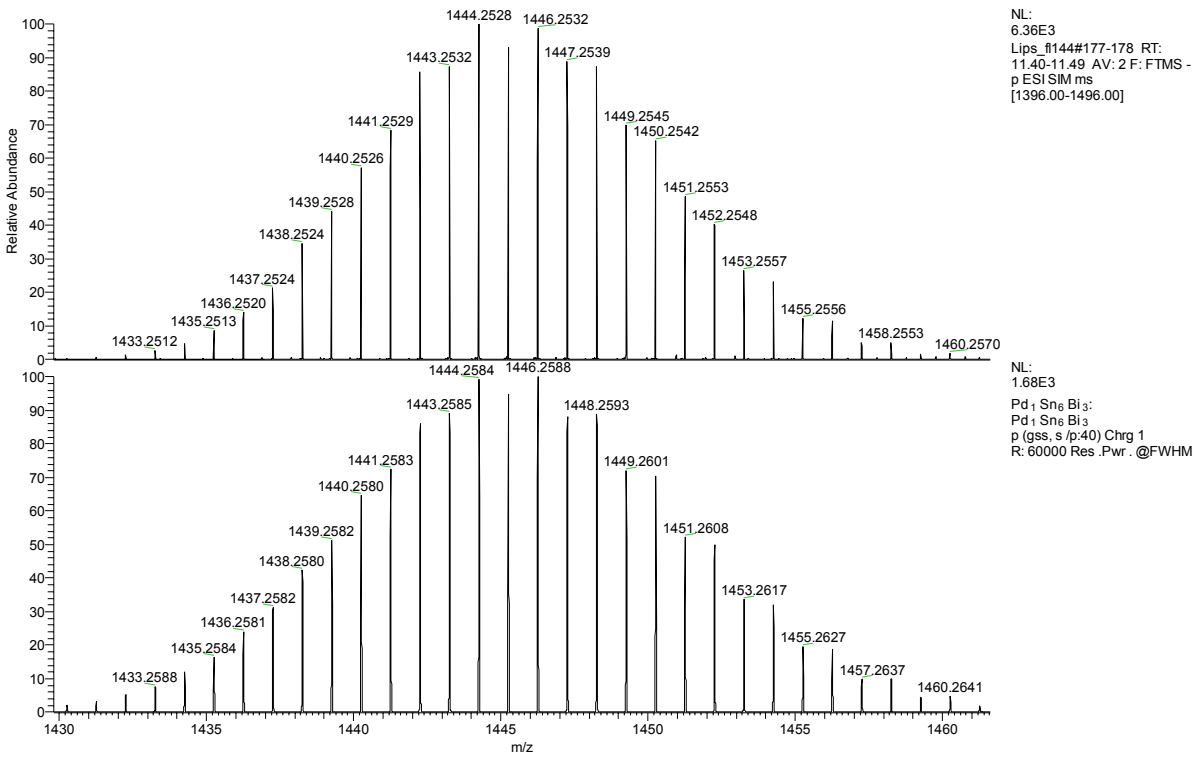

Figure S7. Measured (top) and simulated (bottom) spectrum of the fragment $[PdSn_6Bi_3]^-$.

5.3 ESI-MS Investigation of Compound 1

Compound **1** was dissolved in dimethylformamide (dmf) at -60 °C (Figure S8 and S9).

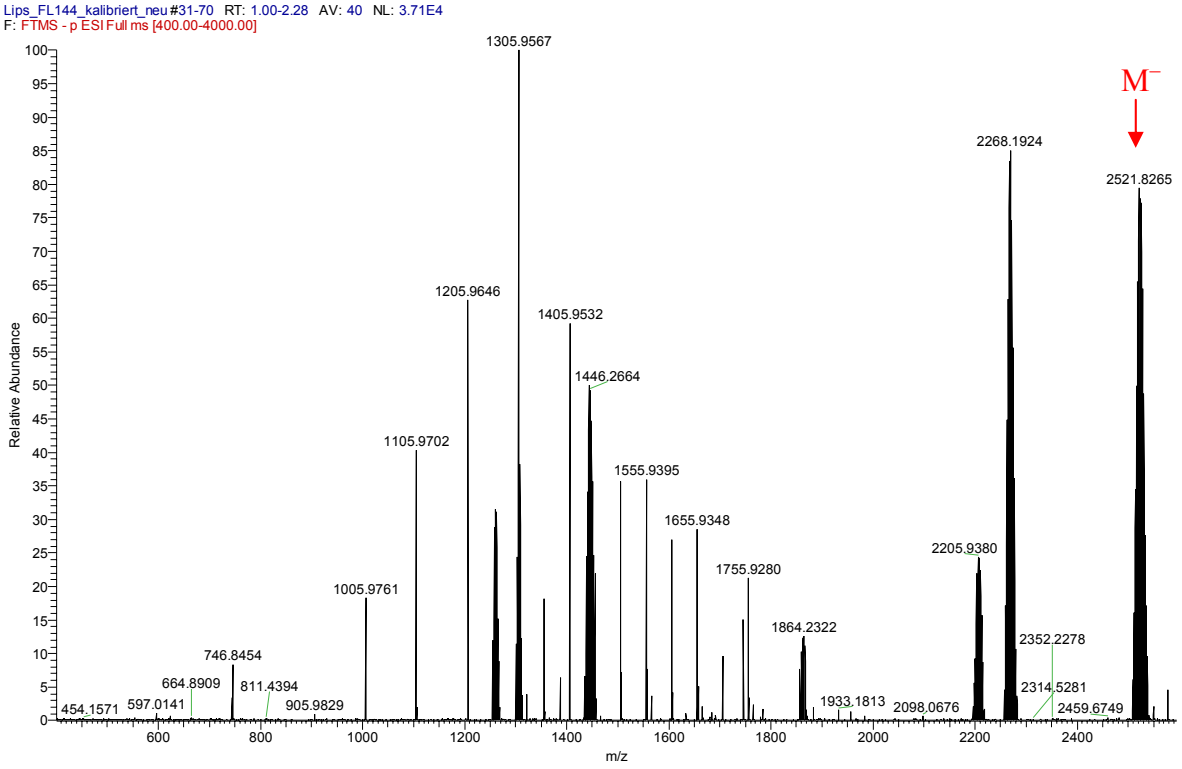

Figure S8. Overview of the ESI mass spectrum of the dissolved compound **1** in dmf.

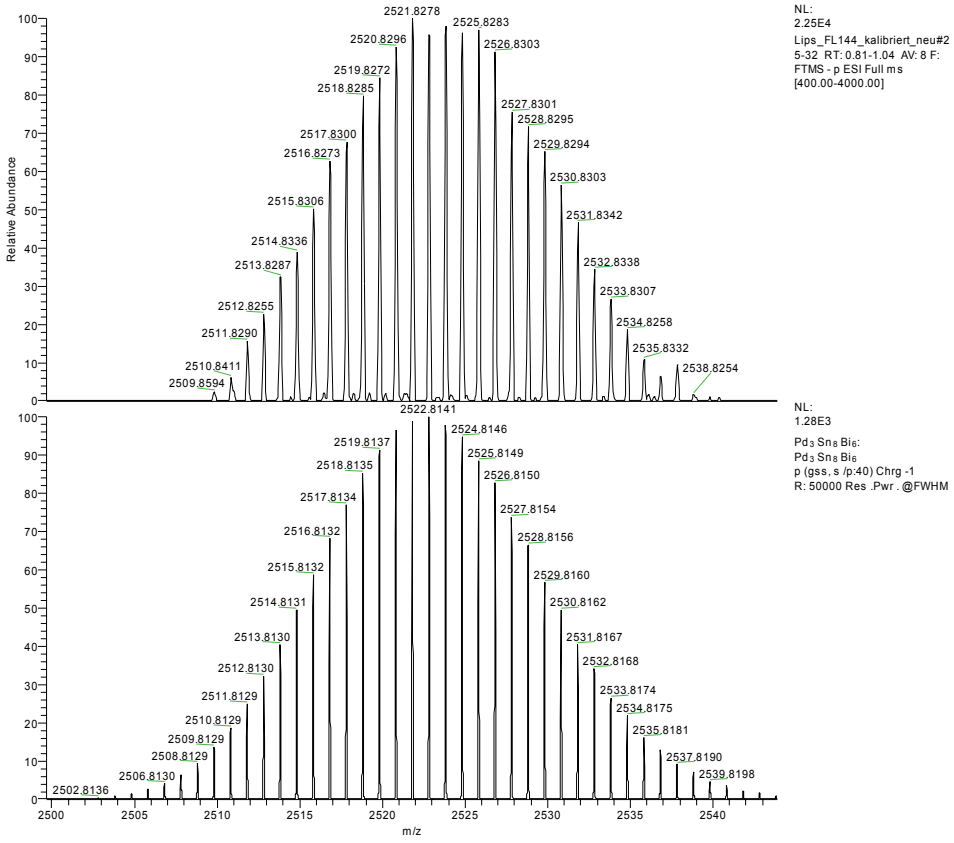

Figure S9. Measured (top) and simulated (bottom) spectrum of the cluster $[Pd_3Sn_8Bi_6]^-$.

6 Quantum Chemical Investigations

6.1 Computational Methods

The density functional theoretical (DFT) [6, 7] investigations were undertaken by means of the program system TURBOMOLE [8, 9] using the RIDFT program [10, 11] with the Becke-Perdew 86 (BP86) functional [12-14] and the gridsize m3. Basis sets were of def2-TZVP quality [15] (TZVP = triple zeta valence plus polarization) for Pd, Sn, Bi. For Pd (ECP-28), Sn (ECP-28) [16] and Bi atoms (ECP-60) [16], effective core potentials have been used for consideration of relativistic corrections and to reduce the computational effort. The high negative charge was compensated for by employment of the COSMO model [17, 18]. Simultaneous optimizations of geometric and electronic structures were performed without symmetry restrictions for $[Pd_3Sn_8Bi_6]^{4-}$ (C_1), also allowing for convergence into local minima at higher symmetry.

6.2 Quantum chemical investigations of the anion in compound 1

6.2.1 Investigation of the Sn/Bi atom distribution of $[Pd_3Sn_8Bi_6]^{4-}$

All 292 isomers of $[Pd_3Sn_4Bi_9]^{4-}$ have been investigated. The absolute and relative energies with respect to the most stable **Isomer 1** are categorized by the occupation of C, B or A positions (see Figure S10) and the structural motif of the Bi atoms presented in Table S3. Table S4 provides a

comparison of the experimentally determined interatomic distances with those of the six calculated isomers (1, 101, 13, 108, 15, 95).

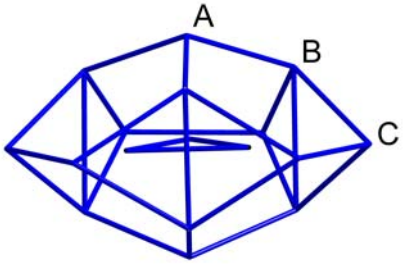

Figure S10. Definition of A, B, and C positions of Sn and Bi atoms in the anion $[Pd_3Sn_8Bi_6]^{4-}$.

The energy sequence in relation to the Sn/Bi distribution over the atomic sites of the intermetalloid cluster anion follows two basic rules if the minority atom type Bi is considered:
I) length of the Bi-atom chain and II) position of the Bi atoms in the cluster anion. e.g., short Bi atom chains are favoured and isomers with Bi atoms occupying C positions are favoured in comparision to A positions. The B position is the worst for Bi atoms. The energetically most stable isomer is the one with Bi atoms occupying all C positions and Sn atoms on A and B positions in combination with three two-membered Bi atom chains. Isomers with five or four Bi atoms on C positions in combination with two- to three-membered Bi atom chains are by 18-31 $kJ \cdot mol^{-1}$ disfavoured to the most stable one. If just one or no C position is taken by a Bi atom in combination with five- or six-membered Bi atom chains the isomers are disfavoured by 139-165 $kJ \cdot mol^{-1}$.

Table S3. Absolute and relative energies of all 292 isomers. Relative energies are given with respect to the most stable **Isomer 1**.

Isomer	E /Hartree	ΔE /kJmol^{-1}	Bi atom positions	Bi atom chain
Pd3Sn8Bi6Isomer1	-3390,040156804	**0,00**	6*C	3*Bi 2
Pd3Sn8Bi6Isomer101	-3390,033417075	**17,69**	5*C, 1*A	2*Bi 2, 1*isolated
Pd3Sn8Bi6Isomer13	-3390,031915159	**21,64**	5*C, 1*B	1*Bi 3, 1*Bi 2, 1*isolated
Pd3Sn8Bi6Isomer96	-3390,031411099	**22,96**	4*C, 2*A	1*Bi 2, 4* isolated
Pd3Sn8Bi6Isomer25	-3390,031023708	**23,98**	4*C, 2*B	2*Bi 2, 2*isolated
Pd3Sn8Bi6Isomer19	-3390,030965521	**24,13**	4*C, 1*B, 1*A	1*Bi 2, 4*isolated
Pd3Sn8Bi6Isomer35	-3390,030659246	**24,94**	5*C, 1*B	1*Bi 4, 1*Bi 2
Pd3Sn8Bi6Isomer34	-3390,029614713	**27,68**	4*C, 1*B, 1*A	1*Bi 3, 1*Bi 2, 1*isolated
Pd3Sn8Bi6Isomer121	-3390,029515909	**27,94**	4*C, 2*A	1*Bi 2, 4*isolated
Pd3Sn8Bi6Isomer176	-3390,028499139	**30,61**	4*C, 2*A	1*Bi 2, 4*isolated
Pd3Sn8Bi6Isomer38	-3390,028421560	**30,81**	4*C, 1*B, 1*A	2*Bi 2, 2*isolated
Pd3Sn8Bi6Isomer108	-3390,027796185	**32,45**	4*C, 1*B, 1*A	1*Bi 3, 3*isolated
Pd3Sn8Bi6Isomer104	-3390,027078803	**34,34**	5*C, 1*B	1*Bi 5, 1*isolated
Pd3Sn8Bi6Isomer41	-3390,025953137	**37,29**	4*C, 2*B	1*Bi 3, 1*Bi 2, 1*isolated
Pd3Sn8Bi6Isomer103	-3390,025891970	**37,45**	4*C, 1*B, 1*A	1*Bi 4, 2*isolated
Pd3Sn8Bi6Isomer143	-3390,025841900	**37,58**	4*C, 1*B, 1*A	1*Bi 3, 3*isolated
Pd3Sn8Bi6Isomer27	-3390,025592106	**38,24**	4*C, 2*B	1*Bi 4, 2*isolated

Pd3Sn8Bi6Isomer36	-3390,025365049	**38,84**	4*C, 2*B	1*Bi 4, 1*Bi 2
Pd3Sn8Bi6Isomer7	-3390,024630170	**40,76**	4*C, 1*B, 1*A	2*Bi 2, 2*isolated
Pd3Sn8Bi6Isomer115	-3390,024348928	**41,50**	4*C, 2*B	2*Bi 3
Pd3Sn8Bi6Isomer15	-3390,024089077	**42,19**	4*C, 2*B	1*Bi 4, 2*isolated
Pd3Sn8Bi6Isomer17	-3390,023995154	**42,43**	4*C, 2*B	1*Bi 3, 1*Bi 2, 1*isolated
Pd3Sn8Bi6Isomer197	-3390,023989107	**42,45**	4*C, 1*B, 1*A	1*Bi 4, 2*isolated
Pd3Sn8Bi6Isomer26	-3390,023975811	**42,48**	4*C, 2*B	1*Bi 4, 2*isolated
Pd3Sn8Bi6Isomer20	-3390,023576580	**43,53**	3*C, 2*B, 1*A	1*Bi 2, 4*isolated
Pd3Sn8Bi6Isomer162	-3390,023334323	**44,17**	3*C, 2*B, 1*A	1*Bi 3, 3*isolated
Pd3Sn8Bi6Isomer31	-3390,023322092	**44,20**	4*C, 1*B, 1*A	1*Bi 4, 1*Bi 2
Pd3Sn8Bi6Isomer114	-3390,023108451	**44,76**	4*C, 2*B	2* Bi 3
Pd3Sn8Bi6Isomer43	-3390,023025751	**44,98**	4*C, 2*B	1*Bi 4, 1*Bi 2
Pd3Sn8Bi6Isomer14	-3390,022568577	**46,18**	4*C, 2*B	1*Bi 4, 2*isolated
Pd3Sn8Bi6Isomer16	-3390,022475795	**46,42**	4*C, 2*B	1*Bi 3, 1*Bi 2, 1*isolated
Pd3Sn8Bi6Isomer113	-3390,022381487	**46,67**	4*C, 2*B	1*Bi 4, 2*isolated
Pd3Sn8Bi6Isomer129	-3390,022328492	**46,81**	3*C, 1*B, 2*A	1*Bi 2, 4*isolated
Pd3Sn8Bi6Isomer46	-3390,022230511	**47,06**	4*C, 2*A	2* Bi 2, 2*isolated
Pd3Sn8Bi6Isomer32	-3390,022004904	**47,66**	4*C, 1*B, 1*A	1*Bi 3, 1*Bi 2, 1*isolated
Pd3Sn8Bi6Isomer98	-3390,021877879	**47,99**	4*C, 1*B, 1*A	1*Bi 4, 2*isolated
Pd3Sn8Bi6Isomer42	-3390,021421494	**49,19**	4*C, 2*B	1*Bi 4, 1*Bi 2
Pd3Sn8Bi6Isomer18	-3390,021409731	**49,22**	3*C, 3*B	2* Bi 2, 2*isolated
Pd3Sn8Bi6Isomer153	-3390,021238820	**49,67**	4*C, 2*B	1*Bi 5, 1*isolated
Pd3Sn8Bi6Isomer65	-3390,020870145	**50,64**	4*C, 1*B, 1*A	1*Bi 3, 1*Bi 2, 1*isolated
Pd3Sn8Bi6Isomer37	-3390,020367062	**51,96**	3*C, 3*B	1*Bi 3, 1*Bi 2, 1*isolated
Pd3Sn8Bi6Isomer95	-3390,020245316	**52,28**	4*C, 1*B, 1*A	1*Bi 5, 1*isolated
Pd3Sn8Bi6Isomer151	-3390,020041928	**52,81**	4*C, 2*B	1*Bi 4, 2*isolated
Pd3Sn8Bi6Isomer152	-3390,019986126	**52,96**	4*C, 2*B	1*Bi 5, 1*isolated
Pd3Sn8Bi6Isomer106	-3390,019940418	**53,08**	4*C, 2*B	1*Bi 5, 1*isolated
Pd3Sn8Bi6Isomer161	-3390,019931997	**53,10**	3*C, 2*B, 1*A	1*Bi 3, 3*isolated
Pd3Sn8Bi6Isomer124	-3390,019849050	**53,32**	4*C, 1*B, 1*A	1*Bi 4, 2*isolated
Pd3Sn8Bi6Isomer21	-3390,019527457	**54,16**	3*C, 2*B, 1*A	1*Bi 3, 3*isolated
Pd3Sn8Bi6Isomer9	-3390,019509975	**54,21**	3*C, 2*B, 1*A	2* Bi 2, 2*isolated
Pd3Sn8Bi6Isomer212	-3390,019171045	**55,10**	3*C, 2*B, 1*A	1*Bi 3, 1*Bi 2, 1*isolated
Pd3Sn8Bi6Isomer28	-3390,019039622	**55,44**	3*C, 3*B	1*Bi 3, 3*isolated
Pd3Sn8Bi6Isomer183	-3390,018849382	**55,94**	3*C, 1*B, 2*A	1*Bi 3, 3*isolated
Pd3Sn8Bi6Isomer163	-3390,018789955	**56,10**	3*C, 2*B, 1*A	1*Bi 4, 2*isolated
Pd3Sn8Bi6Isomer138	-3390,018779331	**56,13**	3*C, 2*B, 1*A	1*Bi 3, 1*Bi 2, 1*isolated
Pd3Sn8Bi6Isomer170	-3390,018769542	**56,15**	3*C, 3*B	1*Bi 3, 1*Bi 2, 1*isolated
Pd3Sn8Bi6Isomer222	-3390,018636380	**56,50**	3*C, 3*B	1*Bi 3, 1*Bi 2, 1*isolated
Pd3Sn8Bi6Isomer178	-3390,018635946	**56,50**	3*C, 1*B, 2*A	1*Bi 3, 3*isolated
Pd3Sn8Bi6Isomer180	-3390,018406129	**57,11**	4*C, 1*B, 1*A	1*Bi 5, 1*isolated
Pd3Sn8Bi6Isomer3	-3390,018403226	**57,11**	4*C, 2*B	2* Bi 3
Pd3Sn8Bi6Isomer148	-3390,018314278	**57,35**	3*C, 2*B, 1*A	2* Bi 2, 1*isolated
Pd3Sn8Bi6Isomer207	-3390,018263586	**57,48**	3*C, 3*B	1*Bi 3, 1*Bi 2, 1*isolated
Pd3Sn8Bi6Isomer202	-3390,017786844	**58,73**	4*C, 2*B	1*Bi 5, 1*isolated
Pd3Sn8Bi6Isomer22	-3390,017606735	**59,20**	3*C, 2*B, 1*A	1*Bi 3, 3*isolated

Pd3Sn8Bi6Isomer204	-3390,017508892	**59,46**	4*C, 2*B	1*Bi 6
Pd3Sn8Bi6Isomer71	-3390,017504467	**59,47**	4*C, 2*B	1*Bi 4, 1*Bi 2
Pd3Sn8Bi6Isomer2	-3390,017125581	**60,47**	4*C, 2*B	2*Bi 3
Pd3Sn8Bi6Isomer171	-3390,017057544	**60,65**	3*C, 3*B	1*Bi 4, 2*isolated
Pd3Sn8Bi6Isomer203	-3390,016628685	**61,77**	4*C, 2*B	1*Bi 6
Pd3Sn8Bi6Isomer52	-3390,016612405	**61,82**	3*C, 1*B, 2*A	2*Bi 2, 2*isolated
Pd3Sn8Bi6Isomer110	-3390,016589001	**61,88**	3*C, 2*B, 1*A	1*Bi 3, 1*Bi 2, 1*isolated
Pd3Sn8Bi6Isomer123	-3390,016584622	**61,89**	3*C, 1*B, 2*A	1*Bi 3, 3*isolated
Pd3Sn8Bi6Isomer4	-3390,016215686	**62,86**	3*C, 3*B	1*Bi 3, 1*Bi 2, 1*isolated
Pd3Sn8Bi6Isomer102	-3390,016039306	**63,32**	4*C, 1*B, 1*A	1*Bi 5, 1*isolated
Pd3Sn8Bi6Isomer81	-3390,015950272	**63,55**	3*C, 2*B, 1*A	1*Bi 4, 2*isolated
Pd3Sn8Bi6Isomer221	-3390,015357165	**65,11**	3*C, 3*B	1*Bi 3, 1*Bi 2, 1*isolated
Pd3Sn8Bi6Isomer80	-3390,015259296	**65,37**	3*C, 2*B, 1*A	1*Bi 3, 1*Bi 2, 1*isolated
Pd3Sn8Bi6Isomer47	-3390,015036070	**65,95**	3*C, 1*B, 2*A	1*Bi 3, 1*Bi 2, 1*isolated
Pd3Sn8Bi6Isomer48	-3390,014815992	**66,53**	4*C, 1*B, 1*A	1*Bi 4, 1*Bi 2
Pd3Sn8Bi6Isomer213	-3390,014563643	**67,19**	3*C, 2*B, 1*A	1*Bi 4, 1*Bi 2
Pd3Sn8Bi6Isomer190	-3390,014559714	**67,20**	3*C, 2*B, 1*A	2* Bi 3
Pd3Sn8Bi6Isomer157	-3390,014523710	**67,30**	3*C, 3*B	3* Bi 2
Pd3Sn8Bi6Isomer68	-3390,014454295	**67,48**	3*C, 2*B, 1*A	1*Bi 3, 1*Bi 2, 1*isolated
Pd3Sn8Bi6Isomer211	-3390,014211579	**68,12**	3*C, 2*B, 1*A	1*Bi 4, 2*isolated
Pd3Sn8Bi6Isomer149	-3390,014196619	**68,16**	3*C, 2*B, 1*A	1*Bi 3, 1*Bi 2, 1*isolated
Pd3Sn8Bi6Isomer127	-3390,014144035	**68,30**	3*C, 2*B, 1*A	1*Bi 3, 1*Bi 2, 1*isolated
Pd3Sn8Bi6Isomer158	-3390,014031550	**68,59**	3*C, 3*B	1*Bi 3, 1*Bi 2, 1*isolated
Pd3Sn8Bi6Isomer107	-3390,013826523	**69,13**	3*C, 3*B	1*Bi 4, 1*Bi 2
Pd3Sn8Bi6Isomer97	-3390,013703304	**69,45**	3*C, 1*B, 2*A	1*Bi 4, 2*isolated
Pd3Sn8Bi6Isomer44	-3390,013604946	**69,71**	3*C, 3*B	1*Bi 3, 1*Bi 2, 1*isolated
Pd3Sn8Bi6Isomer30	-3390,013411728	**70,22**	2*C, 4*B	2*Bi 2, 2*isolated
Pd3Sn8Bi6Isomer23	-3390,013276915	**70,57**	3*C, 2*B, 1*A	1*Bi 4, 2*isolated
Pd3Sn8Bi6Isomer208	-3390,013182616	**70,82**	3*C, 3*B	2*Bi 3
Pd3Sn8Bi6Isomer145	-3390,013053644	**71,16**	3*C, 2*B, 1*A	1*Bi 4, 2*isolated
Pd3Sn8Bi6Isomer147	-3390,013042893	**71,19**	3*C, 2*B, 1*A	1*Bi 4, 2*isolated
Pd3Sn8Bi6Isomer199	-3390,012961479	**71,40**	3*C, 2*B, 1*A	1*Bi 5, 1*isolated
Pd3Sn8Bi6Isomer118	-3390,012947481	**71,44**	3*C, 3*B	2*Bi 3
Pd3Sn8Bi6Isomer73	-3390,012899621	**71,56**	4*C, 2*B	1*Bi 6
Pd3Sn8Bi6Isomer11	-3390,012795279	**71,84**	3*C, 2*B, 1*A	1*Bi 3, 1*Bi 2, 1*isolated
Pd3Sn8Bi6Isomer279	-3390,012584114	**72,39**	2*C, 3*B, 1*A	1*Bi 3, 3*isolated
Pd3Sn8Bi6Isomer67	-3390,012412376	**72,84**	3*C, 2*B, 1*A	1*Bi 4, 1*Bi 2
Pd3Sn8Bi6Isomer223	-3390,012328500	**73,06**	3*C, 3*B	1*Bi 4, 1*Bi 2
Pd3Sn8Bi6Isomer39	-3390,012208923	**73,38**	3*C, 2*B, 1*A	1*Bi 4, 1*Bi 2
Pd3Sn8Bi6Isomer82	-3390,012191326	**73,42**	3*C, 2*B, 1*A	1*Bi 5, 1*isolated
Pd3Sn8Bi6Isomer227	-3390,012125107	**73,60**	3*C, 2*B, 1*A	1*Bi 4, 2*isolated
Pd3Sn8Bi6Isomer8	-3390,011779435	**74,50**	3*C, 2*B, 1*A	1*Bi 4, 2*isolated
Pd3Sn8Bi6Isomer72	-3390,011771219	**74,53**	4*C, 2*B	1*Bi 6
Pd3Sn8Bi6Isomer111	-3390,011742763	**74,60**	3*C, 2*B, 1*A	2* Bi 3
Pd3Sn8Bi6Isomer24	-3390,011715926	**74,67**	2*C, 3*B, 1*A	1*Bi 3, 3*isolated
Pd3Sn8Bi6Isomer137	-3390,011578498	**75,03**	3*C, 2*B, 1*A	1*Bi 5, 1*isolated

Pd3Sn8Bi6Isomer60	-3390,011575429	**75,04**	3*C, 2*B, 1*A	1*Bi 4, 1*Bi 2
Pd3Sn8Bi6Isomer177	-3390,011485434	**75,28**	3*C, 1*B, 2*A	1*Bi 4, 2*isolated
Pd3Sn8Bi6Isomer29	-3390,011423138	**75,44**	3*C, 3*B	1*Bi 4, 2*isolated
Pd3Sn8Bi6Isomer122	-3390,011419366	**75,45**	3*C, 1*B, 2*A	1*Bi 4, 2*isolated
Pd3Sn8Bi6Isomer262	-3390,011408122	**75,48**	3*C, 2*B, 1*A	1*Bi 5, 1*isolated
Pd3Sn8Bi6Isomer94	-3390,011153835	**76,15**	4*C, 1*B, 1*A	1*Bi 6
Pd3Sn8Bi6Isomer205	-3390,011082052	**76,33**	3*C, 3*B	1*Bi 5, 1*isolated
Pd3Sn8Bi6Isomer88	-3390,011058490	**76,40**	3*C, 3*B	1*Bi 5, 1*isolated
Pd3Sn8Bi6Isomer216	-3390,011032675	**76,46**	2*C, 3*B, 1*A	2*Bi 2, 2*isolated
Pd3Sn8Bi6Isomer156	-3390,010925010	**76,75**	3*C, 3*B	3* Bi 2
Pd3Sn8Bi6Isomer116	-3390,010865039	**76,90**	3*C, 3*B	2* Bi 3
Pd3Sn8Bi6Isomer45	-3390,010851114	**76,94**	3*C, 3*B	1*Bi 4, 1*Bi 2
Pd3Sn8Bi6Isomer272	-3390,010519840	**77,81**	3*C, 3*B	1*Bi 5, 1*isolated
Pd3Sn8Bi6Isomer210	-3390,010516925	**77,82**	2*C, 4*B	1*Bi 3, 1*Bi 2, 1*isolated
Pd3Sn8Bi6Isomer6	-3390,010487540	**77,90**	2*C, 2*B, 2*A	2* Bi 2, 2*isolated
Pd3Sn8Bi6Isomer154	-3390,010480997	**77,91**	3*C, 3*B	1*Bi 4, 1*Bi 2
Pd3Sn8Bi6Isomer69	-3390,010353222	**78,25**	3*C, 2*B, 1*A	1*Bi 4, 1*Bi 2
Pd3Sn8Bi6Isomer117	-3390,010328632	**78,31**	3*C, 3*B	1*Bi 4, 1*Bi 2
Pd3Sn8Bi6Isomer76	-3390,010210661	**78,62**	3*C, 3*B	1*Bi 4, 1*Bi 2
Pd3Sn8Bi6Isomer256	-3390,010108143	**78,89**	2*C, 3*B, 1*A	1*Bi 3, 1*Bi 2, 1*isolated
Pd3Sn8Bi6Isomer181	-3390,009986283	**79,21**	2*C, 3*B, 1*A	1*Bi 4, 2*isolated
Pd3Sn8Bi6Isomer50	-3390,009718841	**79,91**	3*C, 2*B, 1*A	2*Bi 3
Pd3Sn8Bi6Isomer66	-3390,009046010	**81,68**	3*C, 2*B, 1*A	1*Bi 5, 1*isolated
Pd3Sn8Bi6Isomer109	-3390,009043681	**81,69**	3*C, 2*B, 1*A	1*Bi 5, 1*isolated
Pd3Sn8Bi6Isomer146	-3390,008993121	**81,82**	3*C, 2*B, 1*A	1*Bi 5, 1*isolated
Pd3Sn8Bi6Isomer139	-3390,008883652	**82,11**	2*C, 3*B, 1*A	3*Bi 2
Pd3Sn8Bi6Isomer209	-3390,008804747	**82,31**	2*C, 4*B	1*Bi 3, 1*Bi 2, 1*isolated
Pd3Sn8Bi6Isomer5	-3390,008608754	**82,83**	2*C, 2*B, 2*A	1*Bi 3, 3*isolated
Pd3Sn8Bi6Isomer266	-3390,008552522	**82,98**	2*C, 3*B, 1*A	2*Bi 2, 2*isolated
Pd3Sn8Bi6Isomer271	-3390,008424778	**83,31**	3*C, 3*B	1*Bi 5, 1*isolated
Pd3Sn8Bi6Isomer79	-3390,008357751	**83,49**	2*C, 4*B	3*2 Bi
Pd3Sn8Bi6Isomer89	-3390,008289604	**83,67**	3*C, 3*B	1*Bi 5, 1*isolated
Pd3Sn8Bi6Isomer194	-3390,008169873	**83,98**	2*C, 3*B, 1*A	1*Bi 3, 1*Bi 2, 1*isolated
Pd3Sn8Bi6Isomer155	-3390,008065041	**84,26**	3*C, 3*B	1*Bi 5, 1*isolated
Pd3Sn8Bi6Isomer40	-3390,007850938	**84,82**	2*C, 3*B, 1*A	1*Bi 3, 1*Bi 2, 1*isolated
Pd3Sn8Bi6Isomer173	-3390,007829573	**84,87**	2*C, 4*B	1*Bi3, 1*Bi 2, 1*isolated
Pd3Sn8Bi6Isomer105	-3390,007770589	**85,03**	4*C, 2*B	1*Bi 6
Pd3Sn8Bi6Isomer75	-3390,007579073	**85,53**	3*C, 3*B	1*Bi 4, 1*Bi 2
Pd3Sn8Bi6Isomer70	-3390,007553497	**85,60**	2*C, 3*B, 1*A	1*Bi 3, 1*Bi 2, 1*isolated
Pd3Sn8Bi6Isomer189	-3390,007410961	**85,97**	3*C, 2*B, 1*A	1*Bi 6
Pd3Sn8Bi6Isomer263	-3390,007390342	**86,03**	3*C, 2*B, 1*A	1*Bi 6
Pd3Sn8Bi6Isomer160	-3390,007367824	**86,09**	2*C, 4*B	3*Bi 2
Pd3Sn8Bi6Isomer226	-3390,007361862	**86,10**	2*C, 4*B	1*Bi 3, 1*Bi 2, 1*isolated
Pd3Sn8Bi6Isomer172	-3390,007305694	**86,25**	2*C, 4*B	1*Bi 3, 1*Bi 2, 1*isolated
Pd3Sn8Bi6Isomer132	-3390,007113801	**86,75**	2*C, 2*B, 2*A	1*Bi 5, 1*isolated
Pd3Sn8Bi6Isomer237	-3390,007005472	**87,04**	3*C, 2*B, 1*A	1*Bi 6
Pd3Sn8Bi6Isomer78	-3390,006996600	**87,06**	2*C, 4*B	3*Bi 2

Pd3Sn8Bi6Isomer244	-3390,006931271	**87,23**	2*C, 2*B, 2*A	1*Bi 4, 2*isolated
Pd3Sn8Bi6Isomer165	-3390,006920635	**87,26**	2*C, 3*B, 1*A	1*Bi 4, 2*isolated
Pd3Sn8Bi6Isomer201	-3390,006908163	**87,29**	2*C, 3*B, 1*A	2*Bi 3
Pd3Sn8Bi6Isomer77	-3390,006898618	**87,32**	3*C, 3*B	1*Bi 4, 1*Bi 2
Pd3Sn8Bi6Isomer191	-3390,006787042	**87,61**	2*C, 3*B, 1*A	1*Bi 3, 1*Bi 2, 1*isolated
Pd3Sn8Bi6Isomer289	-3390,006576421	**88,16**	2*C, 4*B	1*Bi 4, 2*isolated
Pd3Sn8Bi6Isomer141	-3390,006470288	**88,44**	2*C, 3*B, 1*A	3*Bi 2
Pd3Sn8Bi6Isomer150	-3390,006376478	**88,69**	2*C, 3*B, 1*A	1*Bi 3, 1*Bi 2, 1*isolated
Pd3Sn8Bi6Isomer246	-3390,006257418	**89,00**	2*C, 2*B, 2*A	1*Bi 4, 1*Bi 2
Pd3Sn8Bi6Isomer167	-3390,006234375	**89,06**	2*C, 3*B, 1*A	1*Bi 4, 2*isolated
Pd3Sn8Bi6Isomer126	-3390,006227559	**89,08**	3*C, 2*B, 1*A	1*Bi 5, 1*isolated
Pd3Sn8Bi6Isomer261	-3390,006112171	**89,38**	3*C, 2*B, 1*A	1*Bi 5, 1*isolated
Pd3Sn8Bi6Isomer135	-3390,006012498	**89,64**	2*C, 2*B, 2*A	1*Bi 3, 1*Bi 2, 1*isolated
Pd3Sn8Bi6Isomer74	-3390,005894452	**89,95**	3*C, 3*B	1*Bi 5, 1*isolated
Pd3Sn8Bi6Isomer12	-3390,005838635	**90,10**	2*C, 3*B, 1*A	1*Bi 4, 2*isolated
Pd3Sn8Bi6Isomer241	-3390,005777952	**90,26**	2*C, 3*B, 1*A	1*Bi 3, 1*Bi 2, 1*isolated
Pd3Sn8Bi6Isomer159	-3390,005638995	**90,63**	2*C, 4*B	3* Bi 2
Pd3Sn8Bi6Isomer10	-3390,005633379	**90,64**	3*C, 2*B, 1*A	1*Bi 5, 1*isolated
Pd3Sn8Bi6Isomer225	-3390,005614628	**90,69**	2*C, 4*B	1*Bi 3, 1*Bi 2, 1*isolated
Pd3Sn8Bi6Isomer131	-3390,005562022	**90,83**	2*C, 2*B, 2*A	1*Bi 4, 2*isolated
Pd3Sn8Bi6Isomer175	-3390,005327824	**91,44**	2*C, 4*B	1*Bi 3, 1* Bi 2, 1*isolated
Pd3Sn8Bi6Isomer59	-3390,005253785	**91,64**	3*C, 2*B, 1*A	1*Bi 6
Pd3Sn8Bi6Isomer133	-3390,005229708	**91,70**	2*C, 2*B, 2*A	1*Bi 4, 2*isolated
Pd3Sn8Bi6Isomer245	-3390,005116664	**92,00**	2*C, 2*B, 2*A	1*Bi 5, 1*isolated
Pd3Sn8Bi6Isomer54	-3390,005107532	**92,02**	2*C, 2*B, 2*A	1*Bi 3, 1*Bi 2, 1*isolated
Pd3Sn8Bi6Isomer288	-3390,005073026	**92,11**	2*C, 4*B	1*Bi 4, 2*isolated
Pd3Sn8Bi6Isomer144	-3390,004949769	**92,44**	3*C, 2*B, 1*A	1*Bi 5, 1*isolated
Pd3Sn8Bi6Isomer187	-3390,004947244	**92,44**	2*C, 2*B, 2*A	2* Bi 3
Pd3Sn8Bi6Isomer130	-3390,004884434	**92,61**	2*C, 2*B, 2*A	1*Bi 4, 2*isolated
Pd3Sn8Bi6Isomer90	-3390,004868536	**92,65**	2*C, 4*B	1*Bi 3, 1*Bi 2, 1*isolated
Pd3Sn8Bi6Isomer280	-3390,004585742	**93,39**	2*C, 3*B, 1*A	1*Bi 5, 1*isolated
Pd3Sn8Bi6Isomer206	-3390,004552588	**93,48**	3*C, 3*B	1*Bi 6
Pd3Sn8Bi6Isomer198	-3390,004545631	**93,50**	3*C, 2*B, 1*A	1*Bi 6
Pd3Sn8Bi6Isomer99	-3390,004480735	**93,67**	3*C, 2*B, 1*A	1*Bi 6
Pd3Sn8Bi6Isomer218	-3390,004422039	**93,82**	2*C, 3*B, 1*A	1*Bi 4, 1*Bi 2
Pd3Sn8Bi6Isomer134	-3390,004327659	**94,07**	2*C, 2*B, 2*A	1*Bi 4, 2*isolated
Pd3Sn8Bi6Isomer277	-3390,004098942	**94,67**	2*C, 4*B	1*Bi 3, 1*Bi 2, 1*isolated
Pd3Sn8Bi6Isomer200	-3390,004061588	**94,77**	2*C, 3*B, 1*A	2* Bi 3
Pd3Sn8Bi6Isomer83	-3390,004006238	**94,91**	2*C, 3*B, 1*A	1*Bi 4, 2*isolated
Pd3Sn8Bi6Isomer84	-3390,003829149	**95,38**	2*C, 3*B, 1*A	1*Bi 4, 2*isolated
Pd3Sn8Bi6Isomer273	-3390,003757851	**95,56**	3*C, 3*B	1*Bi 6
Pd3Sn8Bi6Isomer287	-3390,003713982	**95,68**	2*C, 4*B	1*Bi 4, 1* Bi 2
Pd3Sn8Bi6Isomer186	-3390,003578460	**96,04**	2*C, 2*B, 2*A	1*Bi 5, 1*isolated
Pd3Sn8Bi6Isomer281	-3390,003505696	**96,23**	2*C, 3*B, 1*A	1*Bi 5, 1*isolated
Pd3Sn8Bi6Isomer112	-3390,003353010	**96,63**	2*C, 3*B, 1*A	1*Bi 4, 1*Bi 2
Pd3Sn8Bi6Isomer174	-3390,003182149	**97,08**	2*C, 4*B	1*Bi 3, 1*Bi 2, 1*isolated

Pd3Sn8Bi6Isomer53	-3390,003180214	**97,08**	2*C, 2*B, 2*A	1*Bi 4, 2*isolated
Pd3Sn8Bi6Isomer224	-3390,003131465	**97,21**	2*C, 4*B	2* Bi 3
Pd3Sn8Bi6Isomer185	-3390,003005068	**97,54**	2*C, 2*B, 2*A	1*Bi 5, 1*isolated
Pd3Sn8Bi6Isomer276	-3390,002979328	**97,61**	2*C, 4*B	1*Bi 3, 1*Bi 2, 1*isolated
Pd3Sn8Bi6Isomer120	-3390,002912431	**97,78**	2*C, 4*B	1*Bi 4, 1*Bi2
Pd3Sn8Bi6Isomer49	-3390,002895935	**97,83**	3*C, 2*B, 1*A	1*Bi 6
Pd3Sn8Bi6Isomer55	-3390,002694918	**98,36**	2*C, 2*B, 2*A	1*Bi 4, 1*Bi 2
Pd3Sn8Bi6Isomer217	-3390,002601999	**98,60**	2*C, 3*B, 1*A	1*Bi 4, 1*Bi 2
Pd3Sn8Bi6Isomer164	-3390,002594612	**98,62**	2*C, 3*B, 1*A	1*Bi 5, 1*isolated
Pd3Sn8Bi6Isomer233	-3390,002232895	**99,57**	2*C, 2*B, 2*A	2*Bi 3
Pd3Sn8Bi6Isomer125	-3390,002188332	**99,69**	3*C, 2*B, 1*A	1*Bi 5, 1*isolated
Pd3Sn8Bi6Isomer51	-3390,001951028	**100,31**	2*C, 3*B, 1*A	1*Bi 5, 1*isolated
Pd3Sn8Bi6Isomer33	-3390,001725109	**100,90**	2*C, 3*B, 1*A	1*Bi 5, 1*isolated
Pd3Sn8Bi6Isomer140	-3390,001701330	**100,96**	2*C, 3*B, 1*A	1*Bi 5, 1*isolated
Pd3Sn8Bi6Isomer182	-3390,001625034	**101,16**	2*C, 3*B, 1*A	1*Bi 6
Pd3Sn8Bi6Isomer215	-3390,001425720	**101,69**	2*C, 3*B, 1*A	1*Bi 4, 1*Bi 2
Pd3Sn8Bi6Isomer119	-3390,001421406	**101,70**	2*C, 4*B	1*Bi 4, 1*Bi 2
Pd3Sn8Bi6Isomer238	-3390,001309432	**101,99**	2*C, 3*B, 1*A	1*Bi 5, 1*isolated
Pd3Sn8Bi6Isomer91	-3390,001157875	**102,39**	2*C, 4*B	1*Bi 4, 1*Bi 2
Pd3Sn8Bi6Isomer231	-3390,001140103	**102,44**	2*C, 3*B, 1*A	1*Bi 5, 1*isolated
Pd3Sn8Bi6Isomer268	-3390,001010625	**102,78**	2*C, 3*B, 1*A	1*Bi 4, 1*Bi 2
Pd3Sn8Bi6Isomer57	-3390,000991452	**102,83**	2*C, 2*B, 2*A	1*Bi 4, 1*Bi 2
Pd3Sn8Bi6Isomer128	-3390,000973226	**102,88**	2*C, 3*B, 1*A	1*Bi 5, 1*isolated
Pd3Sn8Bi6Isomer236	-3390,000948050	**102,94**	3*C, 2*B, 1*A	1*Bi 6
Pd3Sn8Bi6Isomer63	-3390,000821880	**103,27**	2*C, 3*B, 1*A	1*Bi 4, 1*Bi 2
Pd3Sn8Bi6Isomer232	-3390,000791990	**103,35**	2*C, 2*B, 2*A	1*Bi 5, 1*isolated
Pd3Sn8Bi6Isomer166	-3390,000631173	**103,77**	2*C, 3*B, 1*A	1*Bi 5, 1*isolated
Pd3Sn8Bi6Isomer214	-3390,000540627	**104,01**	2*C, 3*B, 1*A	1*Bi 4, 1*Bi 2
Pd3Sn8Bi6Isomer267	-3390,000404163	**104,37**	2*C, 3*B, 1*A	1*Bi 4, 1*Bi 2
Pd3Sn8Bi6Isomer142	-3390,000287824	**104,67**	2*C, 3*B, 1*A	1*Bi 5, 1*isolated
Pd3Sn8Bi6Isomer184	-3389,999608192	**106,46**	2*C, 2*B, 2*A	1*Bi 5, 1*isolated
Pd3Sn8Bi6Isomer56	-3389,999388630	**107,04**	2*C, 2*B, 2*A	1*Bi 5, 1*isolated
Pd3Sn8Bi6Isomer179	-3389,999378094	**107,06**	2*C, 2*B, 2*A	1*Bi 6
Pd3Sn8Bi6Isomer86	-3389,999295232	**107,28**	2*C, 3*B, 1*A	1*Bi 5, 1*isolated
Pd3Sn8Bi6Isomer275	-3389,999210446	**107,50**	2*C, 4*B	2* Bi 3
Pd3Sn8Bi6Isomer61	-3389,998960585	**108,16**	2*C, 3*B, 1*A	1*Bi 5, 1*isolated
Pd3Sn8Bi6Isomer278	-3389,998622496	**109,05**	1*C, 5*B	3* Bi 2
Pd3Sn8Bi6Isomer195	-3389,998489893	**109,40**	2*C, 3*B, 1*A	1*Bi 6
Pd3Sn8Bi6Isomer257	-3389,998449355	**109,50**	2*C, 3*B, 1*A	1*Bi 6
Pd3Sn8Bi6Isomer219	-3389,998409330	**109,61**	1*C, 4*B, 1*A	1*Bi 3, 1*Bi 2, 1*isolated
Pd3Sn8Bi6Isomer93	-3389,998026793	**110,61**	2*C, 4*B	1*Bi 5, 1*isolated
Pd3Sn8Bi6Isomer100	-3389,997856062	**111,06**	2*C, 3*B, 1*A	1*Bi 6
Pd3Sn8Bi6Isomer269	-3389,997694096	**111,48**	1*C, 4*B, 1*A	1*Bi 3, 1*Bi 2, 1*isolated
Pd3Sn8Bi6Isomer290	-3389,997136814	**112,95**	1*C, 5*B	1*Bi 3, 1*Bi 2, 1*isolated
Pd3Sn8Bi6Isomer230	-3389,996857942	**113,68**	2*C, 2*B, 2*A	1*Bi 6
Pd3Sn8Bi6Isomer92	-3389,996758508	**113,94**	2*C, 4*B	1*Bi 5, 1*isolated
Pd3Sn8Bi6Isomer255	-3389,996282480	**115,19**	2*C, 3*B, 1*A	1*Bi 6
Pd3Sn8Bi6Isomer284	-3389,996219137	**115,36**	1*C, 4*B, 1*A	1*Bi 4, 2*isolated
Pd3Sn8Bi6Isomer192	-3389,996067023	**115,76**	2*C, 3*B, 1*A	1*Bi 6

Pd3Sn8Bi6Isomer85	-3389,995996299	**115,94**	2*C, 3*B, 1*A	1*Bi 5, 1*isolated
Pd3Sn8Bi6Isomer291	-3389,995908449	**116,17**	1*C, 5*B	1*Bi 3, 1*Bi 2, 1*isolated
Pd3Sn8Bi6Isomer229	-3389,995635212	**116,89**	2*C, 2*B, 2*A	1*Bi 5, 1*isolated
Pd3Sn8Bi6Isomer242	-3389,995431193	**117,43**	2*C, 3*B, 1*A	1*Bi 6
Pd3Sn8Bi6Isomer264	-3389,995211082	**118,00**	2*C, 3*B, 1*A	1*Bi 6
Pd3Sn8Bi6Isomer220	-3389,994685870	**119,38**	1*C, 4*B, 1*A	1*Bi 4, 1*Bi 2
Pd3Sn8Bi6Isomer169	-3389,994681850	**119,39**	1*C, 4*B, 1*A	1*Bi 5, 1*isolated
Pd3Sn8Bi6Isomer265	-3389,994552317	**119,73**	2*C, 3*B, 1*A	1*Bi 6
Pd3Sn8Bi6Isomer168	-3389,994341825	**120,29**	1*C, 4*B, 1*A	1*Bi 5, 1*isolated
Pd3Sn8Bi6Isomer228	-3389,994052439	**121,05**	2*C, 2*B, 2*A	1*Bi 6
Pd3Sn8Bi6Isomer87	-3389,993738232	**121,87**	1*C, 4*B, 1*A	1*Bi 4, 2*isolated
Pd3Sn8Bi6Isomer193	-3389,993715454	**121,93**	2*C, 3*B, 1*A	1*Bi 6
Pd3Sn8Bi6Isomer247	-3389,993612071	**122,20**	1*C, 3*B, 2*A	1*Bi 4, 1*Bi 2
Pd3Sn8Bi6Isomer270	-3389,993480754	**122,55**	1*C, 4*B, 1*A	1*Bi 4, 1*Bi 2
Pd3Sn8Bi6Isomer64	-3389,993414859	**122,72**	2*C, 3*B, 1*A	1*Bi 6
Pd3Sn8Bi6Isomer250	-3389,993384005	**122,80**	1*C, 3*B, 2*A	1*Bi 4, 1*Bi 2
Pd3Sn8Bi6Isomer234	-3389,993222374	**123,22**	1*C, 3*B, 2*A	2* Bi 3
Pd3Sn8Bi6Isomer136	-3389,993187660	**123,32**	1*C, 3*B, 2*A	1*Bi 5, 1*isolated
Pd3Sn8Bi6Isomer285	-3389,992676073	**124,66**	1*C, 4*B, 1*A	1*Bi 5, 1*isolated
Pd3Sn8Bi6Isomer58	-3389,992198666	**125,91**	1*C, 3*B, 2*A	1*Bi 5, 1*isolated
Pd3Sn8Bi6Isomer259	-3389,992127062	**126,10**	1*C, 4*B, 1*A	1*Bi 5, 1*isolated
Pd3Sn8Bi6Isomer274	-3389,991636005	**127,39**	2*C, 4*B	1*Bi 6
Pd3Sn8Bi6Isomer240	-3389,991591166	**127,51**	2*C, 3*B, 1*A	1*Bi 6
Pd3Sn8Bi6Isomer188	-3389,990984055	**129,10**	1*C, 3*B, 2*A	1*Bi 6
Pd3Sn8Bi6Isomer283	-3389,990377450	**130,69**	1*C, 4*B, 1*A	1*Bi 6
Pd3Sn8Bi6Isomer249	-3389,990075501	**131,49**	1*C, 3*B, 2*A	1*Bi 5, 1*isolated
Pd3Sn8Bi6Isomer239	-3389,989648694	**132,61**	2*C, 3*B, 1*A	1*Bi 6
Pd3Sn8Bi6Isomer235	-3389,989520930	**132,94**	1*C, 3*B, 2*A	1*Bi 6
Pd3Sn8Bi6Isomer292	-3389,989452389	**133,12**	6*B	3*Bi 2
Pd3Sn8Bi6Isomer251	-3389,988842464	**134,72**	1*C, 3*B, 2*A	1*Bi 6
Pd3Sn8Bi6Isomer282	-3389,988685661	**135,14**	1*C, 4*B, 1*A	1*Bi 6
Pd3Sn8Bi6Isomer248	-3389,988324149	**136,09**	1*C, 3*B, 2*A	1*Bi 6
Pd3Sn8Bi6Isomer62	-3389,987467510	**138,33**	2*C, 3*B, 1*A	1*Bi 6
Pd3Sn8Bi6Isomer196	-3389,987298382	**138,78**	1*C, 4*B, 1*A	1*Bi 6
Pd3Sn8Bi6Isomer243	-3389,986566776	**140,70**	1*C, 4*B, 1*A	1*Bi 6
Pd3Sn8Bi6Isomer258	-3389,985455728	**143,62**	1*C, 4*B, 1*A	1*Bi 6
Pd3Sn8Bi6Isomer286	-3389,985126267	**144,48**	5*B, 1*A	1*Bi 5, 1*isolated
Pd3Sn8Bi6Isomer254	-3389,980435579	**156,80**	4*B, 2*A	1*Bi 6
Pd3Sn8Bi6Isomer260	-3389,979614741	**158,95**	5*B, 1*A	1*Bi 6
Pd3Sn8Bi6Isomer253	-3389,978502636	**161,87**	4*B, 2*A	1*Bi 6
Pd3Sn8Bi6Isomer252	-3389,977243920	**165,18**	4*B, 2*A	1*Bi 6

Table S4. Comparison of experimental interatomic distances in the anion of **1**, the three calculated anions of lowest energy and three arbitrarily chosen isomers. Deviations are given in parentheses.

Bond type	**Distances /pm**						
	X-ray	ΔE = 0 kJ·mol^{-1} **Isomer 1**	ΔE = 18 kJ·mol^{-1} **Isomer 101**	ΔE = 22 kJ·mol^{-1}* **Isomer 13**	ΔE = 32 kJ·mol^{-1} **Isomer 108**	ΔE = 42 kJ·mol^{-1}* **Isomer 15**	ΔE = 52 kJ·mol^{-1} **Isomer 95**
Sn(1,14)–Sn(2-4, 11-13)	289.75-294.52	293.82-293.87 [4.1-(−0.7); av. 2.4]	293.38-302.34 [3.6-7.8; av 5.7]	291.25-301.09 [1.5-6.6; av 4.1]	294.16-302.54 [4.4-8.0; av. 6.2]	292.31-302.30 [2.6-7.8; av 5.2]	292.96-311.75 [3.2-17.2; av 10.2]
Sn(2-4, 11-13)–Bi(5-10)	301.94-309.11	310.89-311.24 [9.0-2.1; av. 5.6]	305.77-317.27 [3.8-8.2; av 6.0]	308.54-317.05 [6.6-7.9; av 7.3]	303.32-317.87 [1.4-8.8; av. 5.1]	303.96-324.10 [2.0-15.0; av 8.5]	300.20-326.24 [–1.7-17.1; av 18.8]
Sn(2-4)–Sn(11-13)	318.68-326.03	329.01-329.46 [10.3-3.4; av. 6.9]	323.39-326.33 [4.7-0.3; av 5.0]	326.20 331.66 [7.5-5.6; av 6.6]	322.28-326.54 [3.6-0.5; av. 2.1]	319.89-325.49 [1.2-(–0.5); av 0.9]	323.17-324.15 [4.5-1.9; av 3.2]
Bi(5-10)–Bi(5-10)	312.41-314.88	317.18-317.51 [4.8-2.6; av. 3.7]	304.54-320.13 [–7.9-5.3; av 6.6]	303.90-320.92 [–8.5-6.0; av 7.3]	302.54-320.04 [–9.9-5.2; av. 7.6]	303.65-314.82 [–8.8-(–0.1); av 4.5]	300.69-320.13 [–11.7-5.3; av 8.5]
Sn(1,14)–Pd(1-3)	296.39-302.35	302.60-302.80 [9.2-0.5; av. 4.9]	298.09-306.02 [1.7-3.7; av 2.7]	296.48-303.36 [0.1-1.0; av 0.6]	295.29-307.39 [–1.1-5.0; av. 3.1]	293.39-304.93 [–3.0-2.6; av 2.8]	296.23-306.53 [–0.2-4.2; av 2.2]
Sn(2-4, 11-13)–Pd(1-3)	286.87-291.19	293.29 293.66 [6.4-2.5; av. 4.5]	290.95-300.57 [4.1-9.4; av 6.8]	290.86-299.37 [4.0-8.2; av 6.1]	291.76 301.98 [4.9-10.8; av. 7.9]	292.16-300.50 [5.3-9.3; av 7.3]	290.93-310.72 [4.1-19.5; av 11.8]
Bi(5-10)–Pd(1-3)	272.76-275.08	277.67-278.01 [4.9-2.9; av. 3.9]	275.86-279.07 [3.1-4.0; av 7.1]	275.96-279.66 [3.2-4.6; av 3.9]	275.83-278.94 [3.1-3.9; av 3.5]	274.37-278.83 [1.6-3.8; av 5.4]	275.03-278.55 [2.3-3.5; av 2.9]
Pd(1-3)–Pd(1-3)	275.73-277.20	280.58-280.73 [4.9-3.5; av. 2.8]	279.67-283.54 [3.9-6.3; av 5.1]	279.61-283.06 [3.9-5.9; av 4.9]	281.78-286.58 [6.1-9.4; av. 7.8]	283.02-285.41 [7.3-8.2; av 15.5]	282.01-286.19 [6.3-9.0; av 7.7]

6.2.2 Natural Population Analysis (NPA) of the most stable isomer of $[Pd_3Sn_8Bi_6]^{4-}$ according to DFT calculations in D_{3h} symmetry.

Table S5. Natural charges calculated by means of a Natural Population Analysis (NPA) [19] based on the DFT [6, 7] optimized electronic and geometric structure of the anion in **1**.

Atom No	Natural Charge	Natural Population			
		Core	Valence	Rydberg	Total
Pd1	-0.08	7.99	10.03	0.06	18.08
Pd2	-0.08	7.99	10.03	0.06	18.08
Pd3	-0.08	7.99	10.03	0.06	18.08
Bi1	-0.34	12.00	11.33	0.02	23.34
Bi2	-0.34	12.00	11.33	0.02	23.34
Bi3	-0.34	12.00	11.33	0.02	23.34
Bi4	-0.34	12.00	11.33	0.02	23.34
Bi5	-0.34	12.00	11.33	0.02	23.34
Bi6	-0.34	12.00	11.33	0.02	23.34
Sn1	-0.34	18.00	4.31	0.03	22.34
Sn8	-0.34	18.00	4.31	0.03	22.34
Sn2	-0.17	18.00	4.31	0.03	22.34
Sn3	-0.17	18.00	4.31	0.03	22.34
Sn4	-0.17	18.00	4.31	0.03	22.34
Sn5	-0.17	18.00	4.31	0.03	22.34
Sn6	-0.17	18.00	4.31	0.03	22.34
Sn7	-0.17	18.00	4.31	0.03	22.34
Total	–4.00000	240.00	131.54	0.54	372.00

6.2.3 Investigation of the interaction of the Pd_3 triangle with the main group cage $[Sn_8Bi_6]^{4-}$ by comparison of structural parameters and Mulliken population analysis

For the most stable **Isomer 1** the interaction of the Pd triangle with the main group atom cage has been studied by comparison of the geometries (Table S6) and a Mulliken population analysis [20] of the molecular orbitals (MOs). For this purpose the anion in **1** as well as the corresponding fragments $[Pd_3]$ and $[Sn_8Bi_6]^{4-}$ have been calculated in D_{3h} symmetry. All MOs are shown in the following subchapters, plotted by means of the program gOpenMol [21].

It is obvious that the bonding within the cluster is characterized by a high degree of delocalization, hence cluster orbitals that are related to atomic orbitals can be observed. However, in comparison to an atom, the ternary cluster anion possesses a much lower symmetry (calculated as D_{3h}) as a result of distinct compression along the C_3 axis. Thus, the identification of pure s, p, d, and f-type cluster orbitals is complicated or in part impossible due to significant mixing of the respective irreducible representations. Comparison of the MO diagrams of $[Pd_3]$ and $[Sn_8Bi_6]^{4-}$ with that of $[Pd_3Sn_8Bi_6]^{4-}$ (Figure S13) shows that the lowest MOs of the $[Pd_3Sn_8Bi_6]^{4-}$ cluster anion are non-bonding (either representing the bonding within the $[Sn_8Bi_6]^{4-}$ cluster shell, or the bonding in the $[Pd_3]$ cluster), whereas most MOs between the HOMO level and HOMO–19 show nearly equal contributions from both fragments to form cluster orbitals – however both in Pb–Sn/Bi bonding as well as antibonding fashion.

Table S6. Interatomic distances /Å in the $[Pd_3Sn_8Bi_6]^{4-}$ anion in **1** = $\mathbf{[A]^{4-}}$ exp_{av}, averaged for equivalent bonds, and in the calculated anion = $\mathbf{[A]^{4-}}$ calc, in comparison with the according values in calculated fragments $[Pd_3]$ = [**P**] and $[Sn_8Bi_6]^{4-}$ = $\mathbf{[S]^{4-}}$, or $[Pd_3]^{2-}$ = $\mathbf{[P]^{2-}}$ and $[Sn_8Bi_6]^{2-}$ = $\mathbf{[S]^{2-}}$. Grey boxes highlight the values that agree best with those of $\mathbf{[A]^{4-}}$ calc. Atom numbers accord with the labeling scheme in Figure 1. Note that the structure of $\mathbf{[S]^{2-}}$ produces imaginary frequencies indicating deviation from a local minimum.

Distance	$\mathbf{[A]^{4-}}$ $\mathbf{exp_{av}}$	$\mathbf{[A]^{4-}}$ **calc**	$\mathbf{[S]^{4-}}$ **/ [P]**	$\mathbf{[S]^{2-}}$ **/** $\mathbf{[P]^{2-}}$
Sn1,8–Sn2-7	2.917	2.942	2.874 / –	2.891 / –
Sn2-4–Sn5-7	3.224	3.287	3.326 / –	3.239 / –
Sn2-7–Bi	3.056	3.109	2.996 / –	2.924 / –
Bi–Bi	3.136	3.172	3.015 / –	3.219 / –
Pd–Sn1,8	2.993	3.031	–	–
Pd–Sn2-7	2.896	2.934	–	–
Pd–Bi	2.739	2.778	–	–
Pd–Pd	2.768	2.806	– / 2.482	– / 2.608

6.2.3.1 Molecular orbitals of [Pd_3]

3a1’ -8.249 eV

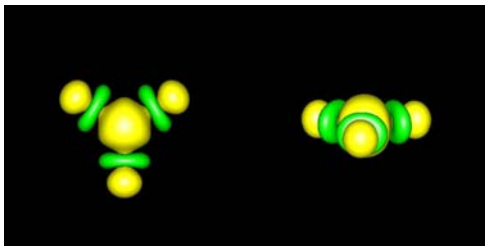

4 e’ -7.559 eV

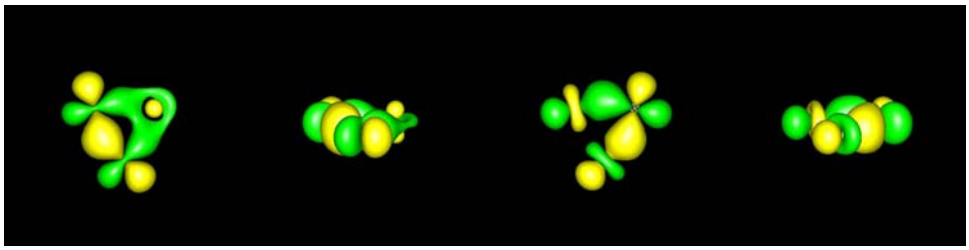

2a2’’ -7.002 eV

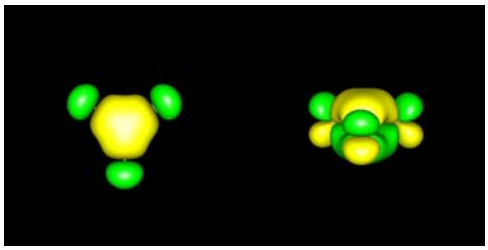

4a1’ -6.550 eV

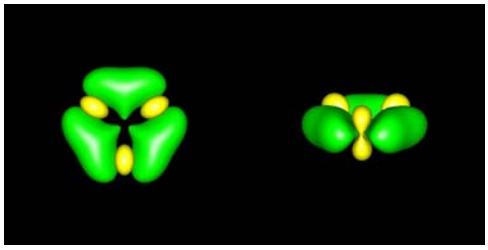

2e’’ -6.177 eV

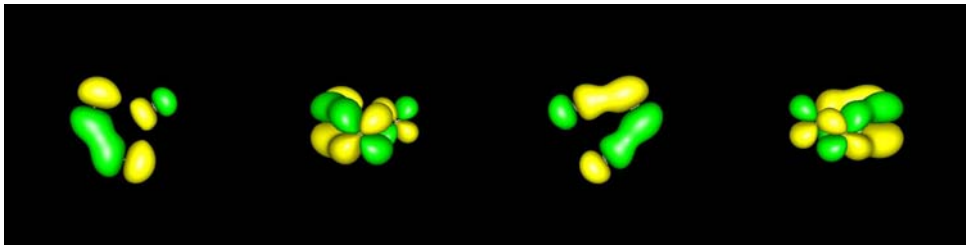

5e’ -5.651 eV

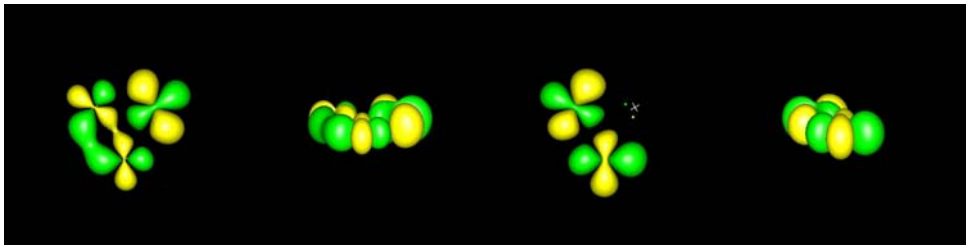

5a1’ -5.461 eV

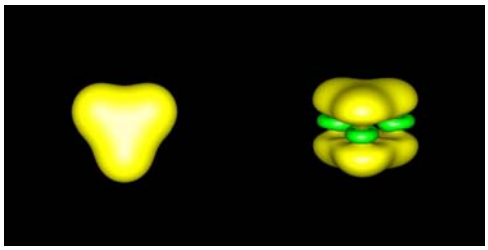

6e’ -5.096 eV

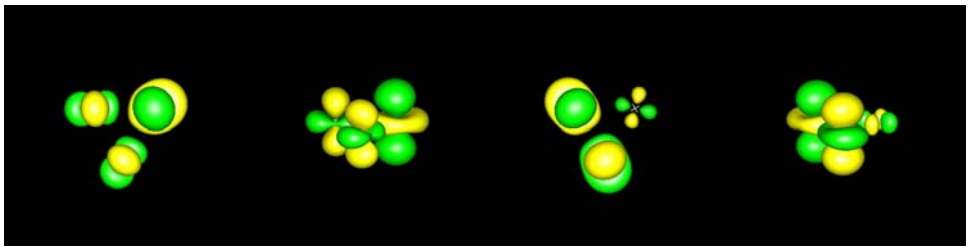

3e’’ -5.067 eV

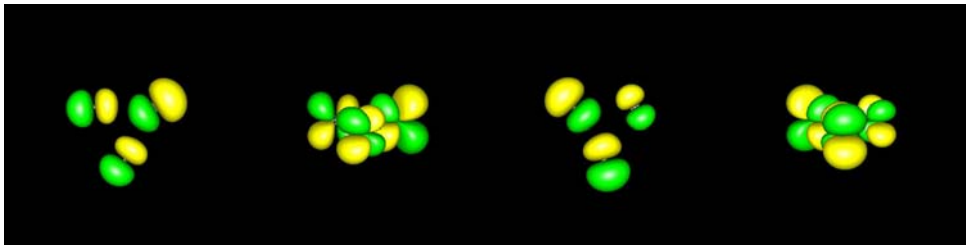

HOMO: 1a1’’ -5.066 eV

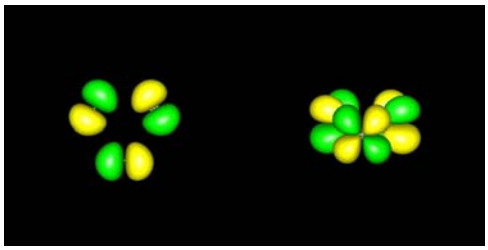

LUMO: 2a2’ -4.961 eV

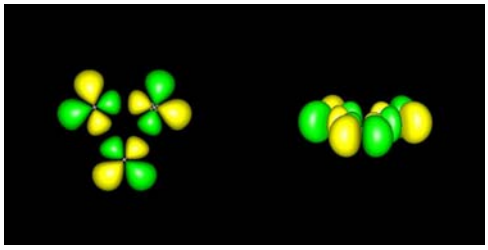

7e’ -2.784 eV

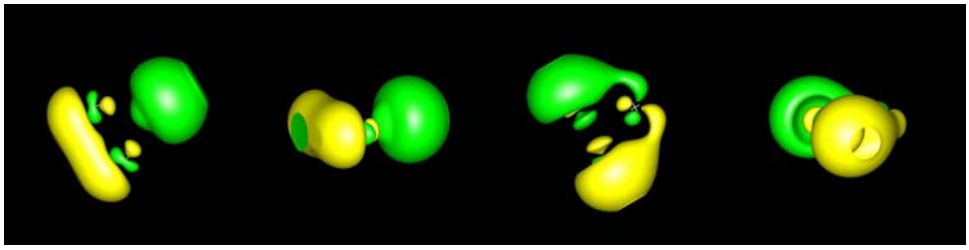

3a2'' -1.383 eV

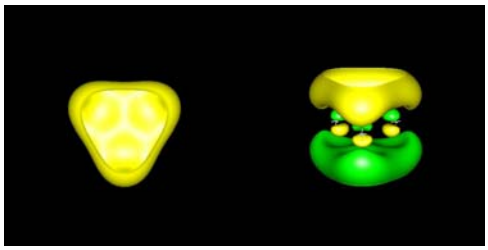

6a1' -0.240 eV

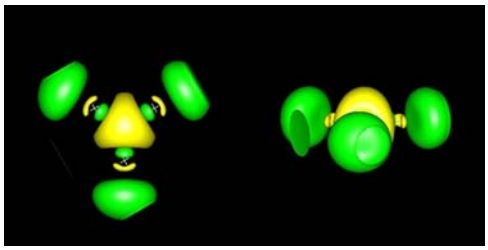

8e' +0.046 eV

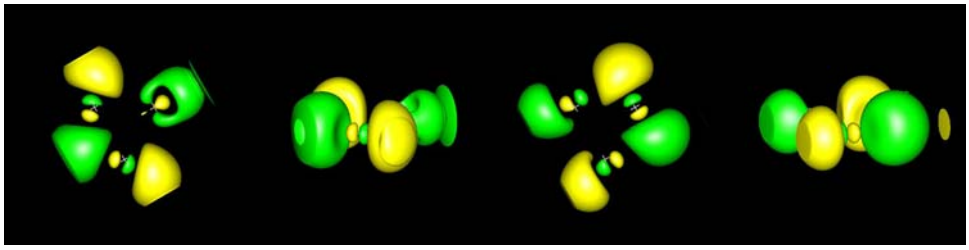

6.2.3.2 Molecular orbitals of $[Sn_8Bi_6]^{4-}$

16a1' -14.398 eV

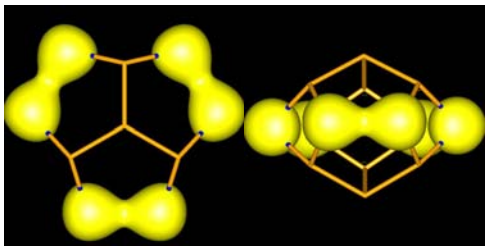

25e' -14.148 eV

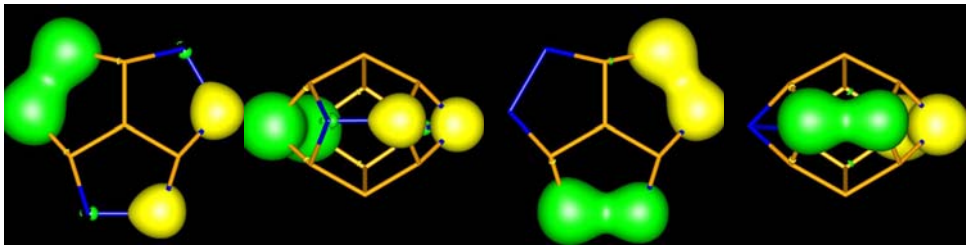

26e’ -13.101 eV

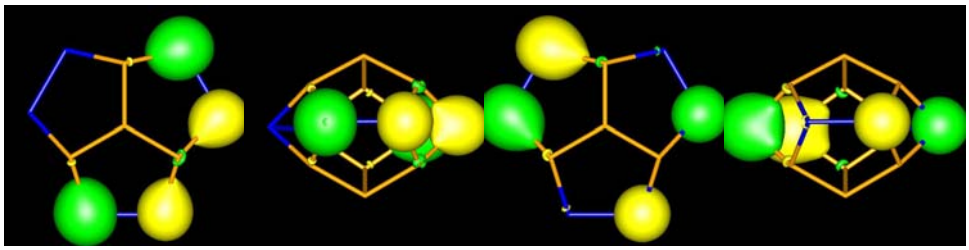

10a2’ -12.667 eV

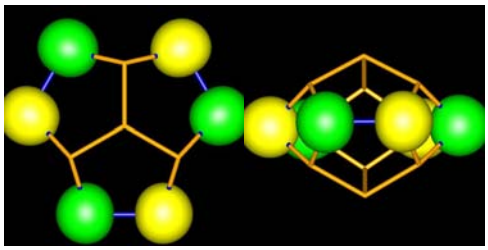

17a1’ -11.120 eV

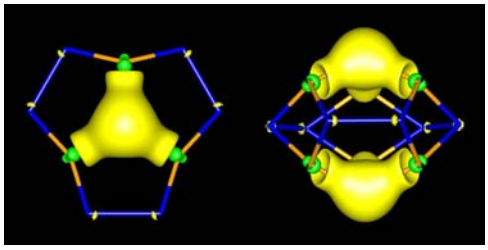

13a2’’ -11.040 eV

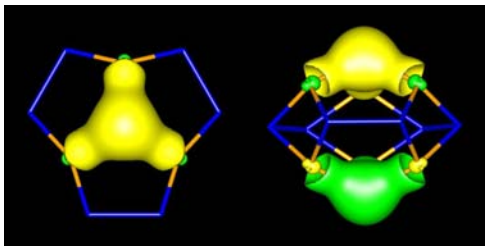

27e’ -9.586 eV

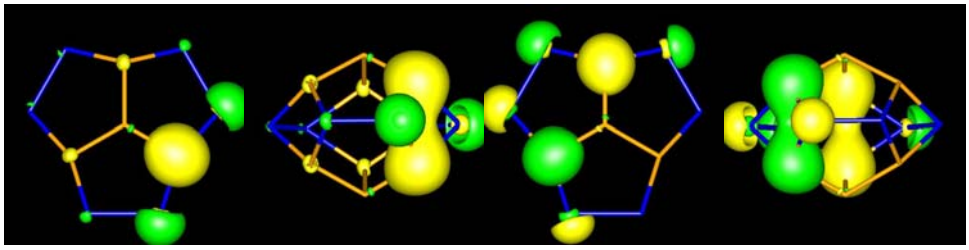

19e’’ -9.413 eV

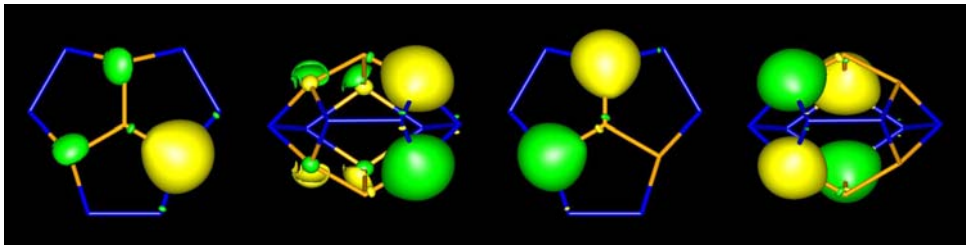

18a1’ -8.603 eV

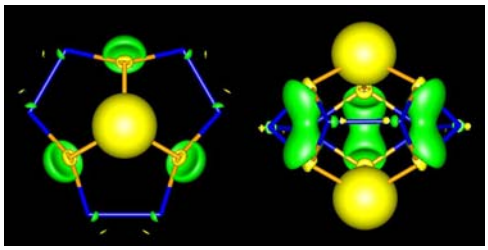

14a2’’ -7.785 eV

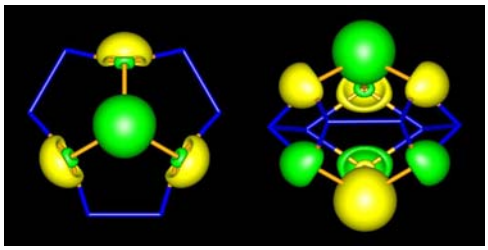

28e’ -5.503 eV

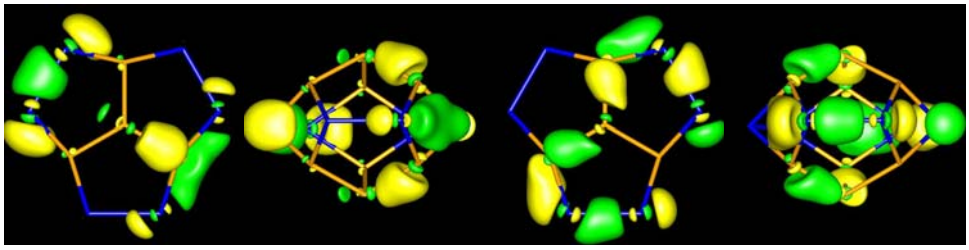

19a1’ -5.462 eV

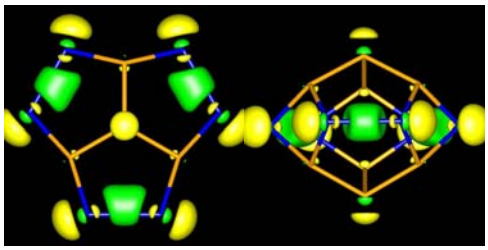

20e’’ -5.341 eV

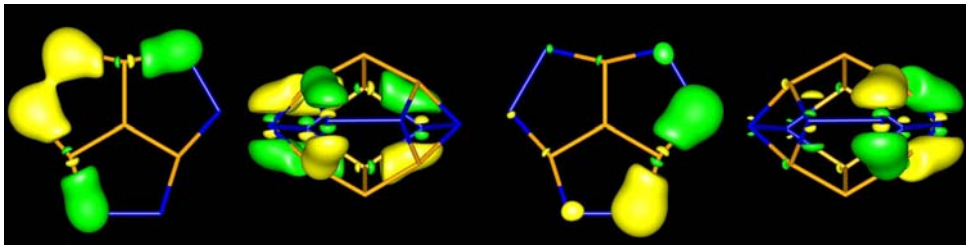

29e’ -5.143 eV

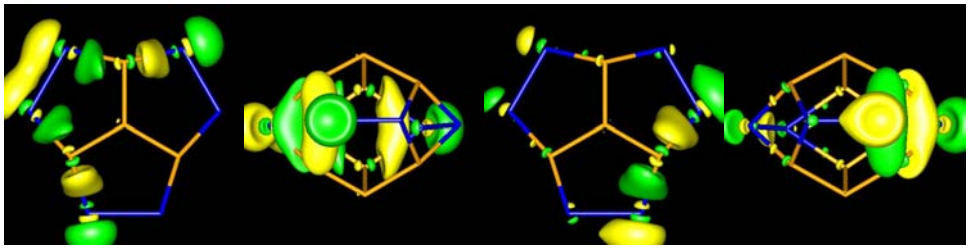

30e’ -4.812 eV

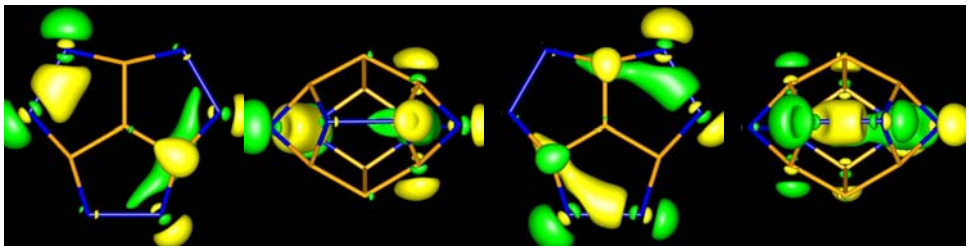

7a1’’ -4.447 eV

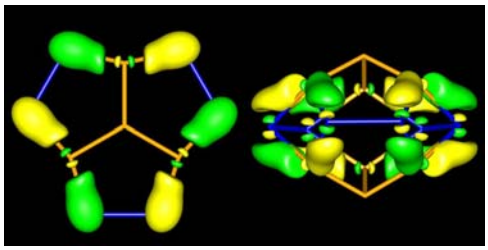

20a1’ -4.375 eV

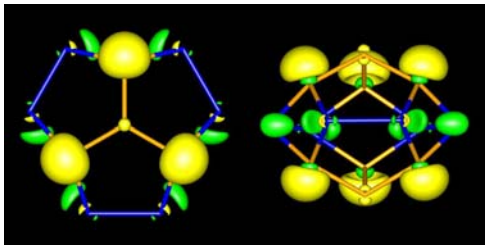

21e’’ -4.163 eV

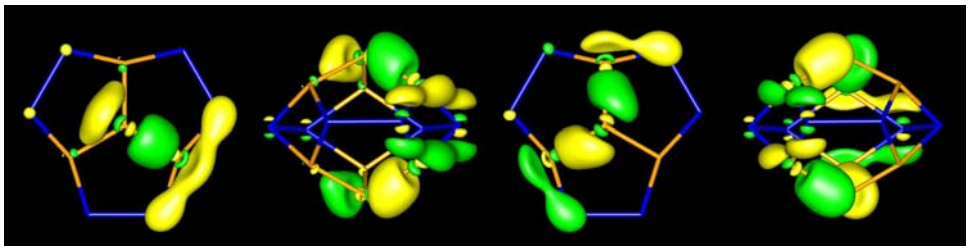

11a2’ -4.163 eV

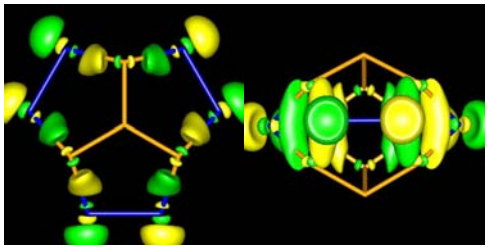

15a2’’ -3.780 eV

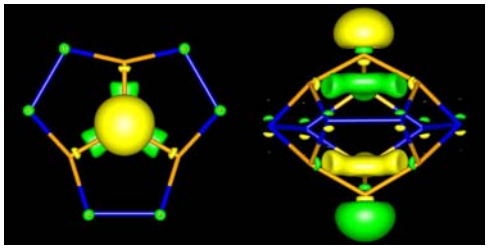

21a1’ -3.520 eV

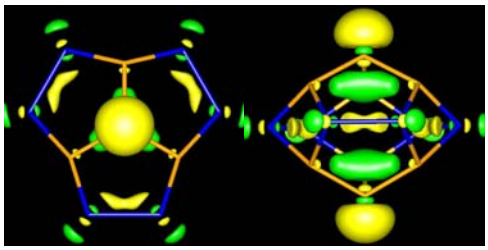

16a2’’ -3.466 eV

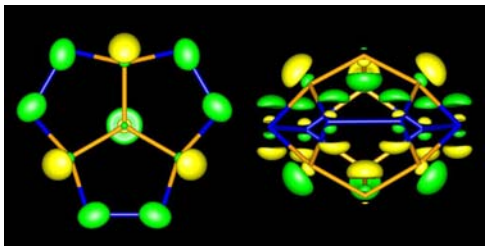

HOMO: 31e’ -3.411 eV

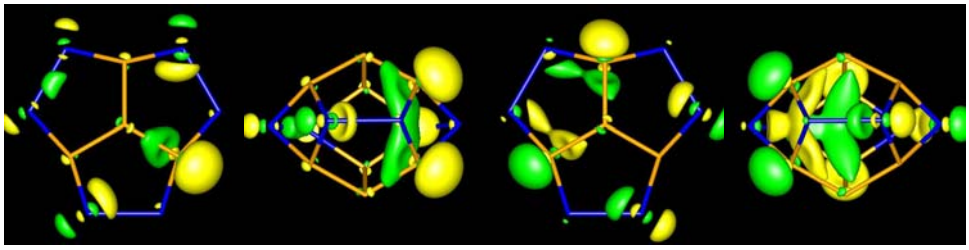

LUMO: 22e’’ -2.081 eV

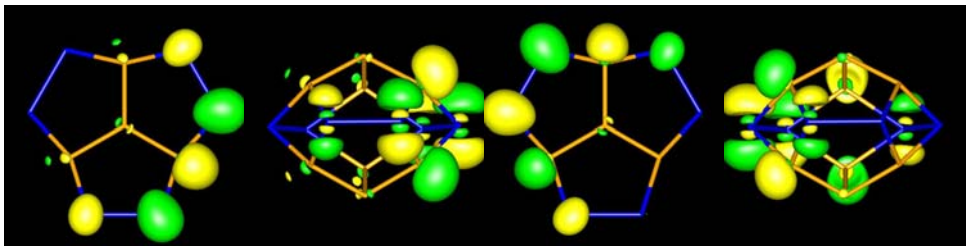

32e’ -1.616 eV

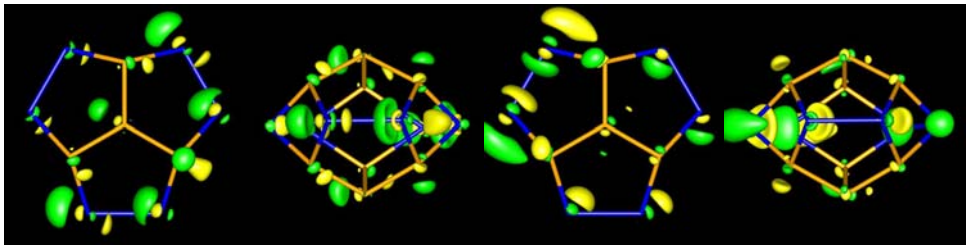

23e’’ -1.423 eV

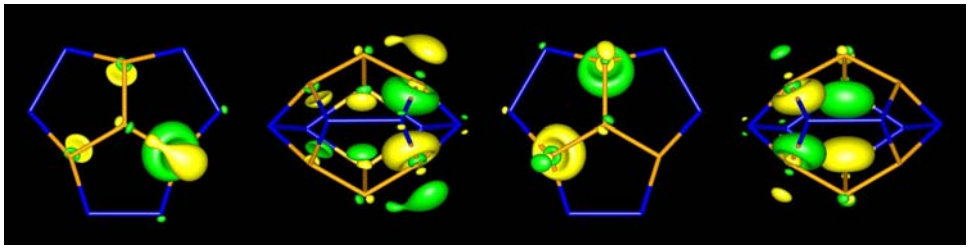

22a1’ -1.387 eV

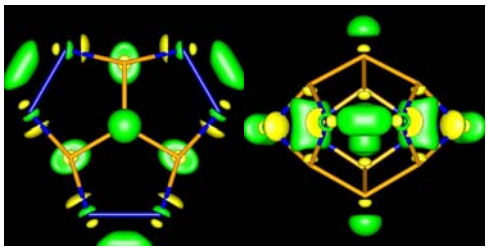

12a2’ -1.226 eV

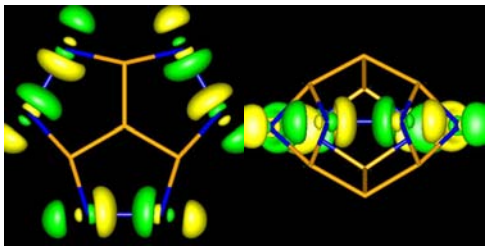

33e’ -1.168 eV

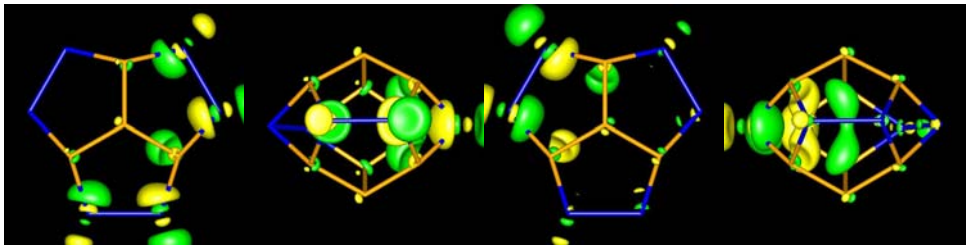

34e’ -0.740 eV

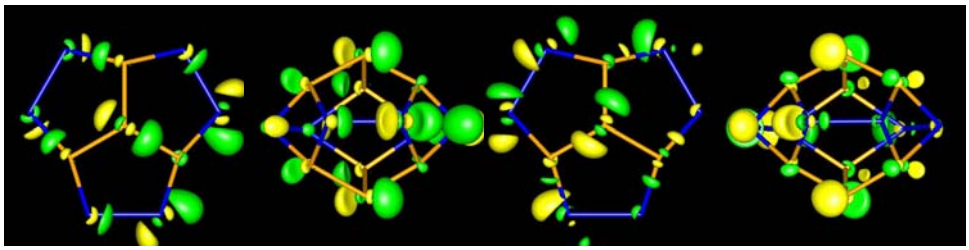

17a2’’ -0.630 eV

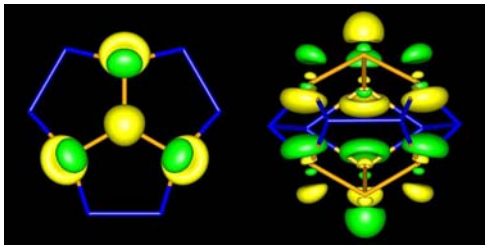

24e’’ -0.536 eV

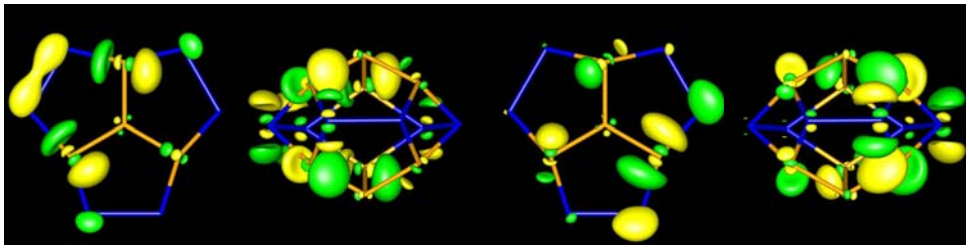

23a1’ -0.242 eV

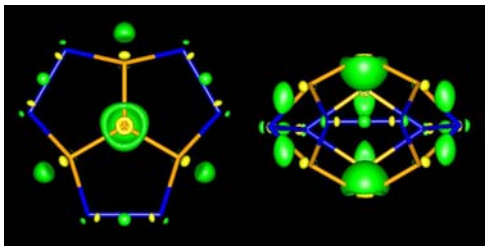

6.2.3.3 Molecular orbitals of $[Pd_3Sn_8Bi_6]^{4-}$

18a1’ -14.371 eV

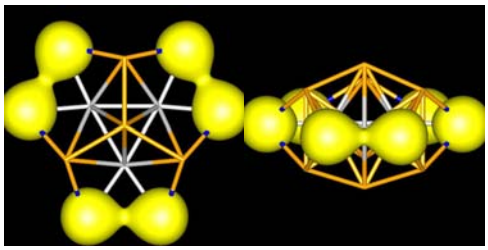

28e’ -14.113 eV

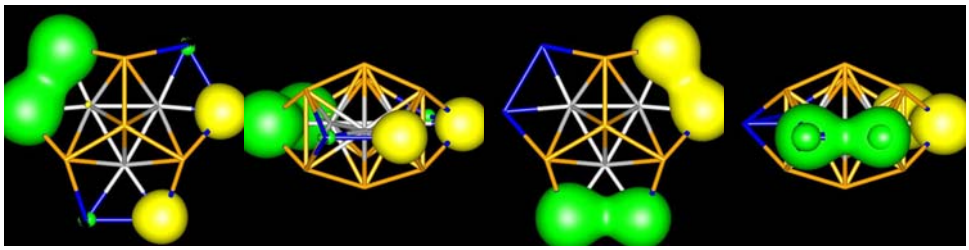

29e’ -13.233 eV

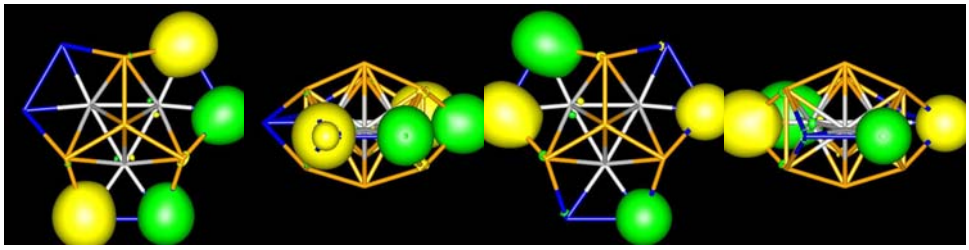

11a2’ -12.919 eV

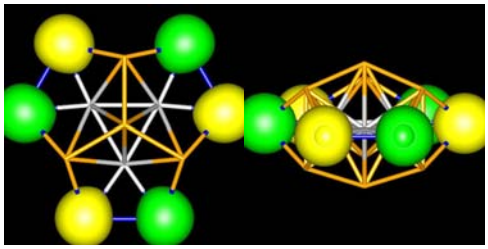

19a1’ -11.663 eV

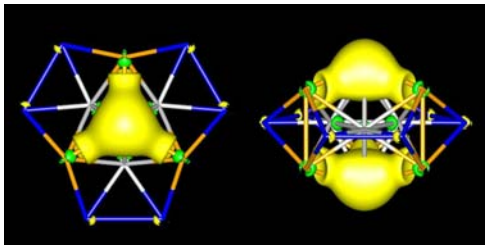

14a2’’ -11.239 eV

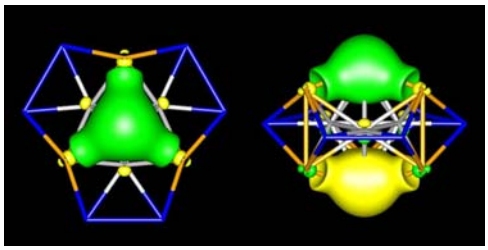

30e’ -10.195 eV

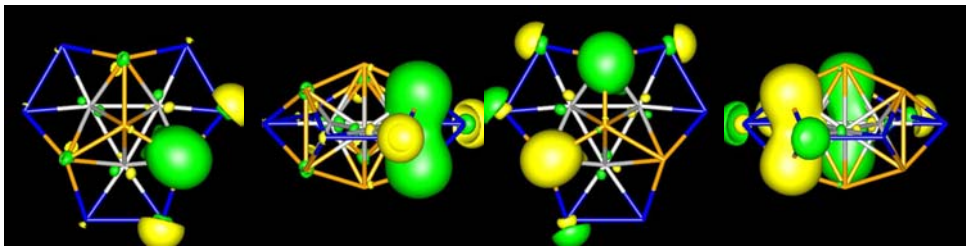

20e’’ -9.747 eV

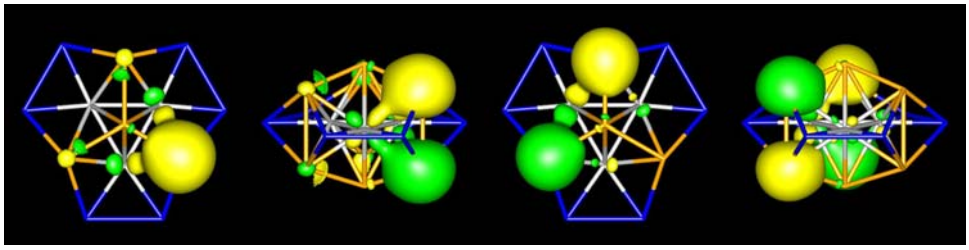

20a1’ -9.177 eV

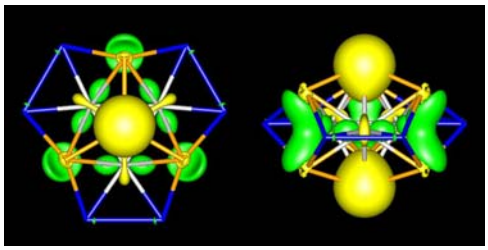

15a2’’ -8.080 eV

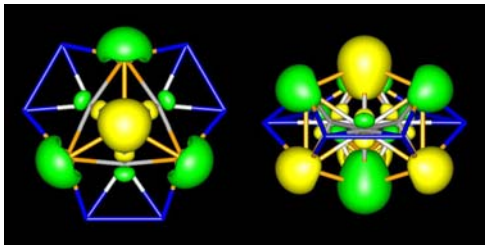

21a1’ -7.027 eV

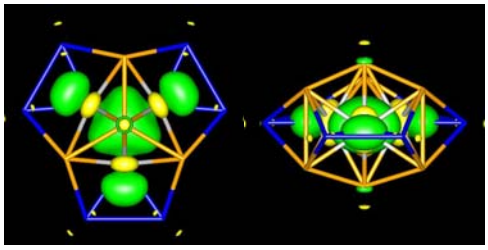

31e’ -6.656 eV

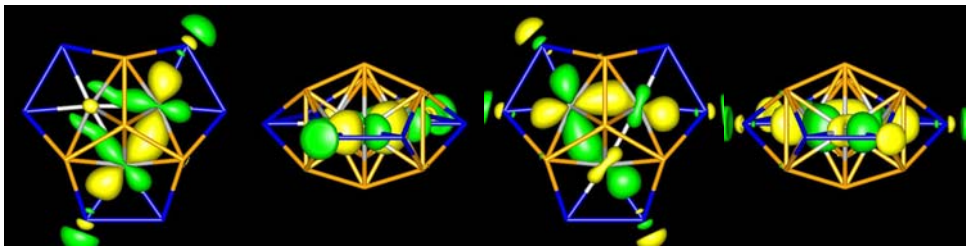

21e’’ -6.170 eV

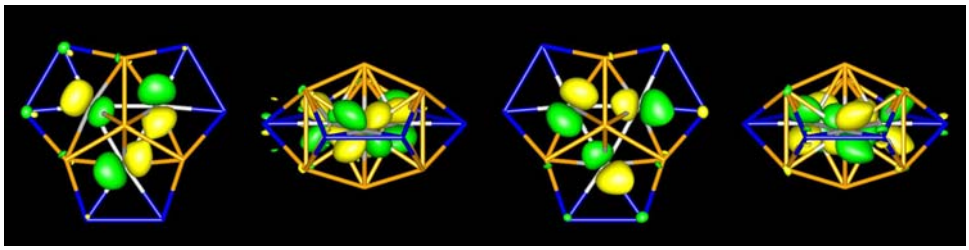

16a2’’ -6.088 eV

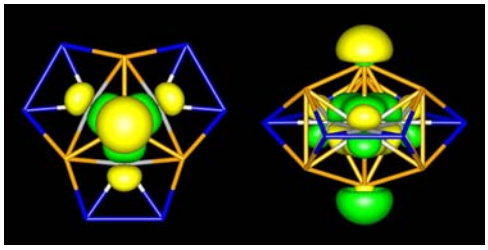

32e’ -6.086 eV

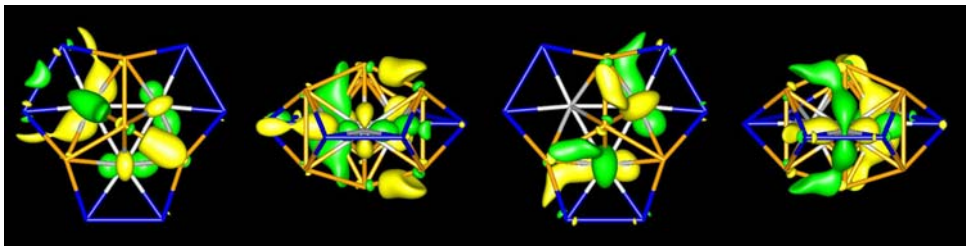

22a1’ -6.069 eV

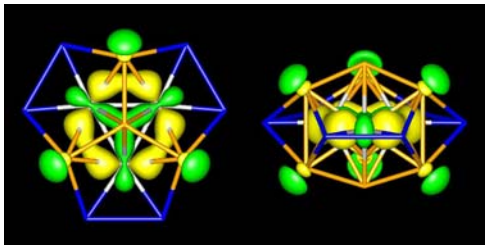

33e’ -5.817 eV

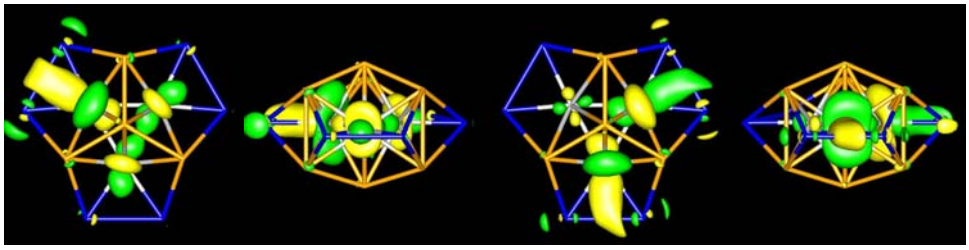

7a1’’ -5.810 eV

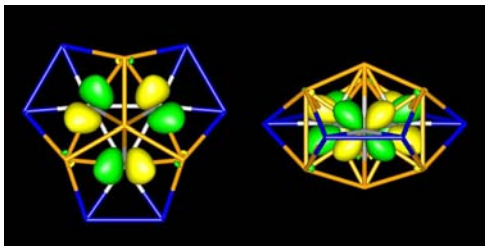

12a2’ -5.662 eV

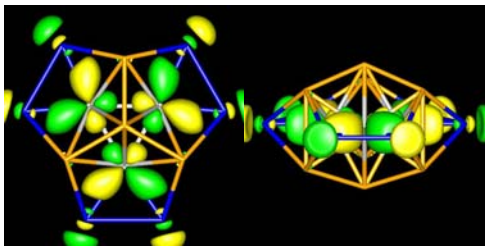

34e’ -5.585 eV

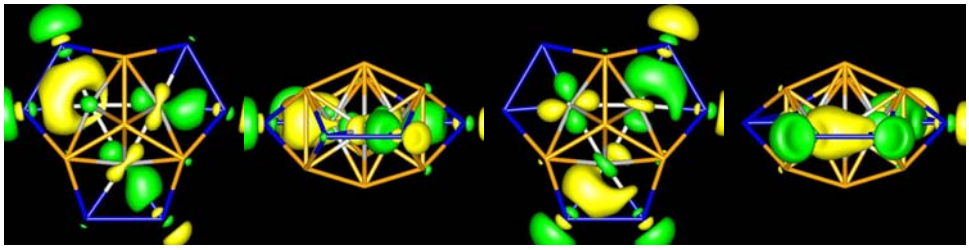

23a1’ -5.347 eV

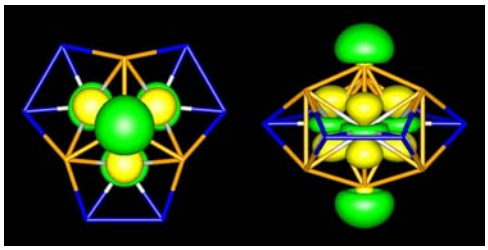

22e’’ -5.319 eV

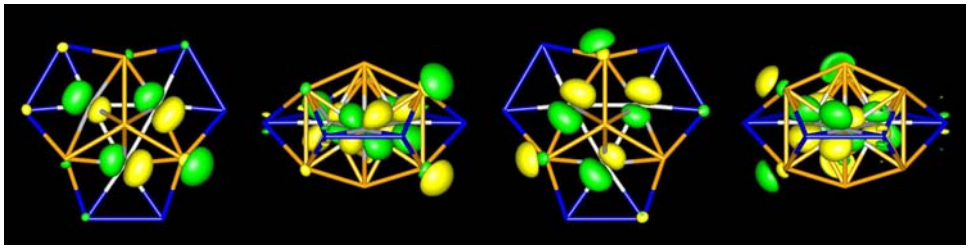

35e’ -4.866 eV

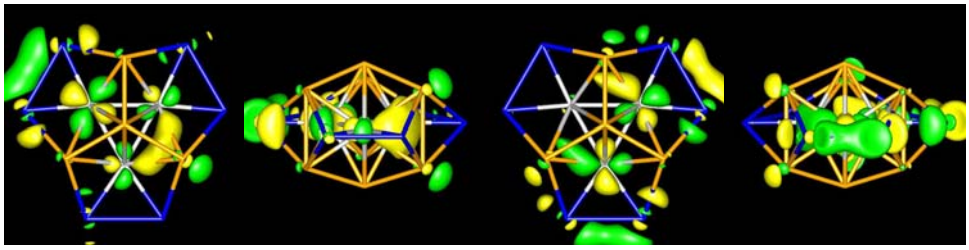

24a1’ -4.824 eV

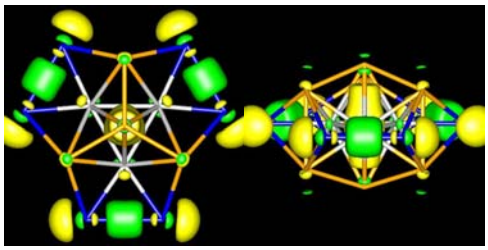

23e’’ -4.768 eV

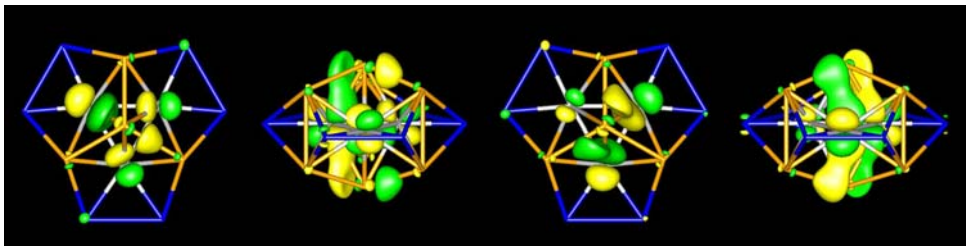

36e’ -4.419 eV

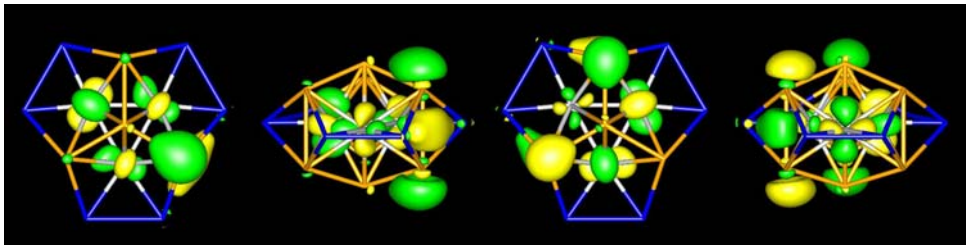

8a1’’ -3.854 eV

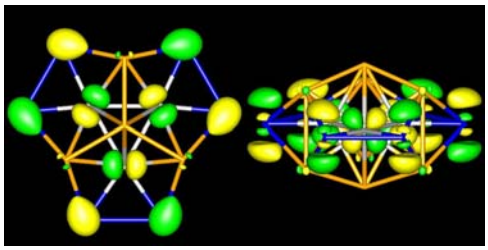

24e’’ -3.849 eV

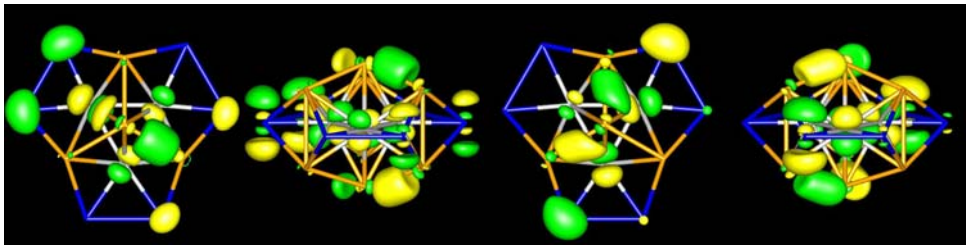

17a2’’ -3.818 eV

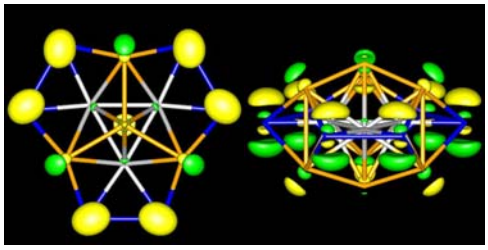

25a1’ -3.783 eV

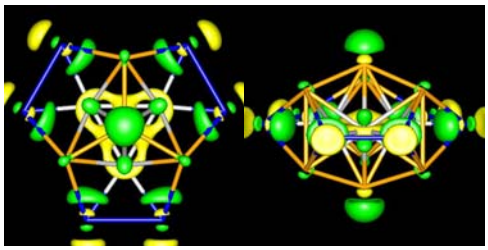

37e’ -3.585 eV

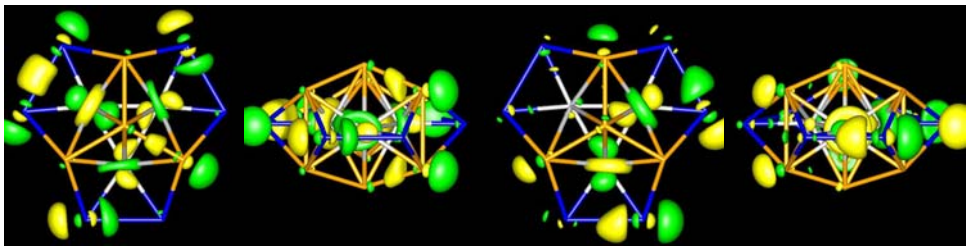

13a2’ -3.551 eV

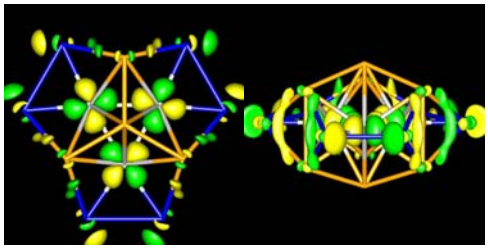

HOMO: 18a2’’ -3.221 eV

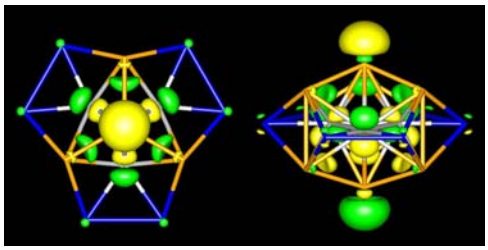

LUMO: 25e’’ -2.378 eV

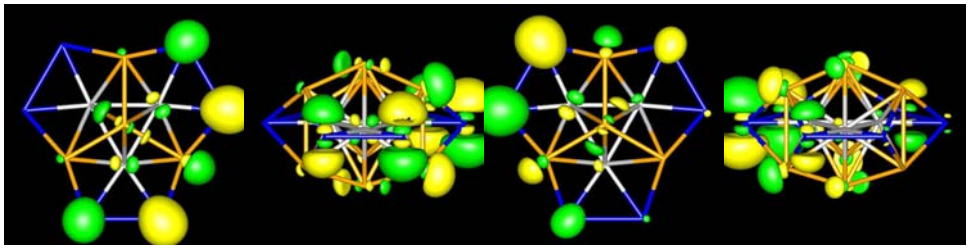

26a1’ -1.570 eV

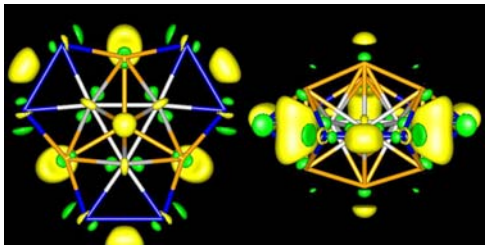

38e’ -1.467 eV

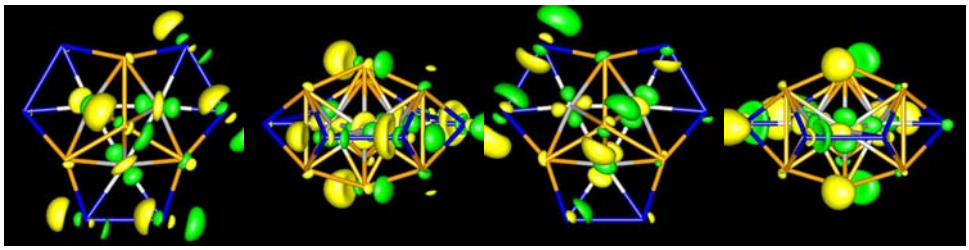

14a2’ -1.348 eV

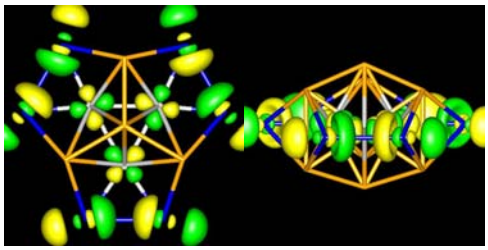

39e’ -1.092 eV

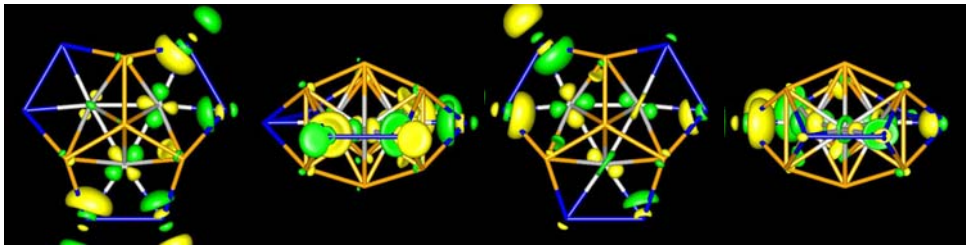

26e’’ -1.079 eV

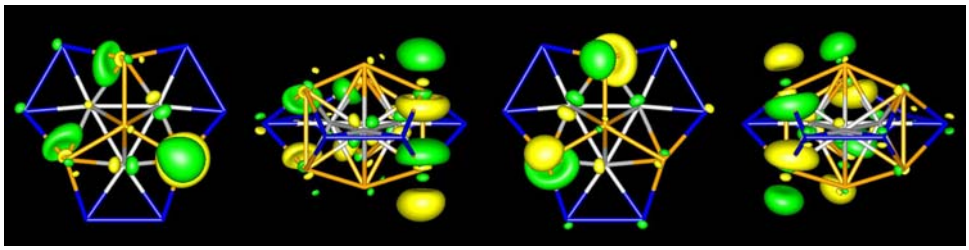

40e’ -0.989 eV

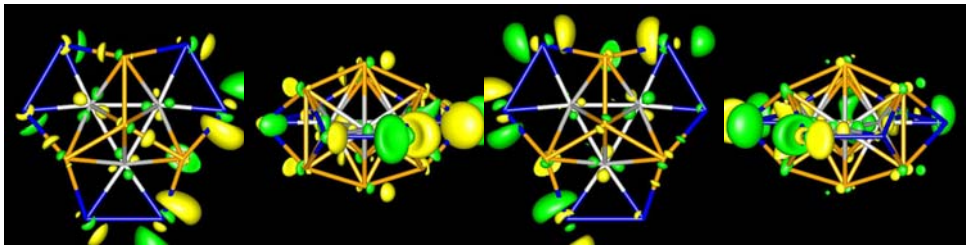

27e’’ -0.664 eV

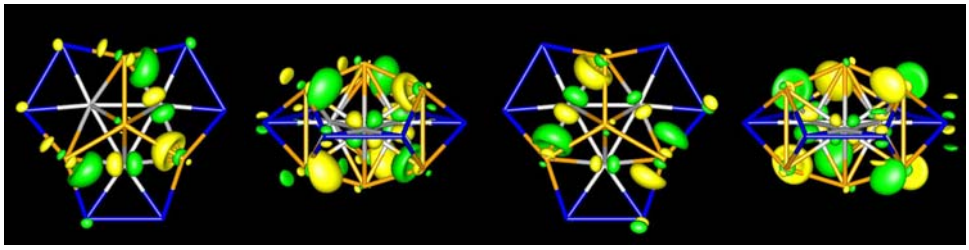

19a2’’ -0.652 eV

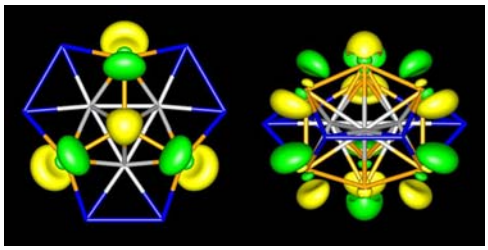

27a1’ -0.346 eV

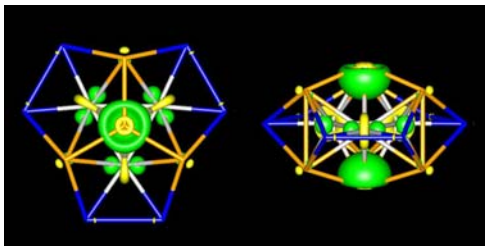

20a2’’ -0.182 eV

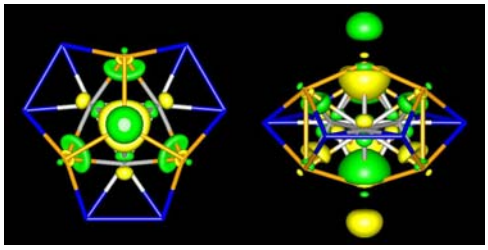

15a2’ -0.173 eV

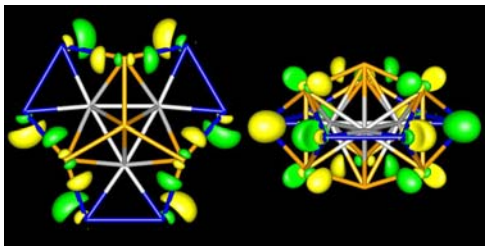

28a1’ -0.091 eV

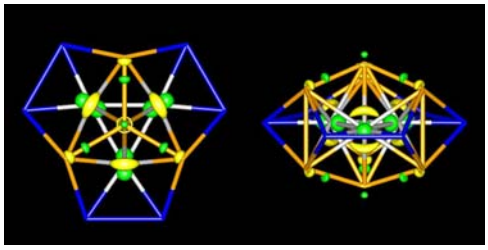

Figure S11. Molecular orbitals of fragments $[Pd_3]$, $[Sn_8Bi_6]^{4-}$, and the cluster anion $[Pd_3Sn_8Bi_6]^{4-}$, according to Mulliken population analysis [20]. For these analyses, the most stable **Isomer 1** has been considered.

6.2.3.4. Fragments of the molecular orbital (MO) schemes for an isolated $[Pd_3]$ cluster (left), and empty $[Sn_8Bi_6]^{4-}$ anion (right), and the $[Pd_3Sn_8Bi_6]^{4-}$ anion

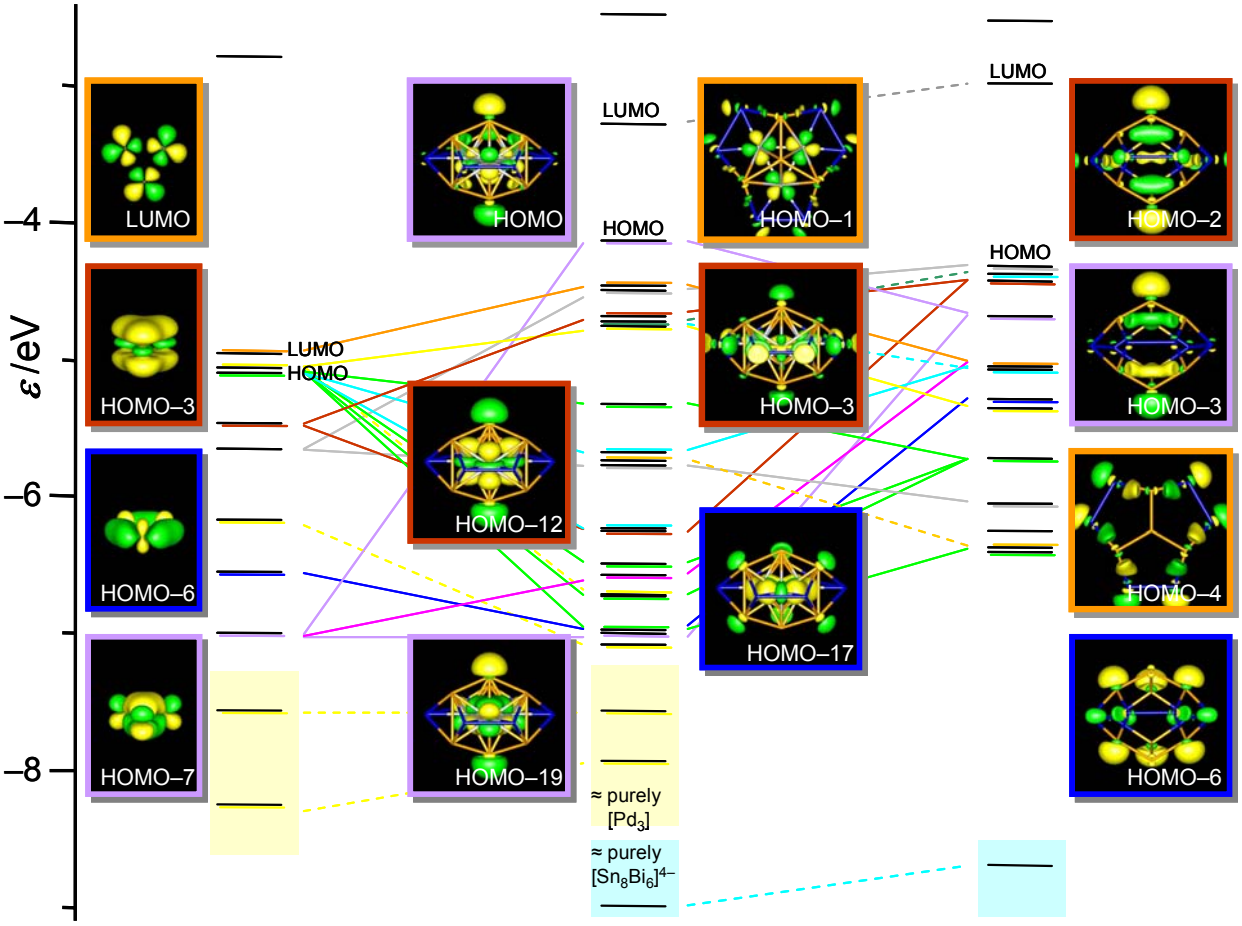

Figure S12. Fragments of the molecular orbital (MO) schemes for an isolated $[Pd_3]$ cluster (left), and empty $[Sn_8Bi_6]^{4-}$ anion (right), and the $[Pd_3Sn_8Bi_6]^{4-}$ anion (center), according to DFT calculations. Combinations of MOs are highlighted by colored lines; dashed lines denote MOs that derive from only one of the fragments. Note that the energies of the charged species have been shifted by about –0.9 eV relative to the energies of the neutral compound in order to adjust the energies of the non-bonding $[Pd_3]$ MOs. The effect that charge compensation using the Cosmo model leads to an energy shift is well-known [22]. The drawn MOs represent examples for s-d-type (blue), d-s-type (red; bonding and anti-bonding MO shown) and p-f-type (violet; bonding and anti-bonding MO shown) cluster orbitals. Not listed MOs of the cluster anion and the empty shell below –9 eV represent combinations of s-type valence orbitals of the main groups atoms that are identical for both the fragment and the ternary cluster anion. Amplitudes are drawn to ±0.03 a.u..

6.2.4. Inspection of the interaction of the Pd_3 triangle with the main group cage $[Sn_8Bi_6]$ by comparison of localized molecular orbitals (LMOs)

The bonding situation was further studied by generation of localized molecular orbitals (LMOs), generated according to the technique developed by Boys [23, 24]. LMOs have been generated for the most stable **Isomer 1** of the anion in **1** and the fragments: $[Pd_3]$ and $[Sn_8Bi_6]^{4-}$ as well as for $[Pd_3]^{2-}$ and $[Sn_8Bi_6]^{2-}$. Vibrational modes were calculated using the program numforce implemented in Turbomole. Even in its lowest energy electronic configuration, $[Sn_8Bi_6]^{2-}$ possesses three imaginary modes. The comparison of LMOs of the fragments for the two models in question, $[Pd_3] + [Sn_8Bi_6]^{4-}$ or $[Pd_3]^{2-} + [Sn_8Bi_6]^{2-}$, with those of $[Pd_3Sn_8Bi_6]^{4-}$ direct toward a "hybrid" situation. Both pairs of fragments possess LMOs that are characteristic of the ternary anion, but at the same time, neither of them shows an exact agreement. However, structural changes within the fragments upon geometry optimization definitely contribute the observed differences. Selected LMOs are shown in the following subchapters, plotted by means of the program gOpenMol [21]. Amplitudes are drawn to ±0.03 a.u..

6.2.4.1 Localized molecular orbitals for $[Pd_3Sn_8Bi_6]^{4-}$

LMO-118 LMO-117 LMO-116 LMO-115 LMO-114 LMO-113

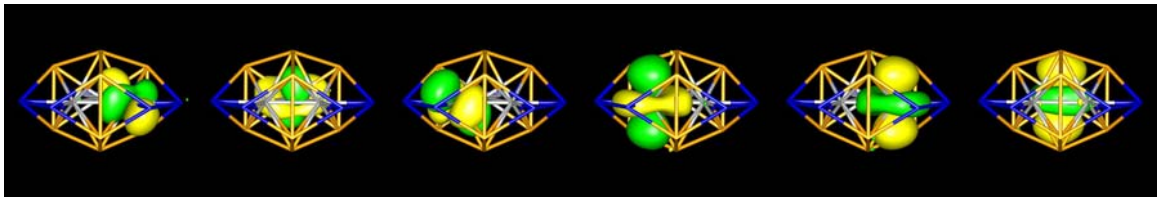

LMO-112 LMO-111 LMO-110 LMO-109 LMO-108 LMO-107

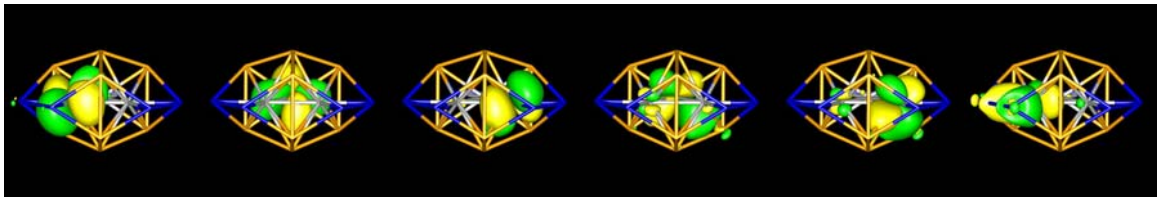

LMO-106 LMO-105 LMO-104 LMO-103 LMO-102 LMO-101

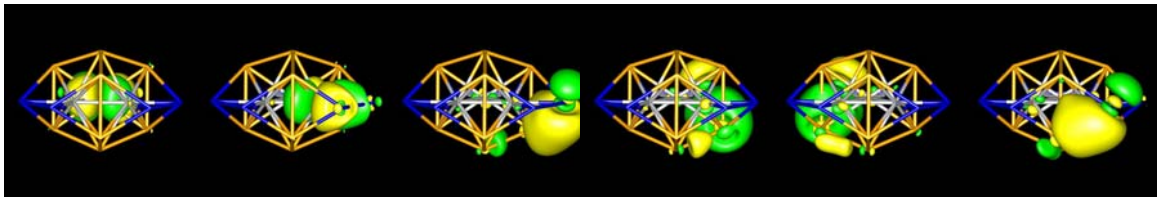

LMO-99 LMO-98 LMO-97 LMO-96 LMO-95 LMO-94

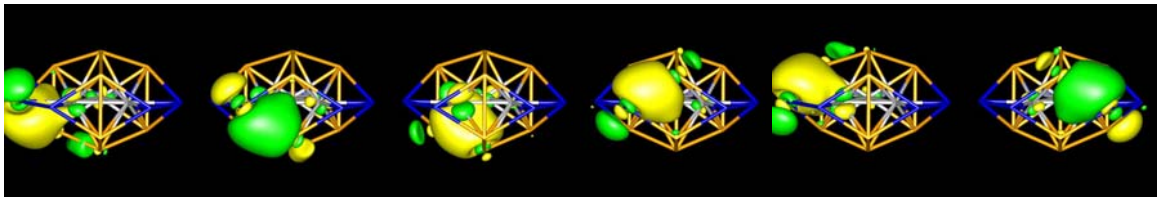

LMO-93 LMO-92 LMO-91 LMO-90 LMO-89 LMO-88

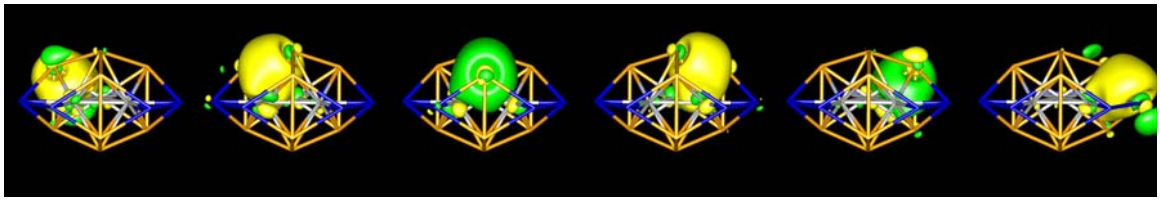

LMO-87 LMO-86 LMO-85 LMO-84 LMO-83 LMO-82

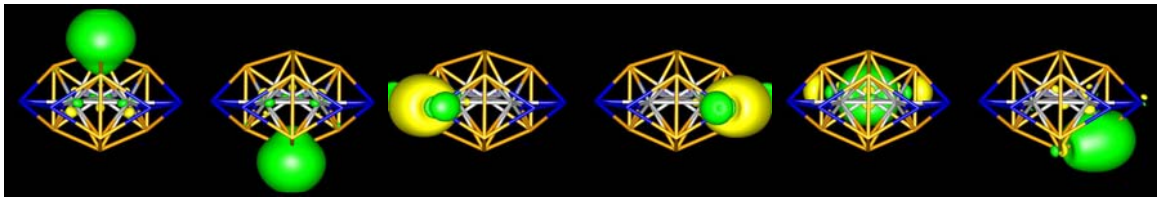

LMO-81 LMO-80 LMO-79 LMO-78 LMO-77 LMO-76

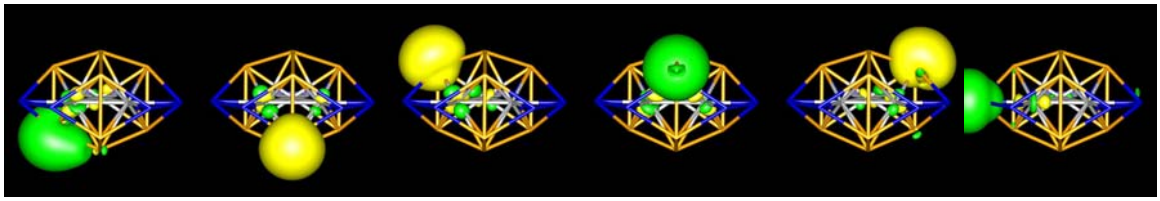

LMO-75 LMO-74 LMO-73 LMO-72 LMO-71

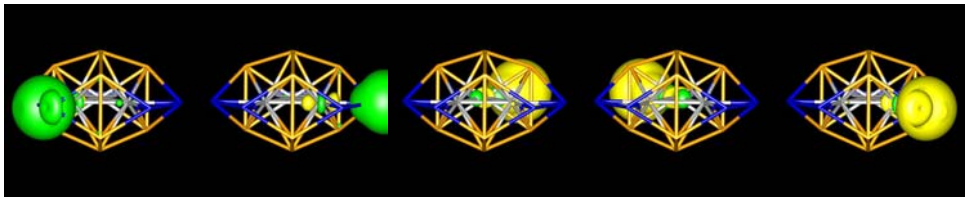

Further LMOs comprise non-bonding d-AOs at Sn (LMO-70 – LMO-31) and d-AOs at Bi (LMO-30 – LMO-1).

6.2.4.2 Localized molecular orbitals for [Pd_3] (top view)

LMO-15 LMO-14 LMO-13 LMO-12 LMO-11 LMO-10

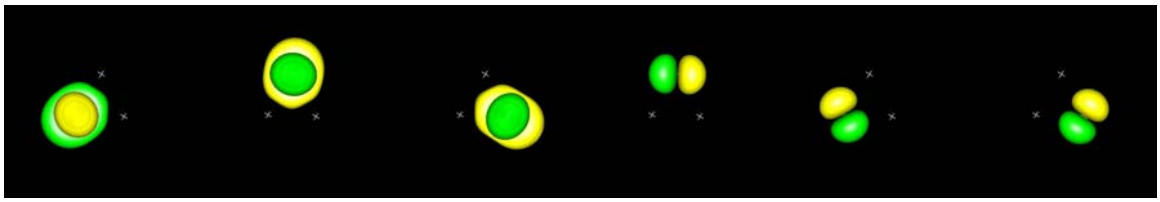

LMO-09 LMO-08 LMO-07 LMO-06 LMO-05 LMO-04

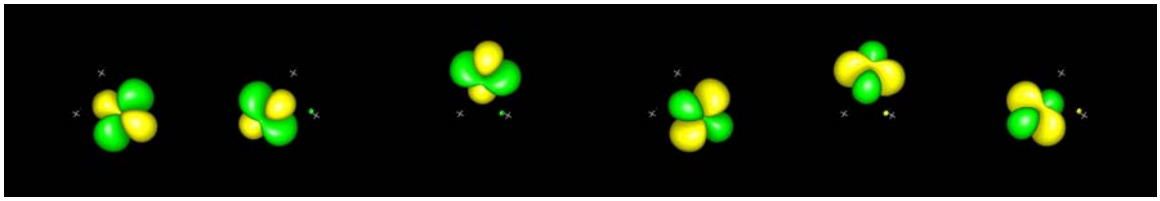

LMO-03 LMO-02 LMO-01

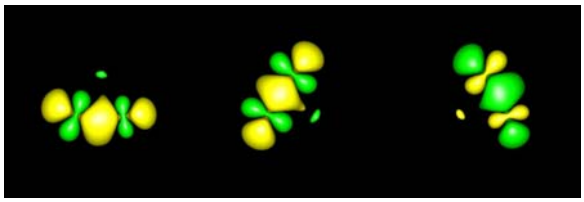

6.2.4.2 Localized molecular orbitals for [Pd_3] (side view)

LMO-15 LMO-14 LMO-13 LMO-12 LMO-11 LMO-10

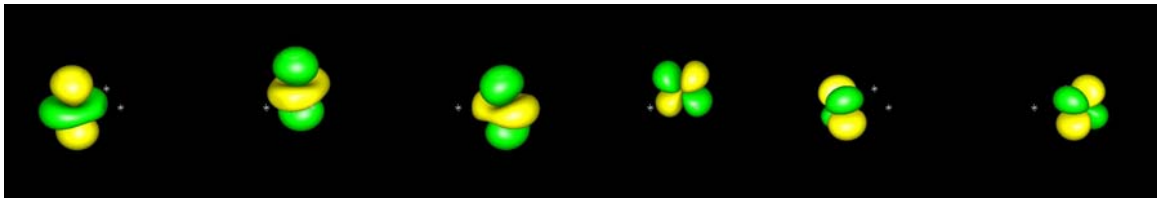

LMO-09 LMO-08 LMO-07 LMO-06 LMO-05 LMO-04

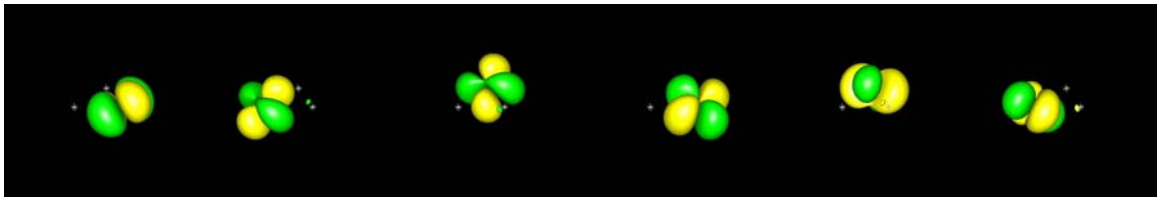

LMO-03 LMO-02 LMO-01

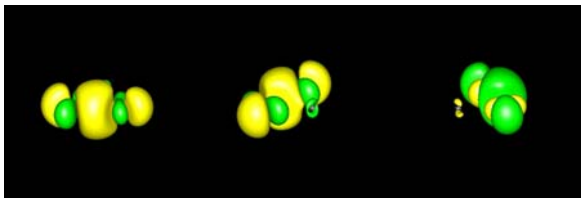

6.2.4.3. Localized molecular orbitals for $[Sn_8Bi_6]^{4-}$

LMO-103 LMO-102 LMO-101 LMO-100 LMO-99 LMO-98

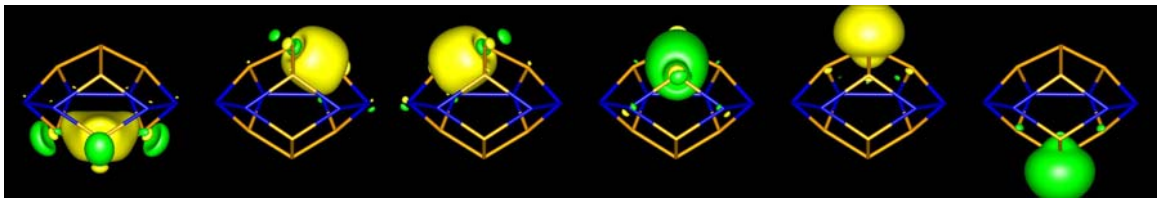

LMO-97 LMO-96 LMO-95 LMO-94 LMO-93 LMO-92

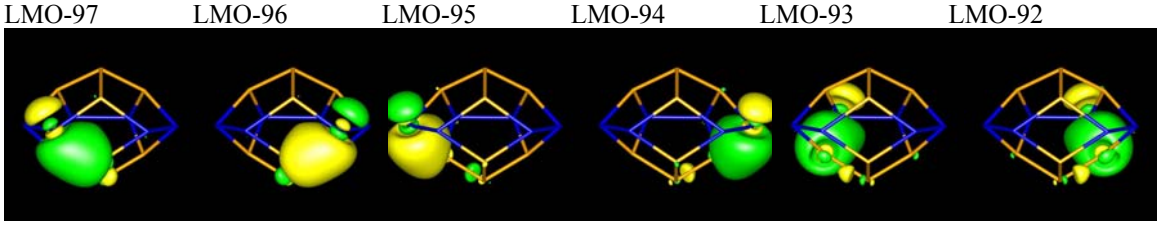

LMO-91 LMO-90 LMO-89 LMO-88 LMO-87 LMO-86

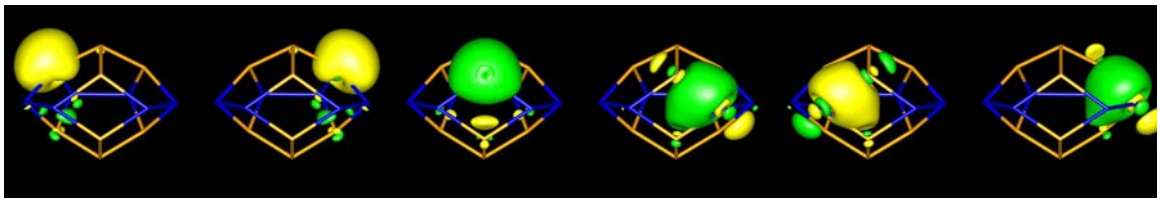

LMO-85 LMO-84 LMO-83 LMO-82 LMO-81 LMO-80

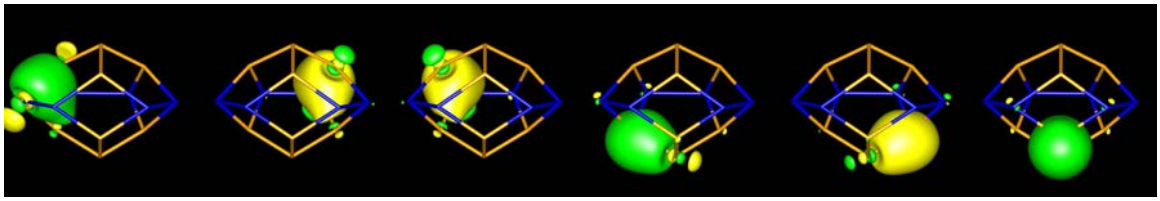

LMO-79 LMO-78 LMO-77 LMO-76 LMO-75 LMO-74

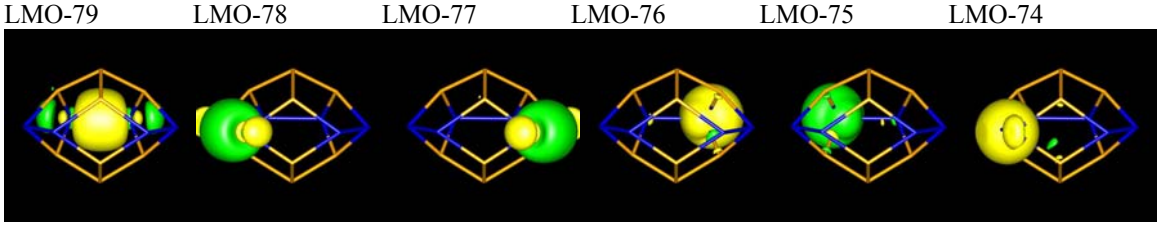

LMO-73 LMO-72 LMO-71

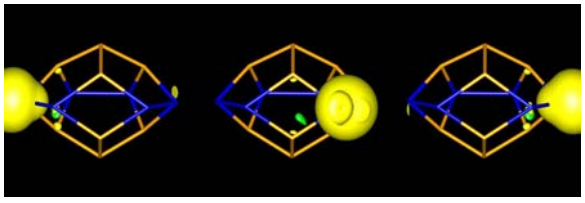

Further LMOs comprise non-bonding d-AOs at Sn (LMO-70 – LMO-31) and d-AOs at Bi (LMO-30 – LMO-1).

6.2.4.4. Localized molecular orbitals for $[Pd_3]^{2-}$ (top view)

LMO-16 LMO-15 LMO-14 LMO-13 LMO-12 LMO-11

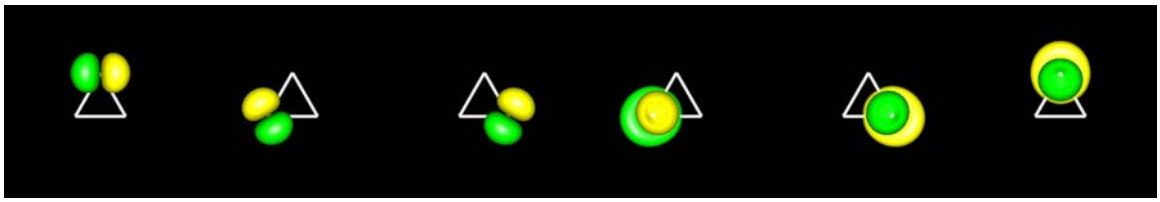

LMO-10 LMO-09 LMO-08 LMO-07 LMO-06 LMO-05

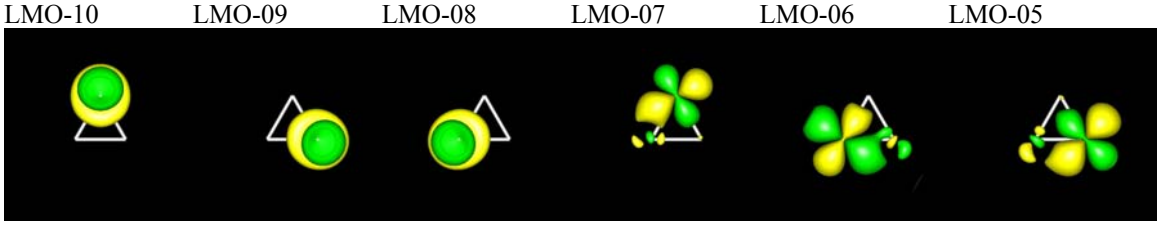

LMO-04 LMO-03 LMO-02 LMO-01

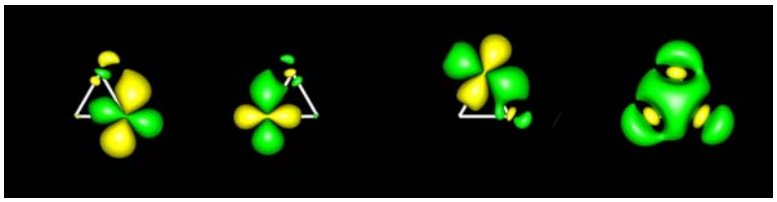

6.2.4.4. Localized molecular orbitals for $[Pd_3]^{2-}$ (side view)

LMO-16 LMO-15 LMO-14 LMO-13 LMO-12 LMO-11

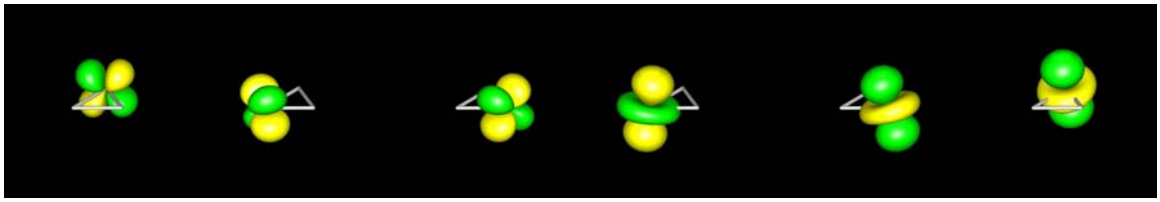

LMO-10 LMO-09 LMO-08 LMO-07 LMO-06 LMO-05

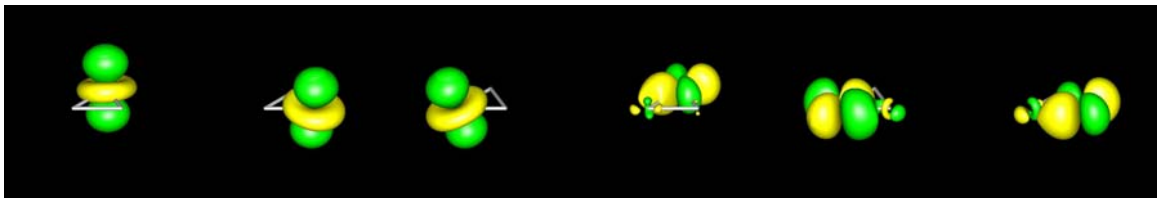

LMO-04 LMO-03 LMO-02 LMO-01

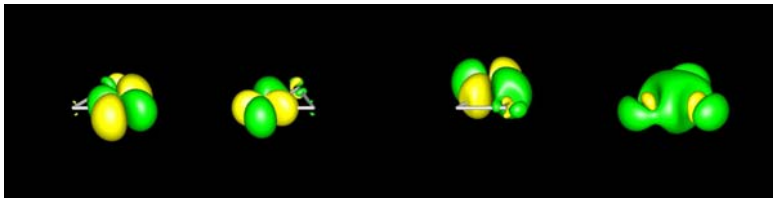

6.2.4.5 Localized molecular orbitals for $[Sn_8Bi_6]^{2-}$

LMO-102 LMO-101 LMO-100 LMO-99 LMO-98 LMO-97

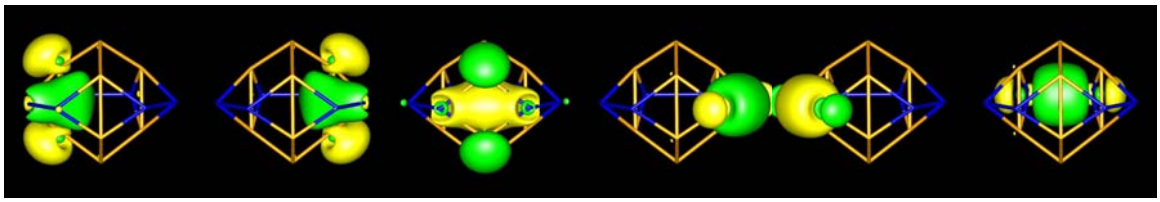

LMO-96 LMO-95 LMO-94 LMO-93 LMO-92 LMO-91

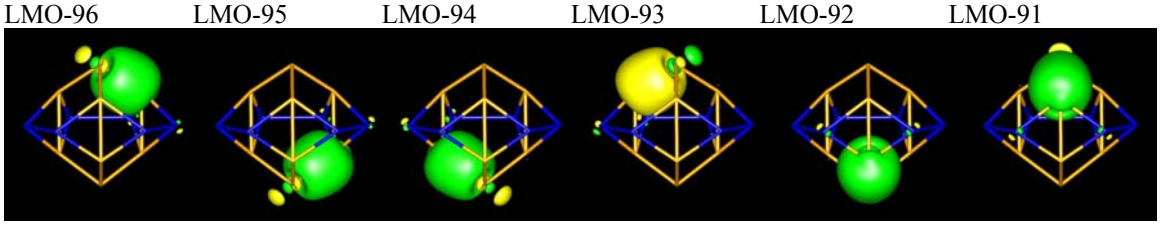

LMO-90 LMO-89 LMO-88 LMO-87 LMO-86 LMO-85

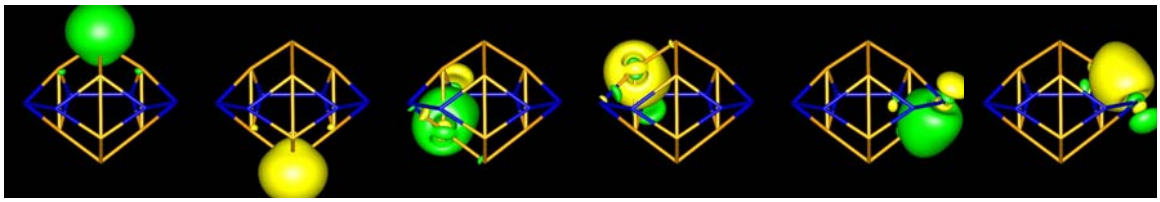

LMO-84 LMO-83 LMO-82 LMO-81 LMO-80 LMO-79

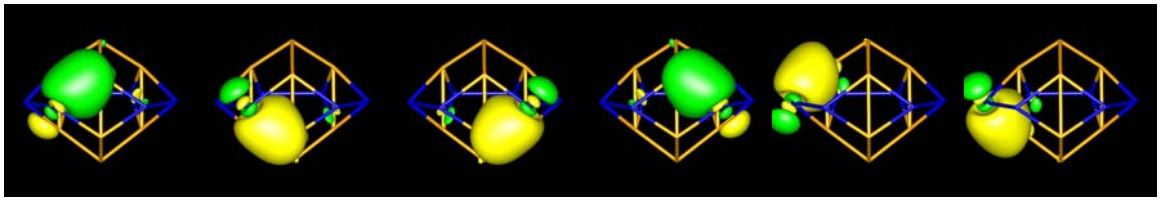

LMO-78 LMO-77 LMO-76 LMO-75 LMO-74 LMO-73

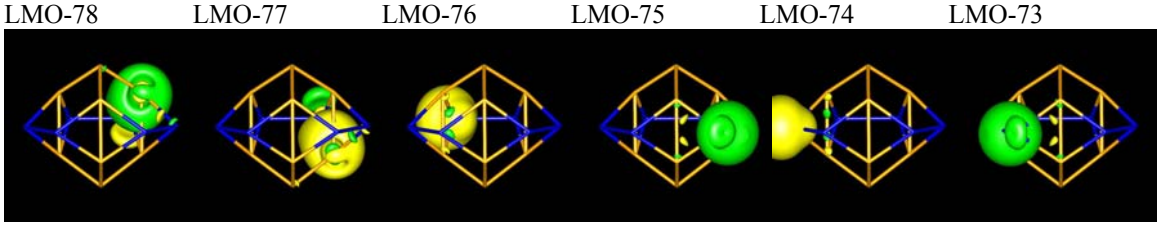

LMO-72 LMO-71

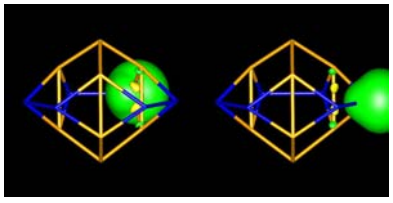

Further LMOs comprise non-bonding d-AOs at Sn (LMO-70 – LMO-31) and d-AOs at Bi (LMO-30 – LMO-1).

Figure S13. Localized molecular orbitals (LMOs) of the cluster anion $[Pd_3Sn_8Bi_6]^{4-}$ and its hypothetical fragments $[Pd_3]$, $[Sn_8Bi_6]^{4-}$, $[Pd_3]^{2-}$ and $[Pd_3Sn_8Bi_6]^{2-}$ according to the analysis of Boys [23, 24]. For the calculations, the most stable **Isomer 1** has been considered.

7 Investigations on the formation of compound 1

7.1 H_2 detection

After the common reaction time of three hours, the reaction solution was analyzed at the Max-Planck-Institute for Terrestrical Microbiology by means of gas chromatography, with a HgO-to-Hg conversion detector (280°C, RGD2; Trace Analytical) after separation at 85°C on Molecular Sieve 5 Å (2m length, 3.2 mm diameter) with synthetic air (80% N_2, 20% O_2) at 10 mL min^{-1} as carrier gas. The gas chromatograph was calibrated with standard gases (Messer Griesheim). For providing identical conditions as described for the formation of **1** in the experimental part of the contribution, the reaction was performed in a glove box before a sample was withdrawn for the analysis. The latter clearly indicated the formation of H_2, as shown in Figure S14. We assume the H_2 to stem from 1,2-diaminoethane (*en*) rather than from 1,2-bis(diphenylphosphino)ethane (dppe), as further outlined below.

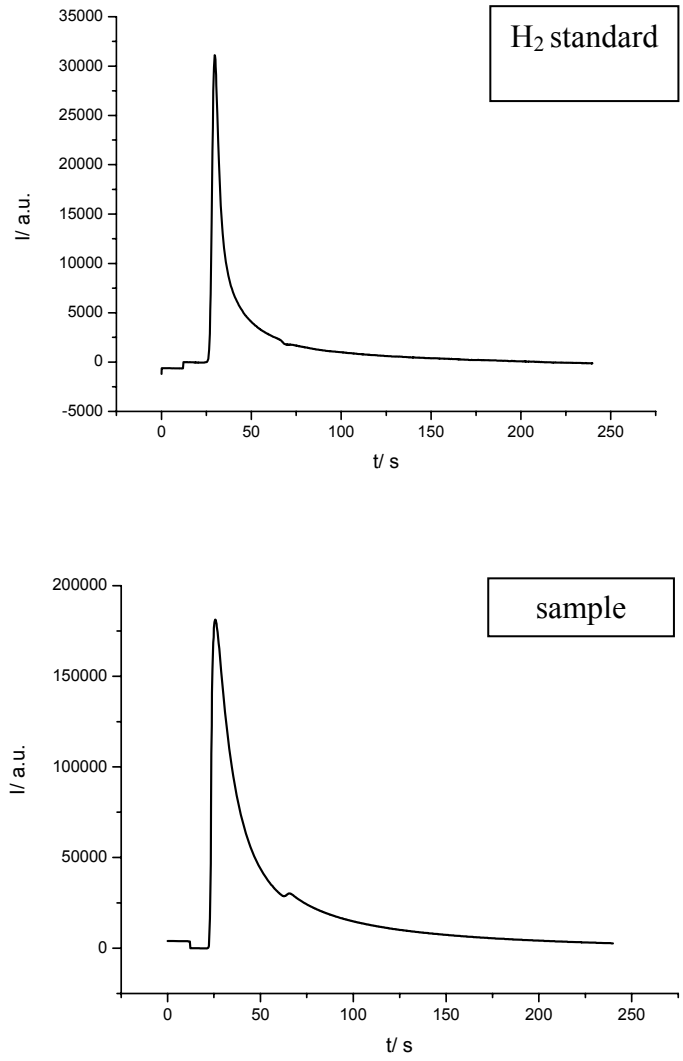

Figure S14. Result of the H_2 detection study, the response for the H_2 standard (top) and the response for the gas volume taken from the reaction mixture (bottom).

7.2 ESI-MS measurement of the reaction solution

ESI-MS measurements of the reaction solution were extended to the mass region 200 to 500 m /z. The according ESI spectrum (Figure S15) shows the presence of $[Bi_2]^-$ units at m/z = 417.9919.

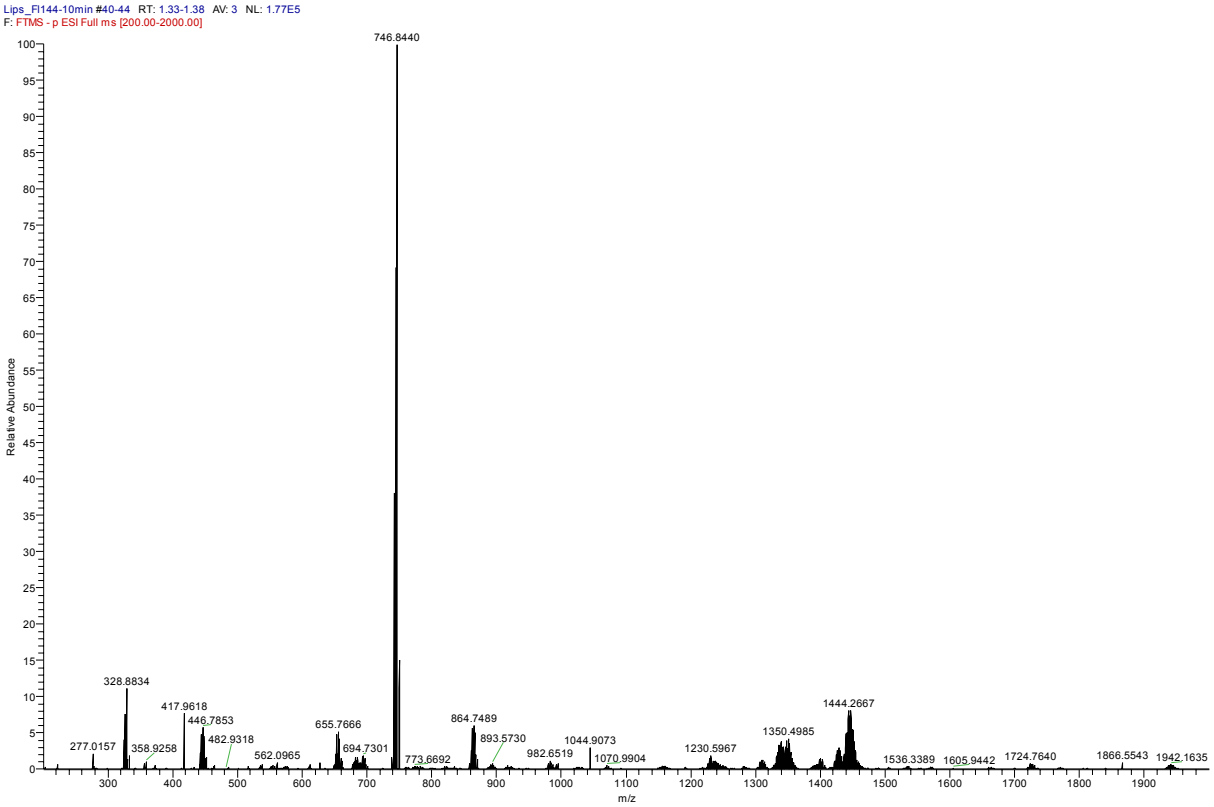

Figure S15. ESI mass spectrum of the precursor solution upon addition of $Pd(dppe)_2$ indicating the presence of $[Bi_2]^-$ units at m/z = 417.9919 (calculated: 417.96078).

7.3 NMR studies of the reaction solution

In order to investigate whether reduced species of dppe are detectable and/or whether dppe releases H_2 (see 7.1), ^{31}P-NMR spectra were recorded (a) after the common reaction time of three hours and (b) after the reaction solutions were allowed to stand for several weeks. The ^{31}P-NMR spectra that were recorded shortly after the combination of the reactants indicate the presence of free dppe ligands at (−12.4 ppm), demonstrating that the reaction has taken place, beside the $Pd(dppe)_2$ complex (31.1 ppm); however none of these spectra shows the formation of any further P containing species (see Figure S16, top). We take this as a clear hint that H_2 decends from *en* as the most acidic species.

After several weeks, one detects another signal at −3.4 ppm that can be assigned to $(Ph_2P)^-$ and a third one at 78.9 ppm which we cannot assign unambiguously to any known phosphorous species (see Figure S16, bottom). We assume that these P-containing species result from ongoing fragmentation of the phosphine under the reductive conditions in solution, but do not seem to play a role in the formation of the title compound. At no time, there is any indication for the formation of a

deprotonated phoshine species, such as $Ph_2PCH^-CH_2PPh_2$, detected upon reaction of $[Sn_9]^{4-}$ with $[IrCl(cod)]_2$ by *Fässler* and co-workers [25], which supports our assumption once more.

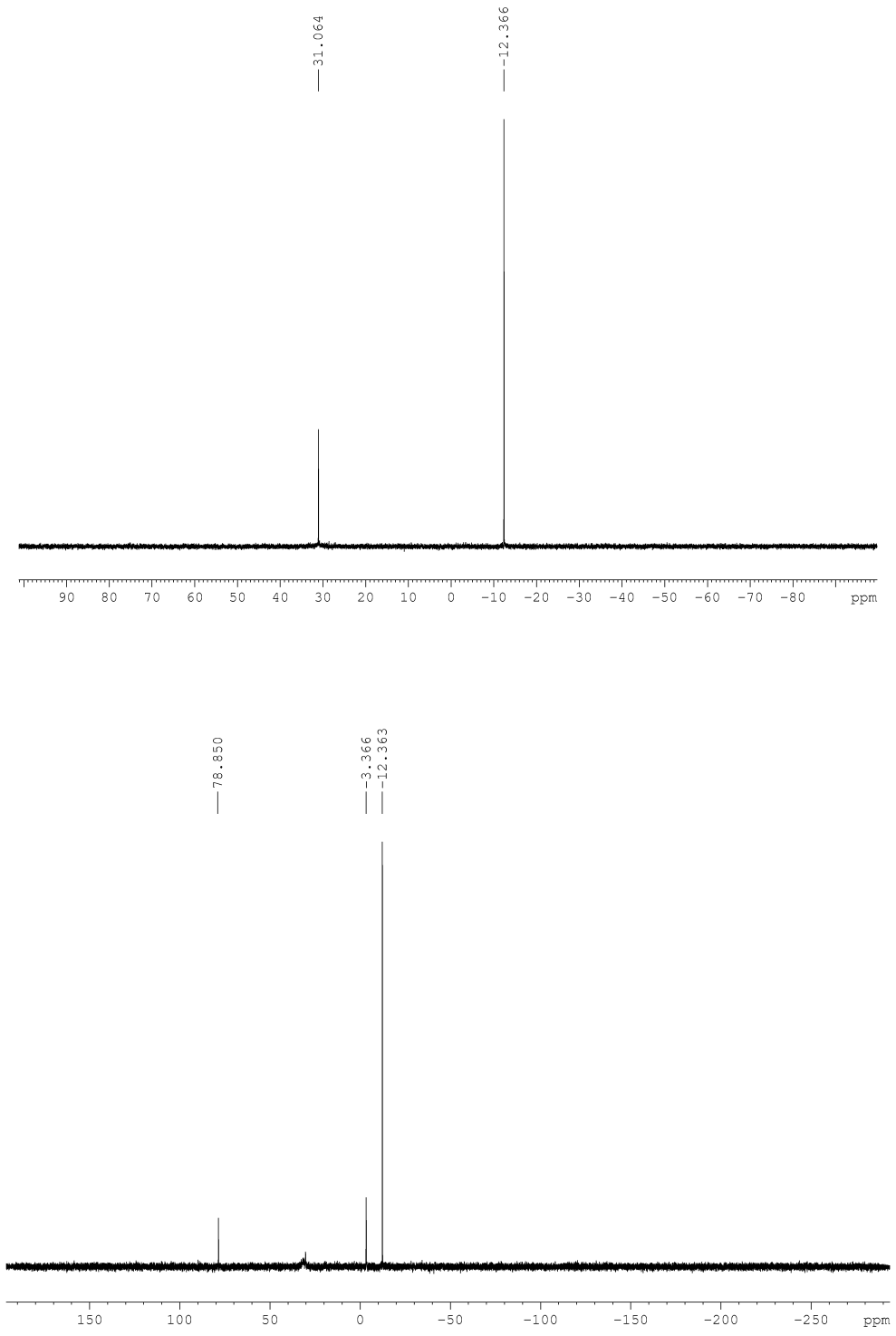

Figure S16. ^{31}P-NMR spectrum of the reaction solution after three hours (top, measured on a Bruker DRX 400 spectrometer with an observed frequency of 162 MHz (^{31}P) at 25 °C) and after several weeks (bottom, measured on a Bruker Avance 300 A spectrometer with an observed frequency of 122 MHz (^{31}P) at 25 °C).

7.5 Proposed reaction scheme and meachanism

According to the results of the studies and analyses outlined in 7.1 - 7.4, we conclude the formation of the title compound **1** in the following reaction scheme [eq (1), detectable products printed in bold]:

$$4\ [Sn_2Bi_2]^{2-} + 3\ Pd(dppe)_2 + 2\ H_2NCH_2CH_2NH_2 \longrightarrow \mathbf{[Pd_3Sn_8Bi_6]^{4-}} + \mathbf{[Bi_2]^{2-}} + 6\ \mathbf{dppe} + 2\ {}^{-}HNCH_2CH_2NH_2 + \mathbf{H_2} \quad (1)$$

Based on the analyses described above, on the nature of the reactants and on the structure of product, we may suggest two possible pathways (A and B) for the formation of the ternary cluster anion in **1**. In order to rationalize the possibility of any of the proposed mechanisms, the postulated intermediate species have been calculated by DFT methods as outlined below. As shown in Figures S17 and S19, both hypothetical pathways would involve (a) the final release of one equivalent of $[Bi_2]^{2-}$ per formula unit of the title compound, (b) electron transfer onto two *en* molecules, and (c) H_2 formation.

Pathway A

The product cluster might have been formed out of a preliminary macrocycle $\{[Pd(Sn_2Bi_2)]_3\}^{q-}$ by reaction with a source for two additional Sn atoms, and simultaneaous electron transfer onto *en* molecules under release of H_2 (see sketch in Figure S18). This suggestion is exclusively based on the structural peculiarities of the title compound that exhibits the according cycle which is capped by two further Sn atoms. No statement can be made on the reactive species releasing the latter, which may be (a) an intact $[Sn_2Bi_2]^{2-}$ anion as source for one Sn atom (under formation of $[Bi_2]^{2-}$ and "Sn^0") or as source for two Sn atoms at two neighboring clusters (under formation of $[Bi_2]^{2-}$) or (b) Sn atoms /anions that derive from further fragmentation of the starting material.

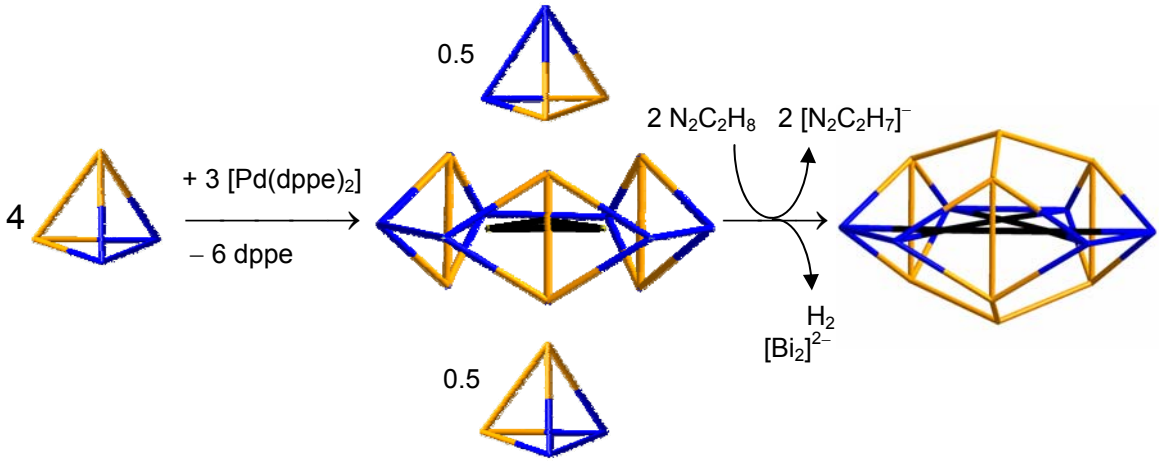

Figure S17. Schematic drawing of the key step in the formation of the anion in **1**, based on the reaction of a precursor macrocycle $\{[Pd(Sn_2Bi_2)]_3\}^{q-}$ with further starting material as source for additional Sn atoms (*pathway A*); note that the two $[Sn_2Bi_2]^{2-}$ tetrahedra that are drawn only count as 0.5 $[Sn_2Bi_2]^{2-}$ per macrocylce on average.

DFT calculations of the intermediate macrocycle $\{[Pd(Sn_2Bi_2)]_3\}^{q-}$ was performed with charges q = −6 (according to the sum of original charges of three $[Sn_2Bi_2]^{2-}$ anions and three Pd^0 atoms) and q = −4 (assumed that the resulting charge of the cluster anion in **1** has been already achieved in this state). In both cases, the geometry optimizations converged into local mimima, but the resulting geometries differ significantly from the geometry of this moiety within the anion in **1** – not only at the still uncapped Sn_3 sites (Figure S18 and Table S7).

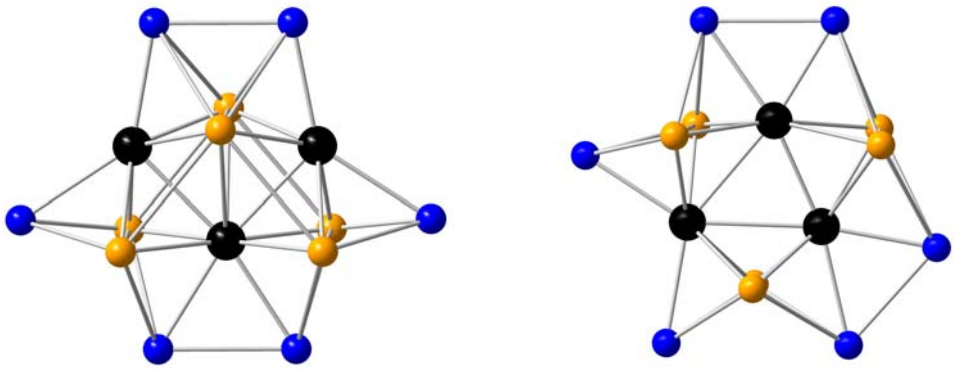

Figures S18. Result of the DFT geometry optimizations of hypothetical macrocycle fragments $\{[Pd(Sn_2Bi_2)]_3\}^{q-}$ with q = −4 (left hand side) or q = −6 (right hand side). Color code: Pd black, Sn orange, Bi blue. Bond lengths are given Table S7.

Table S7. Bond lengths /pm in calculated anions $\{[Pd(Sn_2Bi_2)]_3\}^{q-}$ (q = 4, 6), and in the cluster anion $[Pd_3@Sn_6Bi_8]^{4-}$ in **1** as calculated by the same methods or experimentally observed, for comparison.

bond	$\{[Pd(Sn_2Bi_2)]_3\}^{4-}$	$\{[Pd(Sn_2Bi_2)]_3\}^{6-}$	$[Pd_3@Sn_8Bi_6]^{4-}$ (calc.)	$[Pd_3@Sn_8Bi_6]^{4-}$ (exp.)
Sn−Bi	295.42-315.85	296.94-331.01	310.9-311.2	302.0(2)-309.4(2)
Sn−Sn	340.69-355.49	286.57-338.94	293.8-329.5	289.8(2)-326.1(2)
Pd−Sn	273.85-321.53	272.53-294.43	293.3-302.8	286.8(2)-302.5(2)
Pd−Bi	282.23-299.75	276.53-287.19	277.7-278.0	272.8(2)-275.2(2)
Pd−Pd	295.04-411.44	277.75-319.00	280.58-280.73	275.6(2)-277.4(2)
Bi−Bi	307.00-308.03[a]	310.01-310.05[a]	317.2-317.5	312.4(2)-315.0(2)

[a] Range of the drawn Bi–Bi contacts; all others are longer than 310.1 pm and thus not shown in Figure S18.

Pathway B

As a second possibility for the formation mechanism of the anion in **1**, we suggest a condensation reaction of three cluster precursors containing eight or nine main group element atoms with interstitial Pd atom, $[Pd@Sn_6Bi_2]^{q-}$, $[Pd@Sn_6Bi_3]^{q-}$, or $[Pd@Sn_7Bi_2]^{q-}$; this pathway would be analogous to the formation of condensed or fused icosahedra found in many intermetallic phases [26]. Although the proposed precursor clusters have not yet been isolated, several experimental hints exist in our studies and in the literature for eight atom or nine atom Zintl anions of group 14 or group 15 elements, with or

without interstitial metal atom [27]. A mixed Sn/Bi nine atom cage was previously isolated as by-product at the synthesis of $[Zn_6Sn_3Bi_8]^{4-}$ [28]. Additionally, a Pd-containing nine atom species $[PdSn_6Bi_3]^-$ was indeed detected in the ESI mass spectrum of the reaction solution at the synthesis of compound **1** (see 5.2). In both cases, the precursor clusters would be fragmentation/re-arrangement products of the starting material under release of $[Bi_2]^{2-}$ units. The precursors for such fusion processes calculated and shown in the following were chosen as first suggestions owing to a combination of features: (a) a suitable formula for the production of the fewest amounts of by-product and (b) diamagnetic compositions, (c) suitable structures providing a Bi–Bi bond, (d) relation to a present or previous experimental finding.

A fusion of endohedral eight atom Zintl anions would involve only a few re-arrangment steps of precursor and intermediate species at the formation of the $[Pd_3Sn_8Bi_6]^{4-}$ anion (Figure S19). The second by-product of this pathway should be reformed starting material – according to our observation that the latter co-crystallizes with all compounds containing ternary Zintl anions clusters that we have obtained so far.

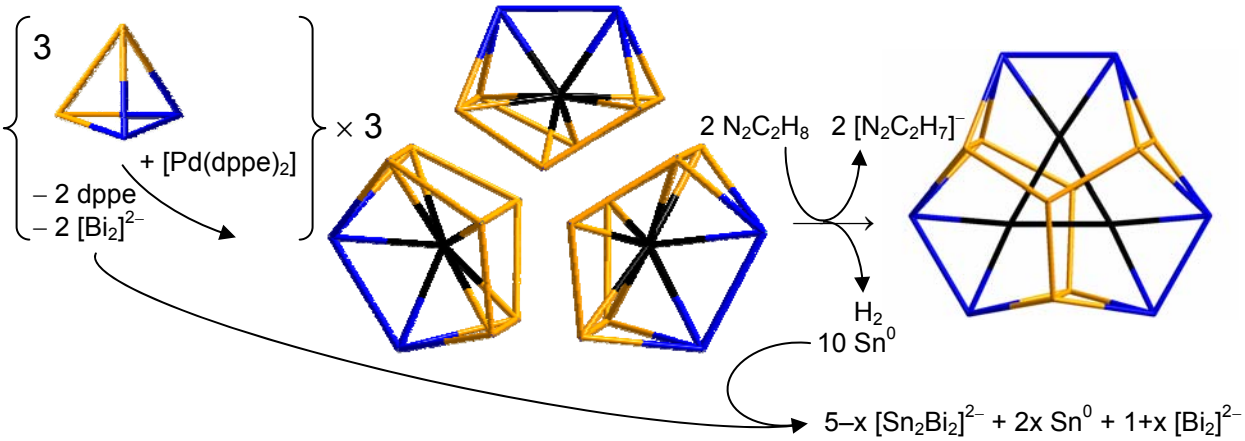

Figure S19. Schematic drawing of the key step in the formation of the anion in **1**, based on the condensation of three precursor clusters $[Pd@Sn_6Bi_2]^{q-}$ into a triply fused cluster anion (*pathway B*). The endohedral eight-atom clusters are reaction products of three equivalents of the starting material $[Sn_2Bi_2]^{2-}$ under release of two equivalents of $[Bi_2]^{2-}$ each, that are (partially) consumed to reform the starting material as by-product of the brutto reaction. Note that $[Bi_2]^{2-}$ as well as Sn^0 and $[Sn_2Bi_2]^{2-}$ were detected as by-products.

DFT calculations of according eight atom cages were performed for $[Pd@Sn_6Bi_2]^{4-}$ and $[Pd@Sn_6Bi_2]^{6-}$ (Figure S20 and Table S8). In both cases, the geometry optimizations converged into local mimima with bond lengths that are similar to those observed in the ternary cluster anion in **1** – except the Pd–Bi bonds that are significantly longer, and the Pd–Sn bonds that are shorter than in the anion in **1**.

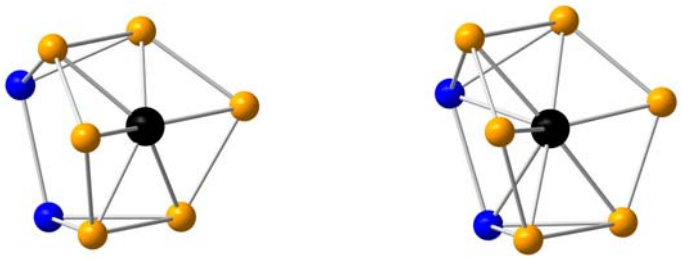

Figures S20. Result of the DFT geometry optimizations of hypothetical cluster anions $[Pd@Sn_6Bi_2]^{4-}$ (left hand side) and $[Pd@Sn_6Bi_2]^{6-}$ (right hand side). Color code: Pd black, Sn orange, Bi blue. Bond lengths are given in Table S8.

Table S8. Bond lengths /pm in calculated anions $[Pd@Sn_6Bi_2]^{q-}$ (q = 4, 6), and in the cluster anion $[Pd_3@Sn_6Bi_8]^{4-}$ in **1** as calculated by the same methods or experimentally observed, for comparison.

bond	$[Pd@Sn_6Bi_2]^{4-}$	$[Pd@Sn_6Bi_2]^{6-}$	$[Pd_3@Sn_8Bi_6]^{4-}$ (calc.)	$[Pd_3@Sn_8Bi_6]^{4-}$ (exp.)
Sn−Bi	300.2-300.6	305.6-305.6	310.9-311.2	302.0(2)-309.4(2)
Sn−Sn	285.9-306.4	285.2-321.6	293.8-329.5	289.8(2)-326.1(2)
Pd−Sn	276.3-281.7	286.1-292.5	293.3-302.8	286.8(2)-302.5(2)
Pd−Bi	369.7-369.8	302.1-302.2	277.7-278.0	272.8(2)-275.2(2)
Bi−Bi	303.5	308.7	317.2-317.5	312.4(2)-315.0(2)

Although a fusion analogous to that shown in Figure S19 would come along with a larger amount of by-product, geometry optimizations of nine atom cages with interstitial Pd atoms have been performed for $[Pd@Sn_6Bi_3]^{3-}$, which was observed in the ESI mass spectrum of the reaction mixture (see 5.2), as well as for $[Pd@Sn_7Bi_2]^{4-}$ and $[Pd@Sn_7Bi_2]^{2-}$, that are based on a trigonal prismatic $[Sn_7Bi_2]^{2-}$ anion which was previously obtained as a by-product in the synthesis of $[Zn_6Sn_3Bi_8]^{4-}$ [27]. For calculation of a variety of isomers of $[Pd@Sn_6Bi_3]^{3-}$, two Bi atoms were involved in a Bi–Bi bond and a third one was placed apart. The starting geometries converged into structures that represent highly distorted, mono-capped square antiprisms. For $[Pd@Sn_7Bi_2]^{2-}$ and $[Pd@Sn_7Bi_2]^{4-}$, the distortion of the resulting mono-capped square antiprism shown in Figure S21, that were obtained as local minimum structures, is only smooth. Other isomers did not converge into reasonable structures with regard to a subsequent condensation of three clusters. Thus, the species shown below may also be viewed as potential precursors in the formation of the anion in **1**. For $[Pd@Sn_6Bi_3]^{3-}$, the reaction would afford more Bi containing by-product, whereas for $[Pd@Sn_7Bi_2]^{q-}$, more Sn atoms would be obtained per formula unit of **1**, than for the condensation of the eight atom cages. The best structural fit between precursor and final cluster anion is observed for $[Pd@Sn_7Bi_2]^{4-}$ – except some dramatically elongated Sn–Bi and Sn–Sn contacts, which seem to be reasonable for a reactive species that will release some of the Sn atoms.

The final decision on the very precursor species requires the inspection of according reaction energies and assistance by further experiments that are underway.

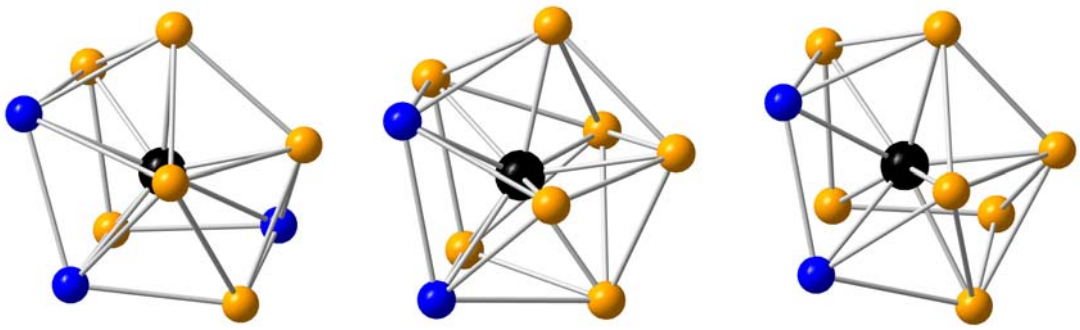

Figures S21. Result of the DFT geometry optimizations of hypothetical cluster anions $[Pd@Sn_6Bi_3]^{3-}$ (left hand side), $[Pd@Sn_7Bi_2]^{2-}$ (center) and $[Pd@Sn_7Bi_2]^{4-}$ (right hand side). Color code: Pd black, Sn orange, Bi blue. Bond lengths are given in Table S9.

Table S9. Bond lengths /pm in calculated anions $[Pd@Sn_{9-x}Bi_x]^{q-}$ (x/q = 3/3, 2/4, 2/2), and in the cluster anion $[Pd_3@Sn_8Bi_6]^{4-}$ in **1** as calculated by the same methods or experimentally observed, for comparison.

bond	$[Pd@Sn_6Bi_3]^{3-}$	$[Pd@Sn_7Bi_2]^{2-}$	$[Pd@Sn_7Bi_2]^{4-}$	$[Pd_3@Sn_8Bi_6]^{4-}$ (calc.)	$[Pd_3@Sn_8Bi_6]^{4-}$ (exp.)
Sn−Bi	299.3-316.42	316.0-329.0	297.8-356.61	310.9-311.2	302.0(2)-309.4(2)
Sn−Sn	305.9-332.05	307.9-334.5	292.3-340.48	293.8-329.5	289.8(2)-326.1(2)
Pd−Sn	267.3-287.34	271.8-282.3	268.3-309.85	293.3-302.8	286.8(2)-302.5(2)
Pd−Bi	282.6-302.57	273.8-273.8	282.6-289.6	277.7-278.0	272.8(2)-275.2(2)
Bi−Bi	322.0	325.0	315.8	317.2-317.5	312.4(2)-315.0(2)

Due to the higher plausibility of the involved reactants and their fusion, and owing to the results of DFT calculations of hypothetical intermediates, we tend to favor *pathway B*, that is, the fusion of pre-formed cages with interstitial Pd atom. We assume that these species are very reactive and have therefore not been isolable so far. While the eight atom clusters, that are assumed to be even more reactive, have not been detectable at all, the nine atom species were observed in the ESI mass spectrum of the present reaction solution. This – along with more similar structural parameters – may be taken as a hint for the latter to play the key role in the formation of the ternary anion in **1**. Apart from the so far unsuccessful isolation of the intermediates, NMR studies might be a useful – although challenging – tool in the final elucidation of the cluster formation mechanisms. However, all attempts to track the formation of the title compound **1** by means of ^{119}Sn NMR studies in solution were unsuccessful so far, which might be aroused by the quadrupole moment of the adjacent Bi nuclei. Reactions with analogous Pt complexes might enable according studies using ^{195}Pt NMR spectroscopy.

8. Micro analysis

The micro analysis of compound **1** was performed at the Campbell Microanalytical Laboratory at the University of Otago (Table S10).

Table S10. Micro analytical results for **1** (% w/w).

atom type	K	Pd	Sn	Bi
measured	3.1-4.0 %	4.8-6.5 %	18.0-19.7 %	32.0-33.6 %
calculated	3.7 %	7.6 %	22.5 %	29.7 %

Due to the very high bismuth concentration in the digest, the optimal analytical ranges for the lighter elements could not be used which affected the precision. An alternative composition that would accord to the higher Bi and lower Sn content, "$[K([2.2.2]crypt)]_4[Pd_3Sn_7Bi_7]$", can be excluded since the compound is diamagnetic whereas the alternative composition would be paramagnetic.

9. References for the Supporting Information

[1] [2.2.2]crypt: 4,7,13,16,21,24-Hexaoxa-1,10-diazabicyclo[8.8.8]hexacosane.

[2] Critchlow, S. C.; Corbett, J. D. *Inorg. Chem.* **1982**, *21,* 3286−3290.

[3] Sheldrick, G. M. SHELXTL 5.1, Bruker AXS Inc. 6300 Enterprise Lane, Madison, WI 53719-1173, USA, **1997**.

[4] Absorption correction was applied with the programs X-RED included in X-Area 1.54, STOE & Cie GmbH, Hilpertstraße 10, D64295 Darmstadt.

[5] a) PLATON: Spek, A. L. *J. Appl. Crystallogr.* **2003**, *36*, 7−13; b) SQUEEZE-Routine: van de Sluis, P.; Spek, A. L. *Acta Crystallogr. Sect. A* **1990**, *46*, 194−201.

[6] Parr, R. G.; Yang, W. *Density Functional Theory of Atoms and Molecules*, Oxford University Press, New York, **1988**.

[7] Ziegler, T. *Chem. Rev.* **1991**, *91*, 651−667.

[8] Ahlrichs, R.; Bär, M.; Häser, M.; Horn, H.; Kölmel, C. *Chem. Phys. Lett.* **1989**, *162*, 165−169.

[9] Treutler, O.; Ahlrichs, R. *J. Chem. Phys.* **1995**, *102*, 346–354.

[10] Eichkorn, K.; Treutler, O.; Öhm, H.; Häser, M.; Ahlrichs, R. *Chem. Phys. Lett.* **1995**, *242*, 652−660.

[11] Eichkorn, K.; Weigend, F.; Treutler, O.; Ahlrichs, R. *Theor. Chem. Acc.* **1997**, *97*, 119−124.

[12] Becke, A. D. *Phys. Rev. A* **1988**, *38*, 3098–3100.

[13] Vosko, S. H.; Wilk, L.; Nusair, M. *Can. J. Phys.* **1980**, *58*, 1200–1211.

[14] Perdew, J. P. *Phys. Rev. B* **1986**, *33*, 8822–8824.

[15] Weigend, F.; Ahlrichs, R. *Phys. Chem. Chem. Phys.* **2005**, *7*, 3297–3305.

[16] Metz, B.; Stoll, H.; Dolg, M. *J. Chem. Phys.* **2000**, *113*, 2563–2569.

[17] Klamt, A.; Schürmann, G. *J. Chem. Soc., Perkin Trans.* **1993**, *2*, 799–805.

[18] Schäfer, A.; Klamt, A.; Sattel, D.; Lohrenz, J. C. W.; Eckert, F. *Phys. Chem. Chem. Phys.* **2000**, *2*, 2187–2193.

[19] Reed, A. E.; Weinstock, R. B.; Weinhold, F. *J. Chem. Phys.* **1985**, *83*, 735–746.

[20] Mulliken, R. S. *J. Chem. Phy*s. **1955**, *23*, 1833–1840.

[21] gOpenMol, Leif Laaksonen, Center for Scientific Computing, Espoo, Finland, Version 3.0, **2005**.

[22] Note that the energies of the charged species have been shifted by –0.9 eV relative to the energies of the neutral compound in order to adjust the energies of the non-bonding [Pd_3]-type MOs. The effect that charge compensation using the COSMO model leads to an energy shift is well-known.

[23] Boys, S. F. *Rev. Mod. Phys.* **1960**, *32*, 296−299.

[24] Foster, J. M.; Boys, S. F. *Rev. Mod. Phys.* **1960**, *32*, 300−302.

[25] Wang, J.-Q.; Stegmaier, S.; Wahl, B.; Fässler, T. F. *Chem. Eur. J.* **2010**, *16*, 1793–1798.

[26] Tillard-Charbonnel, M.; Manteghetti, A.; Belin, C. *Inorg. Chem.* **2000**, *39,* 1684–1696.

[27] a) Corbett, J. D. *Angew. Chem. Int. Ed.* **2000**, *39*, 670−690; b) Scharfe, S.; Fässler, T. F.; Stegmaier, S.; Hoffmann, S. D.; Ruhland, K. *Chem. Eur. J.* **2008**, *14*, 4479–4483; c) Lips, F.; Clérac, R.; Dehnen, S. *Angew. Chem. Int. Ed.* **2011**, *50*, 960−964.

[28] Lips, F.; Dehnen, S. *Angew. Chem. Int. Ed.* **2009**, *48*, 6435−6438.